Cracking the Brain's Code: How do Brain Rhythms Support Information Processing?

A thesis submitted to
The University of Manchester
for the degree of
Doctor of Philosophy
in the Faculty of Biology, Medicine and Health.

2016

Maria Constantinou

School of Biological Sciences

Contents

Word count: 52915

List of Figures

List of Tables

Abbreviations

3xTg-AD	Triple-transgenic model of Alzheimer's disease
AD	Alzheimer's disease
CA1	Cornu ammonis field 1
CA3	Cornu ammonis field 3
DG	Dentate gyrus
EEG	Electroencephalogram
ISI	Inter-spike interval
LEC	Lateral entothinal cortex
LFP	Local field potential
MEC	Medial entothinal cortex
n-BTA	n-spike burst-triggered average
REM	Rapid-eye movement
SPW-R	Sharp-wave ripple
Sub	Subiculum
TE	Transfer entropy

Keywords

Local field potential, Bursting, Hippocampus, Subiculum, Entorhinal cortex, Information theory, Transfer entropy, Neural coding, Computational neuroscience.

The University of Manchester

Maria Constantinou
Doctor of Philosophy
Cracking the brain's code: How do brain rhythms support information processing?
September 27, 2016

The brain processes information sensed from the environment and guides behaviour. A fundamental component in this process is the storage and retrieval of past experiences as memories, which relies on the hippocampal formation. Although there has been a great progress in understanding the underlying neural code by which neurons communicate information, there are still open questions.

Neural activity can be measured extracellularly as either spikes or field potentials. Isolated spikes and bursts of high-frequency spikes followed by silent periods can transmit messages to distant networks. The local field potential (LFP) reflects synaptic activity within a local network. The interplay between the two has been linked to cognitive functions, such as memory, attention and decision making. However, the code by which this neural communication is achieved is not well understood.

We investigated a mechanism by which local network information contained in LFP rhythms can be transmitted to distant networks in the form of spike patterns fired by bursting neurons. Since rhythms within different frequency bands are prevalent during behavioural states, we studied this encoding during different states within the hippocampal formation. In the first paper, using a computational model we show that bursts of different size preferentially lock to the phase of the dominant rhythm within the LFP. We also present examples showing that bursting activity in the subiculum of an anaesthetised rat was phase-locked to delta or theta rhythms as predicted by the model.

In the second paper, we explored possible neural codes by which bursting neurons can encode features of the LFP. We used the computational model reported in the first paper and analysed recordings from the subiculum of anaesthetised rats and the medial entorhinal cortex of an awake behaving rat. We show that bursting neurons encoded information about the instantaneous voltage, phase, slope and/or amplitude of the dominant LFP rhythm (delta or theta) in their firing rate. In addition, some neurons encoded about 10-15% of this information in intra-burst spike counts.

We subsequently studied how the interactions between delta or theta rhythms can transfer information between different areas within the hippocampal formation. In the third paper, we show that delta and theta rhythms can act as separate routes for simultaneously transferring segregate information between the hippocampus and the subiculum of anaesthetised mice. We found that the phase of the rhythms conveyed more information than amplitude.

We next investigated whether neurodegenerative pathology affects this information exchange. We compared information transfer within the hippocampal formation of young transgenic mice exhibiting Alzheimer's disease-like pathology and healthy aged-matched control mice and show that at early stages of the disease the information transmission by LFP rhythm interactions appears to be intact but with some differences.

The outcome of this project supports a burst code for relaying information about local network activity to downstream neurons and underscores the importance of LFP phase, which provides a reference time frame for coordinating neural activity, in information exchange between neural networks.

Declaration

No portion of the work referred to in the thesis has been submitted in support of an application for another degree or qualification of this or any other university or other institute of learning.

Copyright Statement

Acknowledgements

I would like to take this opportunity to acknowledge the people that contributed in making the four years of my PhD project an interesting and enjoyable experience.

Firstly, I would like to sincerely thank my supervisors Dr Marcelo Montemurro and Dr John Gigg for their support, helpful advice, valuable feedback and inspiring conversations throughout the project. I also thank my advisor Dr Jon Turner for useful advice. I thank Prof Stuart Allan who supervised my three-month placement on science public engagement. I would like to thank our collaborators Dr Inés Samengo and Soledad Gonzalo Cogno for their useful comments, feedback and contribution to the second paper, as well as their friendship when I visited the lab in Argentina.

I would like to thank Dr Daniel Elijah for his help at the beginning of my PhD project. I would like to acknowledge and thank Dr Daniel Squirrell for recording most of the data used in this PhD project and detailed explanations of the experimental procedures. I would like to acknowledge the contribution of Claire Scofield who recorded the data from one of the rats used in the second paper. I would like to extend my thanks to my officemates: the three aforementioned, Dr Sarah Fox, Dr Natasha Bray, Dr Fiona Burrows, Khafarae Henry and Sander Tanni, for their support, friendship and interesting academic and non-academic conversations.

I would like to thank my family and friends who have always been by my side, supporting, encouraging and motivating me throughout this academic journey. Finally, I would like to thank my boyfriend Juan Felipe Ramirez-Villegas for his constant support and encouragement over the last year and especially the last month while I was writing this Thesis.

Maria Constantinou, 2016.

Chapter 1

Introduction

1.1 Project motivation

The brain has been puzzling scientists for centuries. As the brain controls a range of functions from heartbeat and breathing to highly intellectual reasoning and creativity, understanding its mechanisms is challenging. In terms of behaviour, input from the sensory systems is translated into neural messages, processed in the central nervous system, and output is sent to the motor system to carry out the decided actions in a stimulus-response manner; for example moving the hand away from a hot surface. Moreover, the brain actively engages behaviour to reach a goal, such as writing a thesis. A vital aspect for guiding goal-driven behaviour is the ability to record and recall prior experiences in the form of memories.

In order to carry out these functions, neurons exchange messages in a 'language' referred to as the neural code. Traditionally, studies in the field of neural coding have focused on stimulus-response recordings from sensory systems and showed that neural firing of action potentials is fundamental to the neural code (examples include Adrian and Zotterman (1926); Hubel and Wiesel (1959); Henry et al. (1974); Georgopoulos et al. (1982)). In the last few decades, accumulating evidence suggests that brain rhythms are also involved in the neural code (for example O'Keefe and Recce (1993); Lisman and Idiart (1995); Montemurro et al. (2008); Kayser et al. (2009)). Brain rhythms are oscillations in extracellular electrical potential reflecting collective neural activity (Logothetis, 2003; Buzsaki et al., 2012). Rhythms within specific frequency bands are associated with different sleep states and behaviours during arousal (recently reviewed in Watson and Buzsaki (2015)). Studies on brain rhythms usually investigate their role in cognitive processing, such as memory and attention (Engel et al., 2001; Ward, 2003; Wang, 2010). Although there has been a huge progress in understanding the brain's functions and the neural code, the role of brain rhythms in information encoding and transmission is still elusive.

This PhD project aimed to determine how information contained in brain rhythms

associated with different behavioural states can be encoded in neural firing. Moreover, this project aimed to explore how brain rhythms can transmit information between distinct neural networks. The hippocampal formation, which is a key structure for memory processing, is ideal for this purpose because, although the brain rhythms associated with different states of arousal, sleep and anaesthesia have been already documented in the literature, their capacity to encode and transmit information within the hippocampal formation has not been studied quantitatively yet. To this end, I used neurocomputational methods to analyse electrophysiological recordings from the hippocampal formation to achieve the aims of the project.

This introduction highlights the relevant background in the study of neural coding, brain rhythms and the hippocampal formation. The aims of the project are then explained and the outline of the thesis, which is written in alternative format, is presented.

1.2 Neural code

Neurons fire action potentials, which are impulses of depolarisation of the neuronal membrane with magnitude of ∼100 mV and lasting ∼1 ms followed by a refractory period of hyperpolarisation (Hodgkin and Huxley, 1939). In addition to single spikes, certain types of neurons can fire two or more spikes in bursts followed by silent periods (Izhikevich, 2010). An overview of the neural code is presented here. Current knowledge about the role of bursting is discussed in more detail in section 1.2.1.

A number of neural codes have been proposed over the past century. The first one was the spike rate code or spike count code in which information about the intensity of stimuli is transmitted by varying the firing rate of the neuron (Adrian and Zotterman, 1926). Subsequently, neurons that encode preferred stimuli in their spike counts have been identified, for example neurons in the primary visual cortex increase their firing rate in response to a preferred orientation of the stimulus (Hubel and Wiesel, 1959; Henry et al., 1974) and neurons in primary motor cortex increase their firing rate in response to the preferred direction of arm movement (Georgopoulos et al., 1982). Moreover, neurons can modify their firing rate to encode different aspects of the stimulus; for example face neurons in inferior temporal cortex increase or decrease their firing rate to transmit global and fine information about faces (Sugase et al., 1999).

Apart from the firing rate of spikes, Bryant and Segundo (1976) provided the first experimental evidence that the exact timing of spikes might be important for stimulus encoding. Mainen and Sejnowski (1995) and De Ruyter Van Steveninck et al. (1997)

then showed that the neural response can depend on the type of stimulus, so that neurons might encode static stimuli in spike counts but dynamic stimuli in spike times. Indeed, further studies confirmed that spikes can be fired with high temporal precision in response to dynamic sensory stimuli repeated over trials (Jones et al., 2004a,b) and quantitative analysis of their encoding capacity showed that spike time codes can convey more information about sensory stimuli than spike count codes (Panzeri et al., 2001; Montemurro et al., 2007a). Moreover, complementary information can be encoded by different temporal codes, such as by a combination of spike count and spike time codes, in a multiplexed code (reviewed in Panzeri et al. (2010)).

Firing of single neurons can also encode complex stimuli, such as abstract concepts, instead of the simple sensory ones discussed so far. For example, concept cells in the human medial temporal lobe can encode a concept, such as a specific person or object (Quian Quiroga et al., 2007, 2009; Quian Quiroga, 2012). Nonetheless, the brain does not have just one dedicated neuron encoding each piece of information, an idea known as 'grandmother cell' (Gross, 2002). Instead, groups of neurons can represent a sensory stimulus or abstract concept in sparse codes or population codes (Britten et al., 1992; Petersen et al., 2002; Panzeri et al., 2003; Quian Quiroga et al., 2008). Neurons can convey information using a combination of codes: for instance, a small group of neurons (sparse code) in the ventroposterior medial nucleus of the thalamus can be combined with a spike time code to transmit more information than the spike times of each individual neuron in the group (Montemurro et al., 2007a). The amount of information that a population of neurons can encode depends on the correlations in their activity and these correlations can either increase or reduce the information capacity of the population (Panzeri et al., 1999; Schneidman et al., 2003; Averbeck et al., 2006).

Firing spike trains is not the only means by which neurons can communicate. Neurons are constantly immersed in fluctuating electrical potentials which can be recorded from the extracellular medium as the local field potential (LFP, explained in section 1.3). The phase of LFP oscillations provides an internally-generated reference frame by which neurons can obtain timing information about the network activity and coordinate their firing. Spike firing relative to this reference signal can be part of the neural code. Indeed, the firing of spatial cells in the hippocampus (explained in section 1.4) with respect to the phase of ongoing LFP rhythms is thought to encode information about space (O'Keefe and Recce, 1993; Skaggs et al., 1996) and memories (Lisman and Idiart, 1995). Moreover, spike firing with respect to the phase of LFP oscillations (phase-of-firing code) can convey more information than spike firing alone in the monkey primary visual (Montemurro et al., 2008) and auditory cortices (Kayser et al., 2009). Multiplex (or nested) codes which combine a phase-of-firing code with temporal and population

codes can further enhance information encoding (Kayser et al., 2009; Panzeri et al., 2010).

Although the LFP can contain information about the network activity, its local nature –spatial reach of ∼0.5–3 mm from the electrode (Logothetis, 2003)– poses a physical restriction on distant neurons from accessing this information. However, one could ask: Is there a mechanism by which downstream networks can have access to this network information? Neurons can transmit information over long distances to downstream neurons by firing action potentials along their axons, which can range in length from a few millimeters to more than a meter (Debanne et al., 2011). Therefore, if some features of LFP rhythms can be encoded in some spike train patterns, the information within LFP could be transmitted to distant downstream neurons by neural firing. In this way, downstream neurons could obtain information about the upstream network activity by only observing the spike trains they receive. In this project, I addressed this question by investigating whether information about LFP can be encoded in spike patterns fired by bursting neurons.

1.2.1 Bursting

Bursting neurons fire two or more high-frequency spikes in bursts followed by silent periods. Bursting is underlined by the interaction of fast and slow currents and thus bursts are dynamically different from firing tonic spikes at a high rate (Izhikevich, 2010). Bursting is abundant in brain regions such as the cortex (Connors et al., 1982; McCormick et al., 1985), thalamus (Steriade et al., 1993a; Guido and Weyand, 1995) and hippocampal formation (Kandel and Spencer, 1961; Ranck, 1973). Originally, bursting was mainly associated with sleep (Steriade et al., 1993a,b) and pathological conditions such as epilepsy (Prince, 1978; McCormick and Contreras, 2001). Increasing evidence from a range of neural systems and animal species has suggested bursts are an important component in neuronal communication.

In the thalamus, bursts are thought to signal the detection of salient stimuli (Guido and Weyand, 1995; Sherman, 2001; Swadlow and Gusev, 2001). Moreover, bursts in the lateral geniculate nucleus of the thalamus encode different simple visual stimuli more reliably than tonic spikes (Alitto et al., 2005) and encode specific features of naturalistic visual stimuli (Lesica and Stanley, 2004). In the hippocampus, bursts are more reliable than spikes for synaptic transmission (Lisman, 1997). In the weakly electric fish, electrosensory cells fire bursts and tonic spikes to encode information about different behaviourally-relevant stimuli in parallel (Oswald et al., 2004; Chacron et al., 2004). In crickets, auditory neurons reliably encode salient increases in the

amplitude of ultrasound stimuli by bursting and this bursting activity also predicts their predator-avoidance responses (Marsat and Pollack, 2006; Sabourin and Pollack, 2009). These are some indicative examples highlighting the role of bursting in diverse systems.

In principle, firing bursts with different spike counts provides a code with many symbols that can represent a signal in a graded manner as proposed by theoretical studies on the encoding capacity of bursting (Kepecs and Lisman, 2003; Samengo et al., 2013). Evidence from computational studies has shown that bursting neurons can encode the slope (Kepecs et al., 2002) and phase (Samengo and Montemurro, 2010) of an input signal in the size of bursts fired.

Motivated from these studies, in the first two papers of this project we investigated whether bursting neurons can encode the phase or some other feature of brain rhythms. To achieve this, we adjusted the model from Samengo and Montemurro (2010) so that the distribution of bursts fired matched the distribution of real bursting neurons and then simulated their responses to signals containing behaviourally-relevant brain rhythms. We then compared these predictions to the analysis of *in-vivo* recordings of bursting activity and LFP. The brain system of choice for this purpose was the rodent hippocampal formation. This is because the hippocampal formation is known to contain bursting neurons (Kandel and Spencer, 1961; Ranck, 1973; Sharp and Green, 1994; Gigg et al., 2000; Latuske et al., 2015), and its anatomy and physiologically-important rhythms have been well-documented in the literature (introduced in section 1.4). In the next section, brain rhythms are introduced.

1.3 Brain rhythms

Brain rhythms refer to the rhythmic fluctuations in extracellular electrical signals which are abundant and constantly present throughout the brain. The first report of extracellular electrical activity relating to behaviour dates back to an abstract by Caton (1875) describing his recordings of electrical currents from the surface of the rabbit and monkey brains. This triggered a new field in neuroscience, the study of brain rhythms, that is still active and expanding to this day. The pivotal point in this field came with the development of the electroencephalogram (EEG) by Berger (1929) who for the first time recorded electrical activity from the exposed cortical surface of a patient undergoing surgery and then refined the method to record from the scalp (Karbowski, 2002). Although initially EEG recordings were dismissed by the community as artefacts, they were praised by Adrian and Matthews (1934) and the importance of the EEG and brain rhythms has since been appreciated (Karbowski, 2002).

Nowadays, EEG is routinely used both in research and clinical settings to record brain rhythm activity from the scalp in humans. The major advantages of EEG that established it as one of the methods of choice for human brain recordings are that it is non-invasive, inexpensive and provides millisecond temporal resolution of electrical brain activity. Different brain rhythms are associated with different stages of the sleep-wake cycle and cognitive functions, as well as pathological states (Engel et al., 2001; Ward, 2003; Wang, 2010; Watson and Buzsaki, 2015). In this section, the origin of the field potentials is explained and their role in cognitive processing is introduced. The brain rhythms in the hippocampal formation are discussed further in section 1.4.4.

1.3.1 The origin of LFP

Extracellular electrical potentials can be recorded from the scalp as the EEG, from the surface of the cortex as the electrocorticogram, or from electrodes inserted into the brain as the intracranial EEG or the LFP (Buzsaki et al., 2012). Extracellular recordings capture both field potentials and spiking activity. The LFP refers to the lowpass-filtered electrical potential signal (usually below 250 or 300 Hz). LFPs can be recorded extracellularly throughout the brain.

The origin of LFP signals is not straightforward because all transmembrane currents, that is ion fluxes in and out of cells, in the vicinity of the electrode contribute to the recorded electrical potential (reviewed in Logothetis (2003); Buzsaki et al. (2012)). The transmembrane currents affecting the signal arise from different sources including synaptic activity (Einevoll et al., 2007; Pettersen et al., 2008), action potentials (Schomburg et al., 2012; Scheffer-Teixeira et al., 2013), calcium spikes (Wong et al., 1979; Schiller et al., 2000), intrinsic resonances (Llinas, 1988; Silva et al., 1991; Leung and Yim, 1991), spike afterhyperpolarizations (Buzsaki et al., 1988; Ylinen et al., 1995), gap junctions (Katsumaru et al., 1988; Cruikshank et al., 2005), neuron-glia interactions (Kang et al., 1998; Poskanzer and Yuste, 2011) and ephaptic coupling (Jefferys, 1995; Anastassiou et al., 2011).

Currents leaving cells and thus entering the extracellular medium create current sources; whereas currents entering cells and thus leaving the extracellular milieu create current sinks (Mitzdorf, 1985). These current sources and sinks form dipoles of electrical potential in the extracellular neural tissue. The amplitude of the potential at a given location is inversely proportional to the distance of its current source or sink and the recording electrode. Therefore, the LFP recorded at an electrode is a weighted sum of all electrical potentials arising from ion fluxes in the surrounding tissue (Mitzdorf, 1985).

The size of the dipoles depends on cell geometry and cytoarchitecture (Einevoll et al., 2013). Pyramidal neurons, which are highly asymmetric, create large dipoles. In contrast, small symmetric neurons have dipoles which cancel out so they have much less contribution to the extracellular potential. Thus, the main contributors to the extracellular potentials are the synaptic currents across pyramidal neurons (Einevoll et al., 2007; Pettersen et al., 2008; Einevoll et al., 2013). The spatial reach of the LFP depends on the correlations among the synaptic inputs to the neurons surrounding the electrode. For uncorrelated inputs, the recorded LFP captures synaptic activity within 0.2 mm; whereas for correlated inputs, the reach of the LFP can encompass activity proportional to the radius of the correlated neural population (Linden et al., 2011).

LFP oscillations within distinct frequency bands, known as brain rhythms, have been associated with a variety of behavioural states (Watson and Buzsaki, 2015). Brain rhythms are usually named with Greek letters, such as alpha, beta, gamma, delta, epsilon and theta rhythms. The boundaries of the frequency bands, as well as the naming, vary considerably among studies and depend on the experimental setup (e.g. awake or anaesthetised) and species (e.g. mouse, rat, cat, monkey or human) from which they are recorded. A historical overview of how some of these terms were coined can be found in the Supplementary Material of Buzsaki and Wang (2012). The link between brain rhythms and cognitive processing is introduced in the following section.

1.3.2 Brain rhythms and cognitive function

Brain rhythms are preserved across evolution as it becomes evident from the similarities in the rhythms recorded from the human brain and non-human primates, mammals, such as cats, rodents and bats (Wang, 2010; Buzsaki, 2015); and also reptiles (Shein-Idelson et al., 2016). This implies an important role for these rhythms in brain function. Moreover, their link with different stages of the sleep-wake cycle and pathological states is a vital component in clinical settings for disease diagnosis and monitoring (Karbowski, 1990).

Brain rhythms have been linked with cognitive processing such as attention, memory, perception and decision making (reviewed in Ward (2003); Wang (2010)). The rhythms involved in memory processing are described in section 1.4.4. Interactions of brain rhythms are thought to mediate top-down processing, for instance to allow predictions about forthcoming events (Engel et al., 2001). Synchronisation and desynchronisation of brain rhythms provide a mechanism for temporal binding of multisensory information (Engel and Singer, 2001). In particular, large scale frequency-specific interactions can combine information from multiple modalities to achieve cognitive processes, such as

decision making and top-down attention (Siegel et al., 2012).

The cognitive role of brain rhythms suggests that they somehow process and transmit information between neural networks. Temporal correlations in the activity of separate networks can allow information flow via synchronised rhythms (Fries, 2005; Womelsdorf et al., 2007). In addition, activity in one network might have a causal effect on another network so that it entrains the latter in order to transmit information, which implies a direction of information flow (Friston, 1994). These two types of interactions are well-defined in the field of neuroimaging, where the first is termed functional connectivity and the latter effective connectivity (Friston, 1994, 2011). Brain rhythm interactions can allow not only functional connectivity but also effective connectivity so as to transmit information about cognitive functions. Indeed, the capacity of brain rhythms to mediate effective connectivity is supported by computational models showing that transitions in coupling between brain rhythms can dynamically change the direction of information flow within interconnected networks along anatomically fixed connections (Battaglia et al., 2012).

Nevertheless, the exact mechanisms of how brain rhythm interactions can mediate effective connectivity are still elusive. Which aspects of the rhythms convey the information between the different networks? Different rhythms can coexist. Hence, do some frequency bands convey more information than others? Different types of coupling between brain rhythms are possible: phase-phase, amplitude-amplitude and phase-amplitude (reviewed in Fell and Axmacher (2011); Buzsaki and Wang (2012)). However, are phase and amplitude equally capable of transmitting information? Is information conveyed by linear correlations in brain rhythms, or does information rely on non-linearities? Do neurological diseases alter these mechanisms?

This PhD project aimed to answer these questions in order to unravel how the interaction of brain rhythms in the hippocampal formation, which is essential for declarative memory and spatial navigation, can process information. Advancements in electrophysiological techniques, such as multiple electrodes (Buzsaki, 2004), allow the acquisition of simultaneous intracranial recordings to investigate effective connectivity between neural networks. To this end, in the last paper, LFP recordings from multiple sites within the hippocampal formation (area CA1 and subiculum) were analysed to quantitatively determine which LFP interactions are involved in information exchange between the two networks and whether these are altered by early stages of neurological disease. The hippocampal formation is introduced in the following section.

1.4 Hippocampal formation

The hippocampal formation is a bilateral structure located in the temporal lobes in humans. Its function and anatomy are very similar in both rodents and primates including humans (Insausti, 1993; Strange et al., 2014). Much of the current knowledge about the hippocampal formation comes from studies using rodents. In this section, the anatomy of the rodent hippocampal formation is described and the role of the hippocampal formation in cognitive functions is outlined.

1.4.1 Anatomy of hippocampal formation

The hippocampal formation (Fig. 1.1) is a compound structure comprising the hippocampus, dentate gyrus, subiculum and entorhinal cortex (Amaral and Witter, 1989; O'Mara et al., 2001). The rodent hippocampus consists of three cornu ammonis fields (CA1, CA2 and CA3). Primates and humans also have a fourth cornu ammonis field (CA4). The hippocampal area CA1 has a characteristic laminar structure comprising the alveus, stratum oriens, stratum pyramidale (pyramidal layer), stratum radiatum and stratum lacunosum moleculare. The subiculum has cytoarchitecture of allocortex which is three layers: molecular layer (continuous from strata lacunosum-moleculare and radiatum of CA1), enlarged pyramidal cell layer (contains soma of principal pyramidal neurons) and polymorphic layer (O'Mara et al., 2001). The entorhinal cortex is multi-laminate, has six functionally distinct layers which are non-homogeneously connected to input and output structures including the hippocampus (reviewed in Gigg (2006); Canto et al. (2008)). The connections within the hippocampal formation are summarised in Fig. 1.2.

The entorhinal cortex, which is divided into medial (MEC) and lateral (LEC) parts, receives sensory information and projects this to the hippocampus (Canto et al., 2008). The entorhinal cortex projects the main input to the hippocampus via the perforant path originating from layer II and the temperoammonic pathway from layer III (Gigg, 2006). The hippocampal area CA3 receives input from the entire dentate gyrus, LEC and MEC (Gigg, 2006). The projections from area CA3 to area CA1 are more segregated: proximal CA3, which borders the dentate gyrus, projects to distal CA1, which borders the subiculum; distal CA3, which borders CA1, projects to proximal CA1, which borders CA3; and medial CA3 projects to medial CA1 (Gigg, 2006). The projections at each stage can process different information. For example CA3 to CA1 connections are involved in memory recall and entorhinal cortex to CA1 in memory acquisition (Brun et al., 2002).

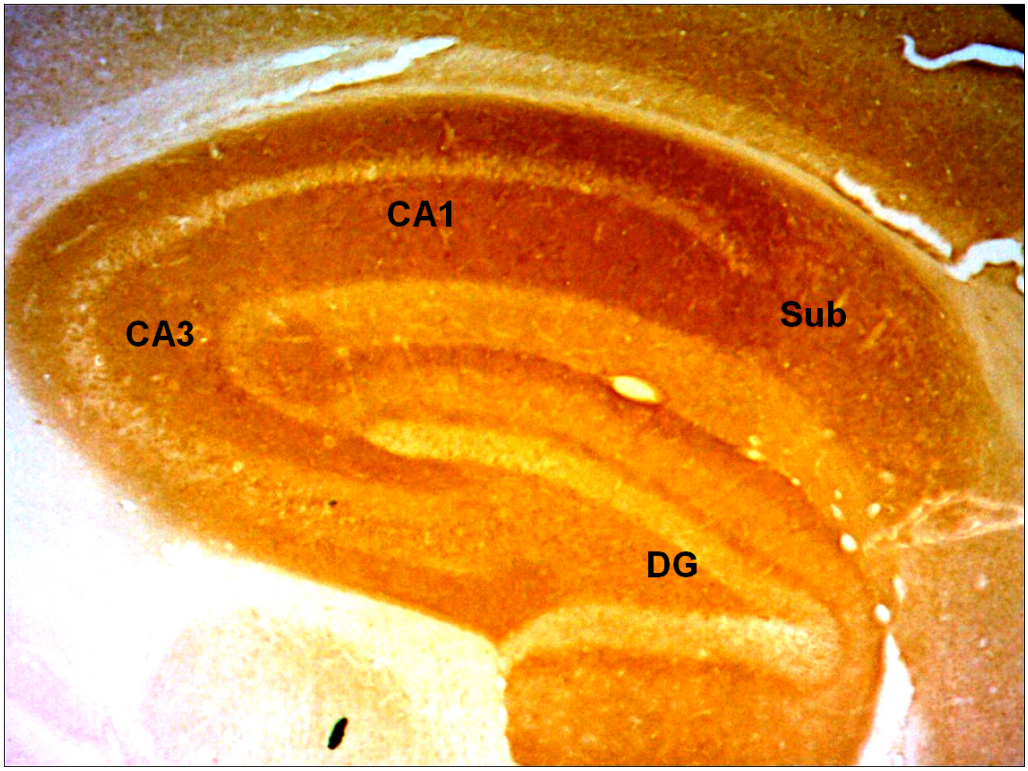

Figure 1.1: Hippocampal formation of a healthy mouse with annotations labelling the hippocampal areas CA1 and CA3, dentate gyrus (DG) and subiculum (Sub). Histological image was provided by Daniel Squirrell who obtained the recordings from mice and rats used in this study.

The subiculum mainly receives input from area CA1 and projects the main output of the hippocampus to the entorhinal cortex and other cortical areas –including the perirhinal, retrosplenial and prefrontal cortices– as well as to subcortical areas –including the thalamus, hypothalamus, amygdala and nucleus accumbens (O'Mara et al., 2001). Proximal CA1 projects to distal subiculum, which borders presubiculum; distal CA1 projects to proximal subiculum, which borders CA1; and medial CA1 projects to medial subiculum. Proximal subiculum and distal CA1 project to LEC. Distal subiculum and proximal CA1 project to MEC. The entorhinal cortex also sends direct input to the subiculum. LEC projects to distal CA1 and proximal subiculum whereas MEC projects to proximal CA1 and distal subiculum (Gigg, 2006). The subiculum and CA1 also receive direct input from the perirhinal cortext, which is involved in object perception, and the postrhinal cortex, which is involved in egocentric spatial and topographical representation. The perirhinal cortex projects to distal CA1 and proximal subiculum, and the postrhinal cortex projects to proximal CA1 and distal subiculum (Witter et al., 2000).

The segregated connections throughout the input-output circuitry of projections within the hippocampal formation support the idea that it can process different types of information (such as spatial and non-spatial) in parallel. Therefore, the hippocampal

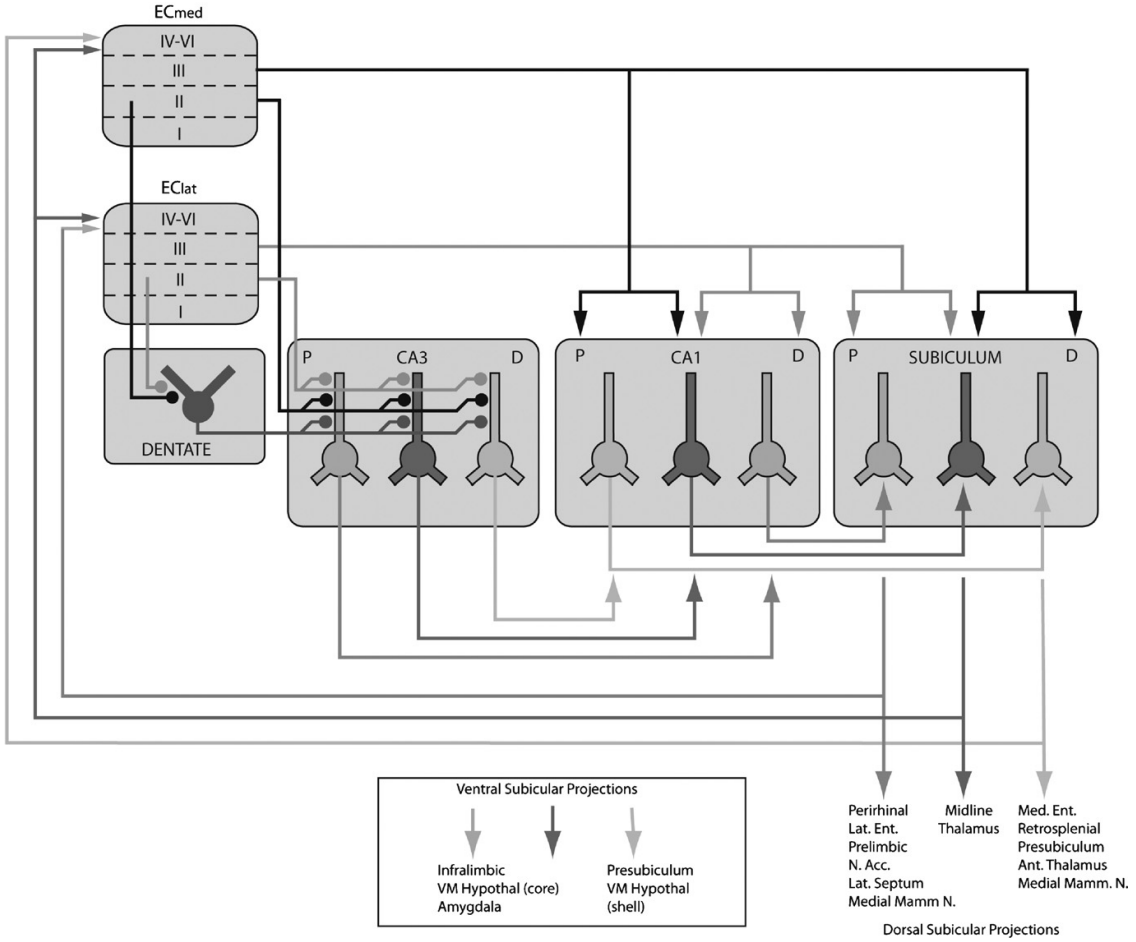

Figure 1.2: Summary of projections within the hippocampal formation described in the text. EClat and ECmed: lateral and medial entorhinal cortex, respectively; D: distal; P: proximal. Figure adapted from Gigg (2006).

formation is an ideal structure to experimentally investigate the idea of dynamic effective connectivity by LFP interactions introduced in section 1.3.2.

1.4.2 Bursting neurons in the hippocampal formation

Bursting in the hippocampal formation has been reported since early studies by Kandel and Spencer (1961) and Ranck (1973). *In-vitro* studies showed that, depending on their firing properties, neurons in the subiculum can be classified as regular spiking if they fire only single spikes or intrinsically bursting if they fire bursts of spikes as well as single spikes (reviewed in O'Mara et al. (2001)). *In-vivo* studies have confirmed the presence of bursting neurons in the subiculum (Sharp and Green, 1994; Gigg et al., 2000; Kim et al., 2012; Kim and Spruston, 2012). More recently, bursting neurons have also been reported *in-vivo* in the MEC (Latuske et al., 2015).

The presence of bursting neurons in the hippocampal formation *in-vivo* suggests that bursting might have a distinct role in the neural code. In this project, we studied the capacity of bursting neurons in the subiculum and the MEC to transmit information about the local network activity (reflected in particular features of ongoing LFP rhythms) to downstream neurons as already introduced in section 1.2.1.

1.4.3 Functions of hippocampal formation

The importance of the hippocampal formation for forming declarative memories, which are memories that can be explicitly expressed, has been first appreciated from studying amnesic patients, with patient H.M. being one of the most famous cases. Patient H.M. had bilateral removal of his medial temporal lobes, including large parts of the hippocampal formation, in order to treat his epilepsy (Scoville and Milner, 1957). After his surgery, the patient was unable to form new declarative memories, that is he suffered from severe anterograde amnesia; even though he could recall memories acquired up until three years before the surgery, he had partial retrograde amnesia (Squire, 2009). Declarative memories are usually divided into semantic which includes facts, concepts and meanings, and episodic which includes the context of life experiences (Dickerson and Eichenbaum, 2010). Although the patient could learn new skills, that is form procedural memories, he could not recall learning them (Squire, 2009). Following decades of research into memory processing, the hippocampal formation has been established as a necessary structure for forming declarative memories but not storing permanently these memories or forming procedural memories (Squire and Wixted, 2011).

Extensive studies of the hippocampal formation in rodents over the past half century have also revealed its importance for spatial navigation, which led to a Nobel Prize in Physiology or Medicine in 2014 (Nobelprize.org, 2016). After the discovery of place cells, which are neurons responding when the animal moves through a location, in hippocampal area CA1 (O'Keefe and Dostrovsky, 1971), the hippocampus has been proposed to form a cognitive map of the space in which the animal navigates (O'Keefe and Nadel, 1978). Since then, more types of spatial cells have been identified in regions of the hippocampal formation. Head direction cells, which fire only when the rodent faces towards a preferred direction, have been found in the postsubiculum (Taube et al., 1990a,b) and the MEC (Giocomo et al., 2014). Grid cells representing space in a hexagonal arrangement have been identified in the MEC (Fyhn et al., 2004; Hafting et al., 2005). Border cells that fire when the animal is near a boundary have been found in the MEC (Solstad et al., 2008). Boundary vector cells that fire when a perceived boundary is at their preferred location have been identified in the subiculum (Lever et al., 2009).

Speed cells, which encode the speed by which the animal moves, have been identified in the MEC (Kropff et al., 2015). The spatial encoding role of the hippocampal formation has been also suggested by imaging studies in humans (Maguire et al., 2000, 2006; Suthana et al., 2009). In addition, recent evidence suggested that grid-like representation of space is also present in humans (Doeller et al., 2010; Jacobs et al., 2013; Horner et al., 2016).

Furthermore, the hippocampal formation has been implicated in encoding non-spatial information. More specifically, neurons in the hippocampal formation may encode the context in which stimuli are perceived during behaviour rather than simple sensory stimuli or spatial cues. For example, non-spatial hippocampal cells in rodents may encode context-dependent representations of episodic memories related to task performance (Wood et al., 2000), such as prospective and retrospective aspects of memory tasks (Ainge et al., 2007). Similarly in humans, concept cells fire in response to complex stimuli, such as visual and acoustic, representing a specific concept which can be a particular person or item (Quian Quiroga et al., 2007, 2009; Quian Quiroga, 2012).

1.4.4 Rhythms in the hippocampal formation

Rhythms in the field potentials within the hippocampal formation are also implicated with specific cognitive functions. The three main rhythms (delta, theta and gamma) in the hippocampal formation are introduced in this section.

1.4.4.1 Delta rhythms

Delta rhythms ($\sim$1–4 Hz) (Siapas and Wilson, 1998) and slow oscillations ($\leq$1 Hz) (Wolansky et al., 2006) are large amplitude rhythms that are prevalent during slow-wave sleep, inactivity and anaesthesia (Wolansky et al., 2006; Sharma et al., 2010; Molle and Born, 2011; Rasch and Born, 2013). The boundary between the two rhythms is not always clear, especially under anaesthesia where the peak of the oscillation is at $\sim$1 Hz (Sharma et al., 2010). In this thesis, we refer to the $\sim$1 Hz oscillation as delta rhythms because in our recordings the band ranged from 0.5 to 2.5 Hz; except in Paper 1 where it was referred to as slow oscillations consistent with the nomenclature under similar experimental conditions (Wolansky et al., 2006).

Delta rhythms are generated by thalamic inputs (Amzica and Ster, 1992; Steriade, 2006) and are thought to mediate memory consolidation during slow-wave sleep (Diekelmann and Born, 2010; Molle and Born, 2011; Born and Wilhelm, 2012; Rasch and Born, 2013). Interestingly, evidence of memory consolidation has also been suggested under

anaesthesia (Culley et al., 2003), suggesting that at least some of the neural activity underlying memory processing is preserved under anaesthesia.

Delta rhythms organise neural activity in 'up' and 'down' states of excitability that enhances or decreases, respectively, neuronal activity in the neocortex (Molle and Born, 2011). During delta rhythms, the hippocampus displays prominent events known as sharp-waves –aperiodic deflections in the LFP (1–50 Hz)– associated with ripples –fast oscillations (100–250 Hz) (Buzsaki et al., 1992; Chrobak and Buzsaki, 1994; Ylinen et al., 1995). Hippocampal ripples are related to cortical spindles (Siapas and Wilson, 1998) and the interactions between these events is thought to form a neural substrate for transferring newly acquired memories from the hippocampus to the neocortex for permanent storage during sleep (Rasch and Born, 2013).

1.4.4.2 Theta rhythms

Theta rhythms refer to the frequency band of ∼3–12 Hz. The frequency range varies between studies depending on the experimental conditions. Indicative examples of hippocampal theta bands reported in the literature are listed in Table 1.1. The theta rhythm can be distinguished in two subtypes based on its sensitivity to the muscarinic acetylcholine receptor inhibitor atropine: the atropine-sensitive theta (∼4–7 Hz) and the atropine-resistant theta (∼7–12 Hz) (Kramis et al., 1975).

Table 1.1: Theta frequency bands within the hippocampal formation in different experimental conditions.

Band (Hz)	Species	Experimental condition
7–12	rats, rabbits	locomotion (Kramis et al., 1975; O'Keefe and Recce, 1993)
6–10	rats	locomotion (Skaggs et al., 1996)
5–10	rats	locomotion, REM sleep (Harris et al., 2002; Patel et al., 2012)
4–10	rats	locomotion, urethane anaesthesia (Lubenov and Siapas, 2009)
4–7	rats, rabbits	awake immobility, urethane anaesthesia (Kramis et al., 1975)
3–5	rats	urethane anaesthesia (Clement et al., 2008)
3–4	mice	urethane anaesthesia (Pagliardini et al., 2013b)
4–8, 3–8	humans	memory task (Lega et al., 2012)

In the hippocampus, theta rhythms are generated by inputs from the medial septum and diagonal band of Broca, which act as the pacemaker for the rhythm (Buzsaki, 2002). Parvalbumin-expressing GABAergic cells in the medial septum projecting to basket cells rhythmically disinhibit pyramidal neurons in the hippocampus (Buzsaki, 2002; Colgin, 2016), while cholinergic neurons in the medial septum slowly depolarise hippocampal pyramidal neurons and basket cells (Buzsaki, 2002). These interactions induce rhythmic inhibitory post-synaptic potentials at the soma of pyramidal neurons.

Moreover, entorhinal input produces rhythmic excitatory post-synaptic potentials at the dendrites of hippocampal pyramidal neurons (Buzsaki, 2002). The interactions of these inhibitory and excitatory post-synaptic potentials produce dipoles of which the sum is the observed theta rhythm in the recorded LFP (Buzsaki, 2002).

Hippocampal theta rhythms are commonly recorded during spatial navigation (O'Keefe and Recce, 1993; Skaggs et al., 1996; McNaughton et al., 2006) and REM sleep (Harris et al., 2002) and are thought to be involved in the declarative memory processing associated with these states. The interplay between theta rhythms, gamma rhythms (introduced in the next subsection) and spiking activity is hypothesised to build internal representations in the hippocampus. Neural firing representing an item of memory, e.g. place cells firing when the animal visits the preferred place field, is locked at a specific phase on the theta cycle (O'Keefe and Recce, 1993). This firing shifts to earlier phases on successive theta cycles, e.g. when the animal traverses the place field, a phenomenon known as theta phase precession (Skaggs et al., 1996). The firing of an ensemble of neurons each representing a specific memory (or portion of the space) is replayed on every theta cycle, and the firing of different ensembles within a theta cycle occurs during gamma cycles superimposed on the theta cycle (Lisman and Idiart, 1995; Jensen and Lisman, 2005, 1998; Buzsaki and Draguhn, 2004; Jensen and Lisman, 2005; Jensen, 2006; Lisman, 2005; Lisman and Buzsaki, 2008; Carr et al., 2012). This hypothesis is mostly based on rodent studies. Experimental evidence from studies with epileptic patients supports the idea that the hippocampal theta rhythms, as well as gamma rhythms, are involved in processing memories in humans (Lega et al., 2012).

The aforementioned evidence suggests that locking of neural firing to the phase of theta rhythms is key in representing information. In light of this, recent studies have shown that theta phase gradually shifts along the septotemporal axis of the hippocampus (Lubenov and Siapas, 2009; Patel et al., 2012) and this spatiotemporal structure of theta can be regarded as a carrier signal containing information about the position of a rat during spatial exploration (Agarwal et al., 2014).

Given the importance of phase-locking in the hippocampal formation, the first part of the project focused on determining whether bursting neurons can encode the phase of some rhythms and the conditions under which such encoding is possible. In order to be able to test a range of possible rhythms, we used a bursting neuron model and then compared the model predictions with the analysis of experimental data. This was the topic of Paper 1.

1.4.4.3 Gamma rhythms

Gamma rhythms refer to the frequency band of ∼30–100 Hz. The exact frequency range varies among studies, e.g. 30–80 Hz (Buzsaki and Draguhn, 2004), 25–100 Hz (Colgin, 2011, 2016) and 30–90 Hz (Buzsaki et al., 2012). The gamma band is further divided into sub-bands based on their interactions with other bands and networks. This sub-band classification varies depending on the study (see Table 1.2). Some authors extend the gamma band to include oscillations with frequencies of >100 Hz (Colgin et al., 2009; Belluscio et al., 2012; Schomburg et al., 2014). Oscillations of >100 Hz are also referred to as epsilon (Freeman, 2007; Belluscio et al., 2012; Schomburg et al., 2014) and high-frequency oscillations (Scheffer-Teixeira et al., 2013) in the literature and can have different physiological roles than gamma rhythms or might arise from spike leakage into the field recording (Scheffer-Teixeira et al., 2013).

Table 1.2: Gamma sub-bands within the hippocampal formation reported in different studies.

Gamma sub-band	Frequencies (Hz)	Study
slow	25–50	Colgin et al. (2009)
fast	65–140	
slow	30–50	Belluscio et al. (2012)
midfrequency	50–90	
fast/epsilon	90–150	
slow	30–80	Schomburg et al. (2014)
midfrequency	60–120	
fast/epsilon	>100	

Gamma rhythms in the hippocampus are generated by the activity of basket cells, which are fast-spiking parvalbumin soma-inhibiting interneurons, and entorhinal input (reviewed recently in Bartos et al. (2007); Buzsaki and Wang (2012); Colgin (2016)). Low gamma or slow gamma (25–55 Hz) arises from CA3 input, whereas fast or mid-frequency gamma (60–100 Hz) arises from MEC input (Colgin, 2016).

Gamma sub-bands interact separately as well as with theta rhythms to couple different networks. More specifically, Colgin et al. (2009) showed that slow gamma was coherent in CA1 and CA3, and fast gamma was coherent in CA1 and MEC of awake rats. In addition, fast and slow gamma were locked to different phases of theta rhythms in area CA1 supporting the idea that: fast gamma coupling with CA1 theta rhythms channels extrinsic inputs from MEC to CA1; whereas slow gamma coupling with CA1 theta rhythms channels intrinsic inputs from CA3 to CA1 (Colgin et al., 2009). These experimental evidence agreed with preceding models proposing the idea of distinct theta-gamma interactions between the entorhinal cortex and hippocampus for memory encoding,

and between areas CA3 and CA1 for memory retrieval (Hasselmo et al., 2002).

The mechanism of LFP rhythm interactions for transmitting separate information might also apply in different contexts. This motivated Paper 3 in this project, which aimed to determine how LFP rhythms in the output part of the hippocampal formation can interact to mediate information exchange.

1.5 Brain rhythms in neurological diseases

Considering that the generation of brain rhythms depends on the underlying neural network, it can be assumed that disruptions in the network by neurological diseases will affect the brain rhythms and this is expected to correlate with cognitive deficits. In rodents, loss of inhibitory interneurons results in disruption of gamma rhythms and impairments in spatial and memory task performance (Fuchs et al., 2007). Abnormal brain rhythms have also been recorded from patients and animal models with a range of neurological disorders, such as epilepsy, schizophrenia, autism, Parkinson's disease and Alzheimer's disease (reviewed in Uhlhaas and Singer (2006, 2010)).

Alzheimer's disease is a neurodegenerative disease (reviewed in Querfurth and LaFerla (2010); Ittner and Gotz (2011)) with characteristic symptoms of cognitive decline and memory problems (Larson et al., 1992). The pathological hallmarks of Alzheimer's disease are β-amyloid plaques and neurofibrillary tangles of hyperphosphorylated protein tau (Querfurth and LaFerla, 2010; Ittner and Gotz, 2011). The hippocampal formation is one of the first brain regions affected by accumulation of β-amyloid plaques and neurofibrillary tangles (Braak and Braak, 1991) and synaptic and neuronal loss (West et al., 1994). As well as loss of anatomical connections, large-scale functional connectivity is disrupted by Alzheimer's disease pathology (He et al., 2009). EEG and MEG studies have reported abnormal brain rhythms in AD patients (de Haan et al., 2009; Stam et al., 2009) suggesting a link between patterns of abnormal rhythms and Alzheimer's disease pathology.

Early diagnosis of neurological diseases is essential for better outcome of treatments, to delay the disease progression and improve the life of patients. Therefore, developing methods that will allow early diagnosis is very important. Identifying abnormal brain rhythms or impaired interactions between brain rhythms can be possible ways to diagnose neurological diseases at early stages. To investigate whether early stages of disease produce any detectable changes in information transfer by brain rhythms, we extended the investigation of information transfer within the rodent hippocampal formation to

a mouse model of Alzheimer's disease. We quantified information transfer by spontaneous LFP in the hippocampal formation of the 3xTg-AD mouse model of Alzheimer's disease and compared it with the information transfer within healthy control mice in order to identify potential impairments.

1.6 Summary

Neurons can transmit information using a combination of codes. Rhythms in the field potential provide an integral component in this information communication. However, a mechanism by which information contained in the LFP can be transferred to distant networks is not known. Bursting is a candidate mechanism for this, since it is reliable and has the capacity to provide more symbols in the neural code by firing events of different size.

LFP interactions, especially phase interactions, are involved in information encoding and transmission. In the hippocampal formation, current hypotheses suggest that delta rhythms coordinate neural excitability for memory consolidation; and neural ensemble activity relative to the phase of theta rhythms encodes memories. In addition, the coupling of oscillations within specific bands can dynamically route and segregate information along anatomical connections, as in the example of gamma sub-bands for memory encoding and retrieval. The exact interactions by which the LFP can mediate this dynamic effective connectivity are still unclear. This project seeks to address these gaps in our knowledge.

1.7 Aims of project

The main aim of this project is to understand how information contained in brain rhythms can be projected to distant networks and how brain rhythms can exchange information between separate neural networks. This aim was achieved in three papers. The specific aims of the project were:

A. To determine the specific conditions by which bursting neurons can lock to LFP phase.

B. To determine the neural code by which bursting neurons can encode information contained in LFP rhythms.

C. To quantitatively determine how the LFP can transfer information between separate networks in the hippocampal formation.

D. To apply the method of quantifying information transfer to investigate whether early stages of neurological disease affect information transfer within the hippocampal formation.

1.8 Alternative format structure

1.8.1 Paper 1

Title: Phase-locking of bursting neuronal firing to dominant LFP frequency components

Authors: Maria Constantinou, Daniel H. Elijah, Daniel Squirrell, John Gigg, Marcelo A. Montemurro

Status of paper: Published in BioSystems and available online at doi:10.1016/j.biosystems.2015.08.004 since 21 August 2015 (see Constantinou et al. (2015)).

Declaration of author contribution: All analyses of experimental and simulated data and model fitting were conducted by MC under the supervision of MM. Initial work with the model was also carried out by DE. Experimental data were recorded by DS during his Masters studies under the supervision of JG. MC wrote the manuscript. MM, JG, DE and DS provided feedback on the manuscript.

Paper overview: This paper addressed aim A. We used a bursting neuron model, which we adjusted to match the firing statistics of subicular neurons, to test the conditions by which bursting output phase-locks to different behaviourally-relevant frequency bands. The model predicted that bursting locks to the phase of the dominant rhythm in the input signal irrespective of the specific frequency of the rhythm. Moreover, bursts of increasing spike count locked to more advanced phases in a graded manner. We tested these predictions by analysing LFP and spiking activity from the rat subiculum under urethane anaesthesia. We observed similar phase locking patterns of bursting neuron output to the phase of the dominant rhythm (delta or theta) in the LFP.

1.8.2 Paper 2

Title: Bursting neurons in the hippocampal formation encode features of LFP rhythms

Authors: Maria Constantinou, Soledad Gonzalo Cogno, Daniel H. Elijah, Emilio Kropff, John Gigg, Inés Samengo and Marcelo A. Montemurro

Status of paper: Published in Frontiers in Computational Neuroscience and available online at doi:10.3389/fncom.2016.00133 since 30 November 2016 (see Constantinou et al. (2016)).

Declaration of author contribution: All analyses of simulated data and model fitting were conducted by MC under the supervision of MM. The analyses of experimental data were conducted by MC and SGC under the supervision of IS and MM. In detail, MC analysed the data from the subiculum and SGC from the entorhinal cortex. MC produced all Figures of the paper, except Figures 5 and 6, which were produced by IS. MC, SGC, IS and MM wrote code. Experimental data from the subiculum were recorded by Daniel Squirrell and Claire Scofield under the supervision of JG. Experimental data from the entorhinal cortex were recorded by EK. MC wrote the draft of the manuscript. MC, SGC, IS and MM finalised the submitted manuscript. DE, JG and EK provided feedback on the manuscript. MC produced all Supplementary Figures and wrote the Supplementary Material , except Supplementary Methods section 1.3 which was written by IS.

Paper overview: This paper addressed aim B. We investigated potential neural codes by which bursting neurons could encode features of the LFP, including the instantaneous voltage, slope, phase and amplitude. We analysed simulations of bursting neuron activity and electrophysiological recordings from the rat hippocampal formation under either urethane anaesthesia or awake behaviour. We show that bursting neurons encode information about features of delta and theta rhythms in their firing rate and some of these neurons also encode a smaller amount of information in their intra-burst spike count. The advantage of this burst code is summarised in Fig. 1.3.

1.8.3 Paper 3

Title: Information transfer by LFP rhythms within the hippocampal formation

Authors: Maria Constantinou, Daniel Squirrell, John Gigg, Marcelo A. Montemurro

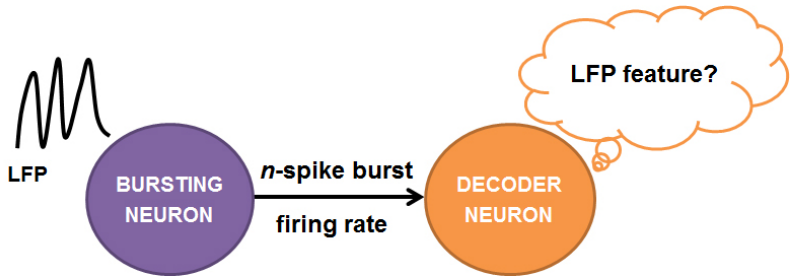

Figure 1.3: Diagram explaining the advantage of a neural code in which bursting neurons encode information about features of the LFP. In the network containing the bursting neuron there is a prominent LFP rhythm. The bursting neuron adjusts its firing rate and spike count to reflect features of this rhythm. The downstream neuron belongs to a separate network that has no direct access to the LFP surrounding the bursting neuron. However, the decoder neuron can obtain information about the upstream network state by only observing the arriving spike patterns.

Status of paper: Manuscript in preparation for eLife

Declaration of author contribution: MC analysed all data and produced all Figures. MC and MM wrote code. Experimental data were recorded by DS for his PhD project under the supervision of JG. MC wrote the manuscript. MM and JG provided feedback on the manuscript.

Paper overview: This paper addressed aim C. We analysed LFP recordings from hippocampal area CA1 and the subiculum of anaesthetised mice to determine how information is exchanged between the two networks. There were two prominent rhythms in the LFP: delta and theta. Therefore, we quantified the information transferred be each rhythm separately. We show that information is transmitted bidirectionally between the two networks by both rhythms. We then asked which aspects of the LFP signal convey the information. We determined that most of the information is conveyed by linear components in the signals. Moreover, the phase of delta and theta rhythms conveyed almost double the amount of information when compared to amplitude.

1.8.4 Supplementary material extending Paper 3

Topic: Information transfer by LFP at early stages of Alzheimer's disease-like pathology in the 3xTg-AD mouse model

Overview: Aim D was addressed by applying the same methodology used in Paper 3 to analyse LFP recordings from hippocampal area CA1 and subiculum of anaesthetised three-month-old 3xTg-AD mice. The results were compared with those obtained for the

three-month-old control mice presented in Paper 3. The outcome was that information transfer in 3xTg-AD and control mice appeared similar, but at the population level there were statistically significant differences between the two phenotypes. The outcome of this part of the study is presented as Supplementary to Paper 3. This was a meta-analysis of data collected by Daniel Squirrell for his PhD project. The results presented in this Supplementary section will be published in combination with the results of the biological investigation into the pathology of Alzheimer's disease in this mouse model (completed by DS).

Chapter 2

Methods

For this PhD project, I analysed electrophysiological data using a range of neurocomputational methods in order to address the aims of each paper. These methods are explained in the Methods section of each paper. In this section, I explain the background of the key methods used to analyse the data, for which a detailed explanation would have been unusually long to include in the methods section of a paper. To perform the data analysis, I wrote custom code or adapted code provided by Marcelo Montemurro to address the specific requirements of each analysis. Data analysis methods were implemented in MATLAB (The MathWorks, Inc.), unless otherwise stated.

2.1 *In vivo* electrophysiology

The electrophysiological data used in this project included LFPs and spiking activity from rats (Papers 1 and 2) and LFPs from healthy mice and 3xTgAD mice (Paper 3). The experimentally recorded data from anaesthetised rodents were obtained by Daniel Squirrell and Claire Scofield under the supervision of John Gigg. The experimental data from the awake behaving rat used in Paper 2 were recorded by Emilio Kropff. The experimental procedures for obtaining these recordings are described in the methods sections of each paper.

2.2 LFP sampling and filtering

Data were recorded with Plexon Recorder/64 (bandwidth: 1 Hz–6 kHz, Plexon Inc., USA). LFP were extracted by lowpass filtering (1-pole Butterworth) the raw recorded signal to obtain the components up to 250 Hz and sampled at 2 kHz. The extracted LFP signal was reverse-filtered with the same 1-pole Butterworth filter to correct for the phase shift distortion caused by the filter.

In order to speed up computation time, LFP signals were resampled to reduce their sampling rate. This was achieved in either of two ways depending on the requirements

of the analysis. The first way was to downsample the original 2 kHz signal by a factor of four to 500 Hz. This was sufficient since the Nyquist frequency of the downsampled signal was 250 Hz and the LFP signals contained no frequency components higher than that. The second way was to decimate the original signal from 2 kHz to 200 Hz. The decimation method was required in this case because the Nyquist frequency of the downsampled signal was 100 Hz. If downsampling was used, then the resulting signal would have a distortion called aliasing (Prandoni and Vetterli, 2008). Examples of this aliasing are illustrated in Fig. 2.1. In the first case, the original 2 kHz signals overlap with both the downsampled and decimated 500 Hz signals (Fig. 2.1A and B). In the second case, the original and decimated 200 Hz signals ovelap whereas the downsampled signal deviates from the original one (Fig. 2.1C and D). This aliasing is caused when signals of different frequencies cannot be distinguished as explained in Fig. 2.2. To prevent aliasing in the resampled signal, the original signal was first lowpass-filtered (Kaiser finite impulse response (FIR) filter) to remove all components above 100 Hz and then samples were discarded by the process called decimation (Prandoni and Vetterli, 2008).

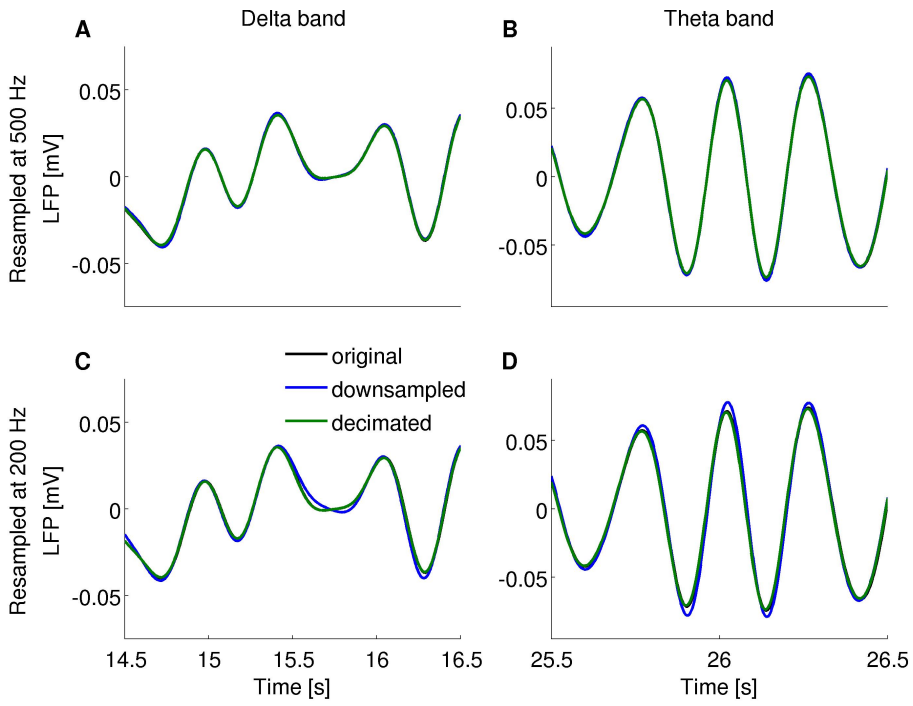

Figure 2.1: Example sections of bandpass-filtered LFP within 0.5-2.5 Hz (A and C) and 2.5-5 Hz (B and D) illustrating downsampling is sufficient for reducing the sampling rate to 500 Hz (A and B) and decimating was required to prevent aliasing in the 200 Hz signals (C and D).

To extract LFP oscillations within specific frequency bands, the LFP signals were filtered with a Kaiser FIR filter. The sharp transition bandwidth was 1.0 Hz, the stopband attenuation was 60 dB and the passband ripple was 0.01 dB. Filtering is also described in the Methods section of each paper. Depending on the requirements of each analy-

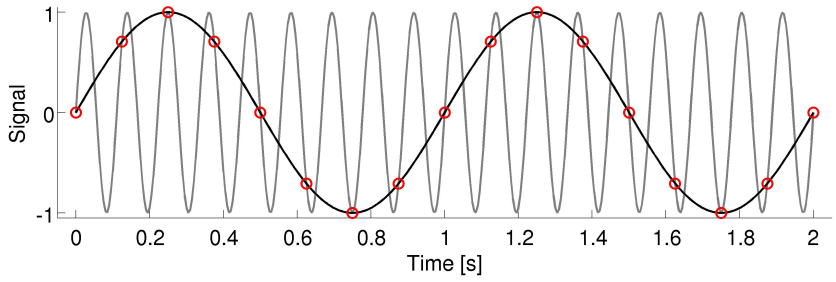

Figure 2.2: Example of two possible sinusoids (black line: 1 Hz; grey line: 9 Hz) that could fit the sampled values (red circles) recorded at a rate of 8 Hz. Aliasing can arise when a signal contains such components of higher frequencies than the Nyquist frequency. The remnants of the higher frequency components can result in the signal distortion observed in Fig. 2.1 when downsampling without lowpass-filtering first to remove all components above the Nyquist frequency.

sis, signals were either narrowband-filtered in overlapping windows of width 1 Hz or bandpass-filtered for specific behaviourally-relevant rhythms such as slow oscillations (0.5-2.5 Hz), anaesthetised theta rhythms (2.5-5 Hz) or awake theta rhythms (6-12 Hz). The cutoff frequencies for each band were chosen based on the spectral analysis of each dataset as explained in each paper. The width of 1 Hz for narrowband filtering was chosen so that we could identify which rhythms are important for information transmission or phase locking and where there is a transition in which rhythms belong to a different band.

2.3 LFP feature extraction

Oscillations can be described by their frequency, amplitude and phase (Fig. 2.3A). The frequency f of an oscillation indicates how many cycles are present in a second. This is inversely proportional to the period $T = 1/f$, which determines the duration of a cycle and is annotated in Fig. 2.3A. The amplitude $A(t)$ is the distance of the peak or trough of the signal from zero. The phase indicates at which point of the cycle is the signal. For instance, the four quarters of the phases of a cycle are coloured differently in Fig. 2.3A.

When an LFP signal is narrowband-filtered to obtain an oscillatory signal $x(t)$ containing only one major frequency so that $x(t)$ is a sinusoid, $x(t)$ can be described by its amplitude $A(t)$ and phase $\phi(t)$ according to Eq. 2.1:

$$x(t) = A(t)\cos[\phi(t)]. \tag{2.1}$$

The signal's amplitude and phase can be computed from the analytical signal $z(t)$ which

is obtained by projecting the signal on the complex plane as described in Eq. 2.2:

$$z(t) = x(t) + \mathrm{i}Q[x(t)] \tag{2.2}$$

where $x(t)$ is the real part of $z(t)$ and $Q[x(t)]$ is a transformation of $x(t)$ to get the imaginary part of $z(t)$. An example point of the analytic signal $z(t)$ is plotted on the complex plane in Fig. 2.3B to depict the quantities $x(t)$ and $Q[x(t)]$ and their relationship with the canonical pair of instantaneous amplitude $A(t)$ and instantaneous phase $\phi(t)$. The instantaneous amplitude $A(t)$ is the absolute value of the transform (Eq.2.3):

$$A(t) = |z(t)| = \sqrt{x(t)^2 + Q[x(t)]^2} \tag{2.3}$$

and the instantaneous phase $\phi(t)$ is the angle between the transform and the positive real axis (Eq.2.7):

$$\phi(t) = \arctan \frac{Q[x(t)]}{x(t)}. \tag{2.4}$$

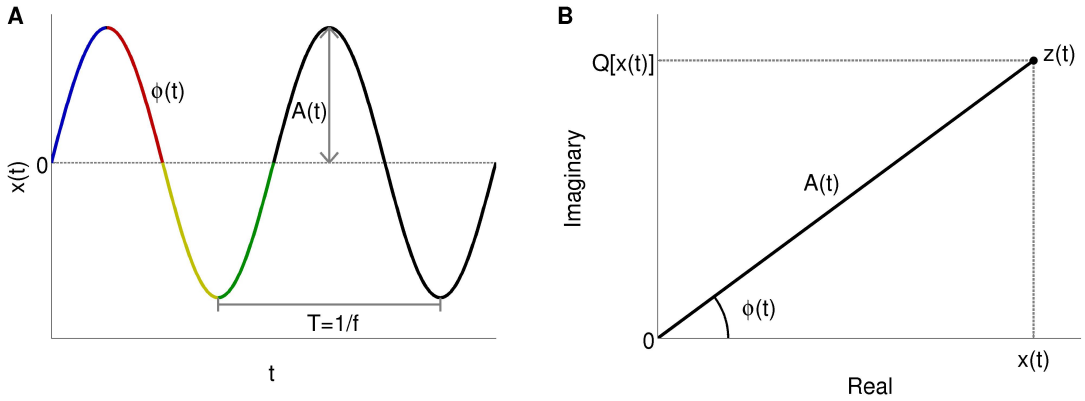

Figure 2.3: (A) Diagram of a sinusoidal signal $x(t)$ plotted against time t showing the phase $\phi(t)$, amplitude $A(t)$ and period T. (B) The analytic signal $z(t)$ for an example time point of signal $x(t)$ is plotted on the complex plane to illustrate how the real $x(t)$ and imaginary part $Q[x(t)]$ are related to the instantaneous phase $\phi(t)$ and instantaneous amplitude $A(t)$.

The imaginary part of $z(t)$ can be computed as the Hilbert transform ($Q[x(t)] = H[x(t)]$) of $x(t)$ using the implementation for the discrete-time series by Marple (1999). The Hilbert transform (Eq.2.5) computes the imaginary part $H[x(t)]$ of the analytic signal of a continuous signal $x(t)$ according to:

$$H[x(t)] = \frac{1}{\pi} \mathrm{p.v.} \int_{-\infty}^{\infty} \frac{x(t)}{t-\tau} d\tau \tag{2.5}$$

(Papoulis, 1977) where p.v. indicates that the integral over infinity is computed via the Cauchy principal value (Cauchy, 1826). This calculation can be easily done using the

Fourier transform so that:

$$Z(f)=\begin{cases}2X(f) & f>0\\ X(0) & f=0\\ 0 & f<0\end{cases} \tag{2.6}$$

where $X(f)=F[x(t)]$ is the continuous-time Fourier transform of signal $x(t)$ over the interval $-\infty<f<\infty$. For band-filtered LFP, which are N-point discrete signals $x[n]$, where $0\leq n\leq N-1$, the discrete-time analytic-like signal $z[n]$ was obtained by:

$$Z[m]=\begin{cases}X[0] & m=0\\ 2X[m] & 1\leq m\leq \frac{N}{2}-1\\ X(\frac{N}{2}) & m=\frac{N}{2}\\ 0 & \frac{N}{2}+1\leq m\leq N-1\end{cases} \tag{2.7}$$

where $X[m]$ is the N-point discrete-time Fourier transform (DTFT) of signal $x[n]$, and then calculating the inverse DTFT of $Z[m]$ (Marple, 1999). This method both preserves the original time series as the real part of the analytic signal:

$$\mathrm{Re}(z[n])=x[n] \tag{2.8}$$

and ensures the real and imaginary parts are orthogonal:

$$\sum_{n=0}^{N-1}\mathrm{Re}(z[n])\mathrm{Im}(z[n])=0 \tag{2.9}$$

(Marple, 1999). Thus, in all analyses presented in this thesis, amplitude and phase were extracted as the absolute and angle, respectively, of the Hilbert transform $z[n]$ of the band-filtered LFP $x[n]$ (Fig. 2.4).

For some of the analyses, the slope of band-filtered LFP signals was also extracted. Slope $s[n]$ was defined as the instantaneous gradient of the LFP signal $x[n]$. This was computed as the difference between two consecutive LFP points divided by the time difference h of those points according to Eq. 2.10:

$$s[n+\frac{1}{2}]=\frac{x[n+1]-x[n]}{h} \tag{2.10}$$

where $0\leq n\leq N-1$. Feature extraction from band-filtered LFP is summarised in Fig. 2.4.

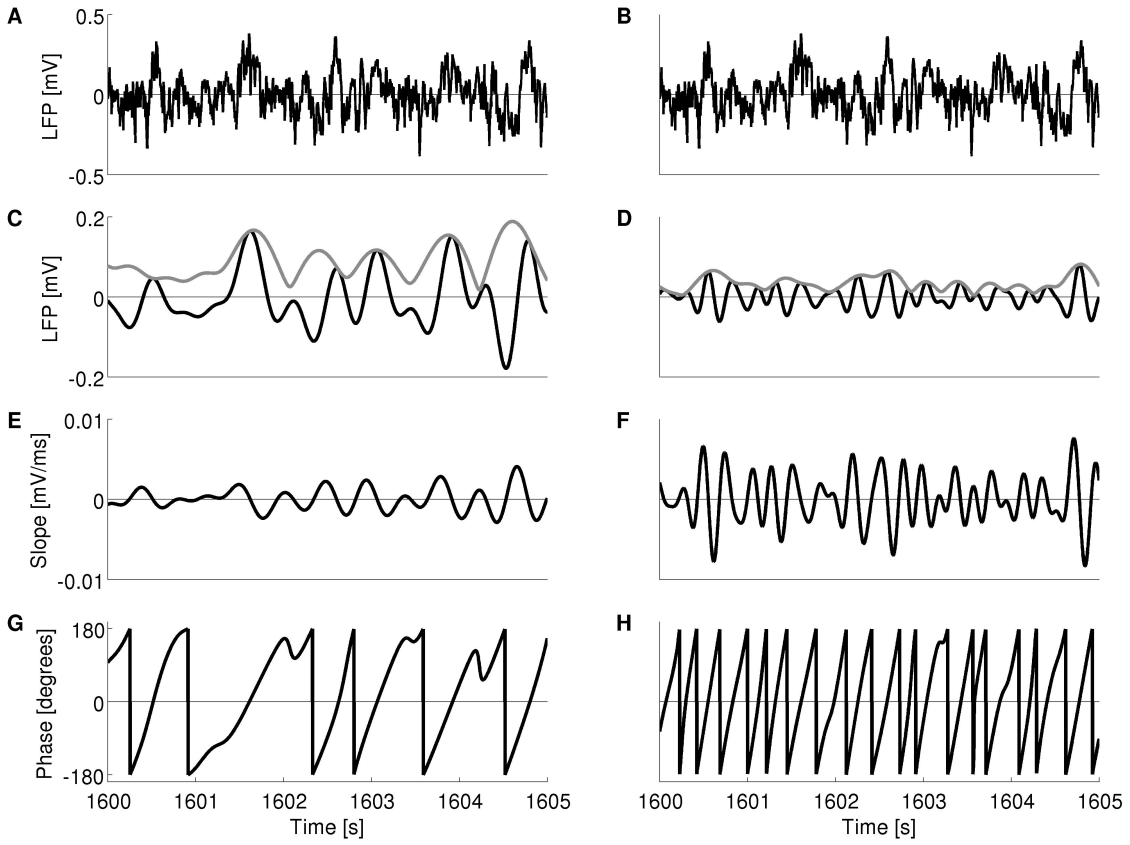

Figure 2.4: A and B: Example segment of raw LFP signal recorded from the subiculum of an anaesthetised rat. C-H: The investigated features of the delta-filtered (C, E and G) and theta-filtered LFP (D, F and H) were the instantaneous voltage (C and D, black lines), the instantaneous amplitude which is the envelope of the signals (C and D, grey lines), the instantaneous slope (E and F) and the instantaneous phase (G and H).

2.4 Spectral analysis

LFP are broadband signals, that is they are composed of a mixture of frequencies. To examine the spectral content of LFP, power spectra and spectrograms were used. These methods along with their advantages and limitations are explained in this section.

2.4.1 Power spectrum

In order to quantify the power of oscillations contained in the LFP recordings, power spectra were computed. There are a number of possible methods for constructing power spectra and some common ones, based on the Fourier decomposition of the signal, are compared here.

LFP are time series data, that is they take some value at each equally-sampled time point. The Fourier transform converts the signal from the time domain to the frequency domain, where it decomposes the signal into sinusoidal components and returns the phase and amplitude of each sinusoidal component (Bremaud, 2002).

The simplest way to construct a power spectrum is the periodogram, which computes the squared modulus of the discrete Fourier transform of the signal (Proakis and Manolakis, 1996). More specifically, the periodogram gives an estimate of the power spectral density of the signal. However, computing the Fourier transform of finite-length signals for which the number of periods is not an integer can result in spectral leakage, that is the creation of artifact frequency components not present in the signal. In order to avoid spectral leakage, a modified periodogram can be computed by first multiplying the signal by a window function to taper the signal and then obtaining the periodogram of this tapered signal (Proakis and Manolakis, 1996). The Hamming window, which is non-negative and decreases to near zero, can be used to reduce the leakage in periodograms (Proakis and Manolakis, 1996). An example periodogram of LFP constructed with the Hamming window is shown in Fig. 2.5A.

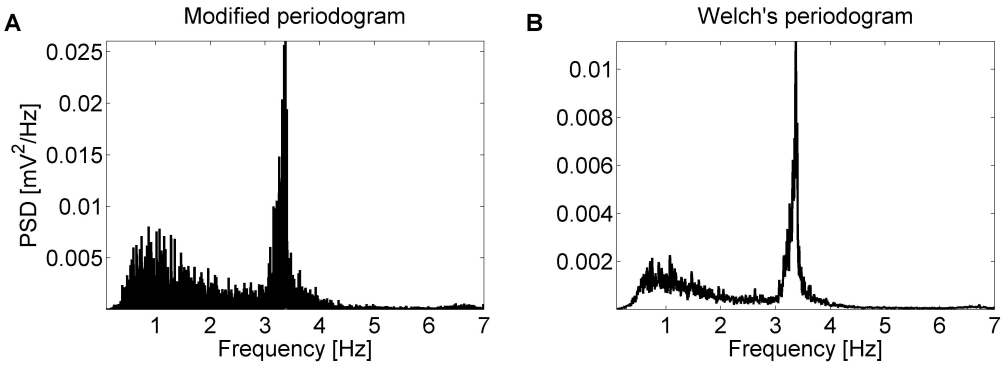

Figure 2.5: Example modified periodogram (A) and Welch's periodogram (B) of LFP recorded from hippocampal area CA1 of an anaesthetised mouse. Both power spectra plotted using Hamming windows. B: For the Welch's periodogram, the windows had length of 180 s and 50% overlap.

As can be seen in Fig. 2.5A, the modified periodogram is very noisy. This is because random variances in the experimental LFP recordings, which are noisy and finite, are reinforced by the squaring in the estimation of the power rather than eliminated. The Welch's method (Welch, 1967) can be used to reduce this noise. The Welch's method divides the signal in a number of overlapping epochs of equal length, computes the modified periodogram of each epoch and averages the periodograms over all epochs. An example Welch's periodogram constructed with overlapping Hamming windows is shown on Fig. 2.5B.

The advantage of the periodogram is that it produces a very sharp peak at frequencies with high power. On the other hand, averaging may result in wider peaks in periodograms constructed with the Welch's method. In our analyses, both the modified periodogram and Welch's periodogram (with the chosen window size) showed the same spectral peaks for the LFP recordings (examples in Fig. 2.5). The Welch's method greatly reduced the noise and thus was used for spectral analysis in all papers in this thesis.

2.4.2 Spectrogram

Periodograms show the spectral composition of LFP but cannot reveal whether and how this composition changes over time. Since LFP are dynamic and LFP rhythms are associated with different network states, visualising transitions in LFP composition is essential to understand the role of different rhythms. To determine how LFP composition changed over time, spectrograms were computed. The spectrogram calculates the squared modulus of the discrete Fourier transform over moving time windows along the signal (Prandoni and Vetterli, 2008).

The time and frequency resolutions of the spectrogram depend on the window size L. Time resolution is equal to the window size $\Delta t = L$ and frequency resolution is proportional to the window size ($\Delta f = 2\pi/L$) so that the area of each time-frequency tile in the spectrogram is $\Delta t \Delta f = 2\pi$ (with discrete time and normalised frequency) (Prandoni and Vetterli, 2008). A long window gives higher frequency resolution but less time precision; whereas a short window gives high time precision but poorer frequency resolution. Therefore, a tradeoff between the two is needed for choosing an optimal window size that will allow identifying separate rhythms that are close by and at the same time locate transitions between rhythms with reasonable time precision.

For the requirements of our analyses, a window size of 2 seconds was chosen so that transitions in LFP rhythms could be identified with a 2-second precision and frequency bands could be separated with resolution of 0.5 Hz. This was sufficient to distinguish transitions between delta and theta rhythms which were the two bands present in LFP signals of at least 30-minute length recorded from anaesthetised rodents. Doubling or halving this window size did not qualitatively change any of the results.

2.5 Information theory

Information theory is a mathematical framework originally devised by Shannon (1948) to quantify the amount of information that can be transmitted by general communica-

tion channels. Its origins date back to attempts to understand information transmission through transatlantic telegraphic cables pioneered by Nyquist (1924, 1928) and Hartley (1928). Shannon recasted the problem of communication into the already established paradigm of statistical physics and defined an entropy measure of information that has become the pivotal quantity from which all other quantities within the mathematical theory of information are constructed (Shannon, 1948). Since then, information theory has found ubiquitous applications in almost all areas of science and engineering where there are entities that exchange information. These applications extend to disciplines including computer science, cryptology, linguistics, economics and biology.

Shortly after its development, the concept of information was applied in neuroscience by the landmark work of MacKay and McCullock (1952) where, for the first time, the capacity of alternative neural codes was quantified. In the last few decades, information theory has been an instrumental tool to quantify the amount of information that can be conveyed by neural codes and to quantitatively compare their capacity in encoding neural messages (examples include De Ruyter Van Steveninck et al. (1997); Strong et al. (1998); Montemurro et al. (2007a, 2008); Kayser et al. (2009)).

In this thesis, information theory was used in Paper 2 to investigate possible neural codes by which bursting neurons can convey information about LFP. Here, I explain the basic concepts of information theory and the properties that make it a useful tool for addressing the requirements of the analysis in Paper 2. The exact details of how information theory was used to analyse the data is described in the Methods section of Paper 2.

2.5.1 Shannon entropy

A discrete signal or variable at any given time point can take one of a number of possible values each having a certain probability. As the number of possible equiprobable values increases, the uncertainty about which value occurs at that point also increases. For example, the outcome of throwing a fair 8-sided die is more uncertain than that of a 6-sided die. Similarly, which letter can occur in a text at random is more uncertain when the text is written by a 26-letter than a 4-letter alphabet –assuming each letter has equal probability to occur. Even if a message consists of one letter only, a 26-letter alphabet could encode more messages than a 4-letter one. Hence, a variable with higher uncertainty can encode more messages.

The uncertainty of a variable having a value x, which occurs with probability $p(x)$, is

quantified as:

$$h(x) = \log_2 \frac{1}{p(x)} \tag{2.11}$$

(Shannon, 1948; MacKay, 2003). This measure is the amount of information that value x can contain. The information contained in a set of variables can be defined as the average uncertainty of the variables weighted by their probability of occurrence. This information can be quantified by computing the entropy of the probability distribution of the set of variables (Shannon, 1948). A set of discrete random variables X with M possible values x, each occurring with a probability $p(x)$, has entropy:

$$H(X) = -\sum_{x \in X} p(x) \log_2 p(x). \tag{2.12}$$

The entropy can take values $0 \leq H(X) \leq \log M$ with $H(X) = 0$ if and only if X contains one value x with $p(x) = 1$ and all other values have $p(x) = 0$. The maximum value of entropy $H(X) = \log M$ is achieved when all M values x occur at equal probability $p(x) = \frac{1}{M}$ (Shannon, 1948). The units of entropy and information depend on the logarithm base. When the logarithm base is 2, the entropy and information have units of bits (Shannon, 1948).

A simple application of Eq. 2.12 is calculating the entropy of a 4-symbol code where $X = \{1,2,3,4\}$. If each symbol x occurs with equal probability $p(x) = \frac{1}{4}$, the entropy of variable X is:

$$H(X) = -\sum_{x=1}^{4} \frac{1}{4} \log_2 \frac{1}{4} = 2 \text{ bits/symbol.} \tag{2.13}$$

This means that the code has an average uncertainty of 2 bits/symbol so that, on average, a symbol can encode $2^{H(X)} = 2^2 = 4$ messages. This coincides with the uncertainty of each symbol calculated with Eq. 2.11: $h(1) = h(2) = h(3) = h(4) = -\log_2 \frac{1}{4} = 2$ bits, which means observing any symbol can discriminate between 4 messages.

If some symbols are more common than others in the code so that $p(x = 1) = \frac{1}{8}$, $p(x = 2) = \frac{3}{8}$, $p(x = 3) = \frac{1}{16}$ and $p(x = 4) = \frac{7}{16}$, the entropy of X is:

$$H(X) = -(\frac{1}{8} \log_2 \frac{1}{8} + \frac{3}{8} \log_2 \frac{3}{8} + \frac{1}{16} \log_2 \frac{1}{16} + \frac{7}{16} \log_2 \frac{7}{16}) = 1.68 \text{ bits/symbol,} \tag{2.14}$$

and the uncertainty of each symbol is $h(1) = 3$ bits, $h(2) = 1.4$ bits, $h(3) = 4$ bits, $h(4) = 1.2$ bits. The second example illustrates that although rare symbols can convey more information than frequenctly-occurring symbols, the average uncertainty of 1.68 bits/symbol means that the code can convey an average of $2^{1.68} = 3.2$ messages per symbol, which is less than the previous code where all symbols were equally probable.

2.5.2 Joint entropy

Entropy can be extended to more than one variables to quantify the uncertainty when these variables co-occur in a measure referred to as joint entropy. For two sets of discrete random variables X and Y with possible values x and y, each occurring with probability $p(x)$ and $p(y)$, respectively, and probability of co-occurring $p(x,y)$, the joint entropy is defined as:

$$H(X,Y) = -\sum_{\substack{x\in X \\ y\in Y}} p(x,y)\log_2 p(x,y) \tag{2.15}$$

(Shannon, 1948). The joint entropy can take values $H(X,Y) \leq H(X)+H(Y)$ with $H(X,Y) = H(X)+H(Y)$ if and only if the two variables are independent, that is when $p(x,y) = p(x)p(y)$ (Shannon, 1948).

2.5.3 Conditional entropy

In some cases, knowing one variable Y can influence the uncertainty about another variable X. The conditional probability of X having a particular value x given Y has a value y is:

$$p(x|y) = \frac{p(x,y)}{\sum_{x\in X} p(x,y)}. \tag{2.16}$$

The uncertainty of X conditional to knowledge of Y can be quantified as the conditional entropy computed by:

$$H(X|Y) = -\sum_{\substack{x\in X \\ y\in Y}} p(x,y)\log_2 p(x|y) = -\sum_{y\in Y} p(y)\sum_{x\in X} p(x|y)\log_2 p(x|y). \tag{2.17}$$

This estimates the average entropy of x for each possible y weighted by the probability of observing that y value (Shannon, 1948). The uncertainty of variable X can either decrease by knowing variable Y if X depends on Y ($H(X|Y) < H(X)$) or stay the same if X and Y are independent ($H(X|Y) = H(X)$) (Shannon, 1948).

Conditional entropy relates to joint entropy by the chain rule:

$$H(X|Y) = H(X,Y) - H(Y). \tag{2.18}$$

The chain rule can also be extended to more than two variables. For instance, for three variables:

$$H(X,Y,Z) = H(X|Y,Z) + H(Y,Z) = H(X|Y,Z) + H(Y|Z) + H(Z) \tag{2.19}$$

(Cover and Thomas, 2006).

2.5.4 Mutual information

How accurately can one predict the value of X by knowing Y? Variable X has an uncertainty equal to entropy $H(X)$. Knowing another variable Y can reduce the uncertainty of X by an amount equal to the conditional entropy $H(X|Y)$. This reduction in uncertainty is the amount of information about X that can be obtained by observing Y. This quantity is referred to as mutual information, or simply information, and is defined by:

$$I(X;Y) = H(X) - H(X|Y) \tag{2.20}$$

(Shannon, 1948; Cover and Thomas, 2006). From the chain rule (Eq. 2.18), Eq. 2.20 can also be written as:

$$I(X;Y) = H(X) + H(Y) - H(X,Y). \tag{2.21}$$

Mutual information captures the dependence between the random variables X and Y and is a symmetric measure because I(X;Y)=I(Y;X). Mutual information can be lower or equal to the entropies of X and Y, that is $I(X;Y) \leq H(X)$ and $I(X;Y) \leq H(Y)$; and can have values $I(X;Y) \geq 0$, where I(X;Y)=0 if the two variables are independent from each other. The greater the value of mutual information, the greater the reduction in uncertainty obtained about one variable by knowing the other variable (Cover and Thomas, 2006).

2.5.5 Application of information theory in neural coding

Mutual information is a non-linear, non-parametric measure since it is computed from the probabilities of observing the possible neural signals in a dataset and, consequently, makes no assumptions about the probability distributions of the data. This is particularly important when analysing neural responses because the distributions of neural signals can vary (Penttonen and Buzsaki, 2003; Buzsaki and Mizuseki, 2014). Moreover, this is a major advantage as compared to other methods, such as correlation and coherence, usually used in the analysis of electrophysiological data (reviewed in Pereda et al. (2005)). Thus, information theory is a valuable tool when studying the neural code (reviewed in Quian Quiroga and Panzeri (2009)).

Information theory has first been applied in the context of stimulus-response experiments, where a stimulus is presented over multiple trials and the spike train responses

are analysed to quantify how much information the neural response can convey about the stimulus (reviewed in Borst and Theunissen (1999)). The implementation of the method for this type of datasets usually makes use of time bins to discretise the spike trains in order to estimate the probabilities to be plugged in the equations for computing the mutual information (De Ruyter Van Steveninck et al., 1997; Strong et al., 1998). In a different setting in which an animal freely moves in space, Skaggs et al. (1993) proposed an alternative implementation of information theory for analysing spike trains by binning the stimulus (location of animal) and considering the firing rate (of spatial neuron) corresponding to each stimulus bin. In the latter, the stimulus can be replaced by any continuous quantity, not only space. We used an adaptation of the latter implementation in Paper 2 to compute information from the firing of bursting neurons in respect to LFP signals (as described in the Methods section of the Paper 2).

Adjusting the underlying representation of the signal, that is changing the definition of signals X and Y in the computation of mutual information, allows the study of different aspects of the signal that might encode information. This has been extensively utilised in the field of neural coding. For example, Montemurro et al. (2008) defined the neural response as either the number of spikes in a time window or the LFP phase at which spikes were fired in order to compare the encoding capacity of spike count and phase-of-firing codes, respectively. Subsequently, Kayser et al. (2009) extended this by defining neural responses from the same recordings in eight different ways: spike count, temporal pattern of spikes, pooled response from a small number of neurons with or without keeping track of individual neuron activity, and labelling each of the four responses with the LFP phase. The use of information theory showed that combinations of these codes have greater encoding capacity than individual codes (Kayser et al., 2009).

The second aim of this project was to determine how bursting neurons can encode features of the LFP. To address this, we compared possible neural codes employed by bursting neurons. As explained in this section, information theory was the optimal method for this purpose. The details of the neural codes studied and the way information theory was implemented are outlined in the Methods section of Paper 2.

2.6 Transfer entropy

The third aim of this project was to determine how interactions in LFPs can exchange information between hippocampal area CA1 and the subiculum. Information exchange need not be bidirectional, that is information might flow in one direction but not the other direction. As mentioned in section 2.5.4, mutual information is a symmetric

measure and thus cannot reveal the direction of information flow from one variable (or signal) to the other. Therefore, mutual information was not an appropriate measure for this purpose. A more recently developed information theoretic method, called transfer entropy (Schreiber, 2000), overcomes this limitation while preserving all the advantages inherent in computing measures from the probability distributions of the recorded data, that is being model-free, non-parametric and non-linear.

To be able to capture the direction of information flow, the past of the signal should also be taken into account. This is because if one variable affects another, it will exert its effect with a time delay. This is the basis of the Wiener-Granger causality principle (Wiener, 1956; Granger, 1969). Transfer entropy follows this causality principle by incorporating a time delay in the calculation to reveal the direction of information transfer. Therefore, transfer entropy was the method of choice for the requirements of Papers 3. In this section, the Wiener-Granger causality principle and its interpretations are explained and then transfer entropy estimation is introduced. The details of how transfer entropy was used to analyse the data in Paper 3 are described in the Methods section of the paper.

2.6.1 Wiener-Granger causality principle

The concept of causality between two signals was first introduced by Wiener (1956) and, subsequently, formulated mathematically by Granger (1969). According to the definition of causality, if the future of a signal can be better predicted by looking at the past of a second signal than by only considering its own past, then the second signal can be causal to the first signal (Wiener, 1956; Granger, 1969). This causality principle is depicted diagrammatically in Fig. 2.6.

The Granger method uses bivariate autoregressive modelling of time series data to quantify the predictions between signals (Granger, 1969). An extension of this to the frequency domain with multivariate data has been provided by the partial directed coherence method (Sameshima and Baccala, 1999; Baccala and Sameshima, 2001). However, both of these methods are linear and also depend on the parameters used to fit the autoregressive model. In contrast, the transfer entropy method can capture non-linear interactions in the LFP and requires no model fitting (Schreiber, 2000). The way transfer entropy was applied in this project is outlined in the next section.

Methods based on the Wiener-Granger causality principle can imply causal interactions between signals, however, cannot distinguish whether there is an actual mechanism by which one signal physically causes the other or whether the captured ‘causality’

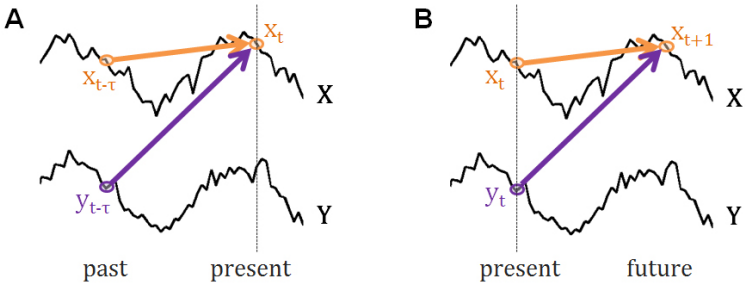

Figure 2.6: Wiener-Granger causality principle. A: Signal Y can be causing signal X if the present value x_t can be better predicted by knowing a past value $y_{t-\tau}$ than only knowing a past value $x_{t-\tau}$. The annotations are the same as the variables used in Besserve et al. (2010). B: Same schematic as in A but annotating signals X and Y with the variables used in the transfer entropy equations used to analyse the data for Paper 3. In this diagram, if knowing the present value y_t improves prediction about the future value $x_{t+\tau}$ compared to only knowing the present value x_t, then Y is thought to cause X.

is due to an indirect effect of interactions with other parts within the system. This is because these methods quantify by how much the past of one signal can predict the present value of another signal but this on its own does not exclude the possibility of other signals in the system causing both of the observed signals with a time delay. Thus, Wiener-Granger causality methods provide a measure of the predictability between two signals rather than a measure of actual causality.

2.6.2 Transfer entropy estimation

Assuming two discrete time series signals X and Y, the present values of the signals at time t are denoted by X_t and Y_t. The present values of the signals depend only on k past values and not on any value before the k^{th} value in the past, so that: $X_t^{(k)} = (X_{t-1}, ..., X_{t-k})$ and $Y_t^{(k)} = (Y_{t-1}, ..., Y_{t-k})$. For these signals, the transfer entropy $T(Y \rightarrow X)$ from signal Y to signal X is given by:

$$T(Y \rightarrow X) = H(X_t | X_t^{(k)}) - H(X_t | X_t^{(k)}, Y_t^{(k)}) \tag{2.22}$$

where $H(X_t|X_t^{(k)})$ is the entropy of the present values of X conditioned to its k past values; and $H(X_t|X_t^{(k)}, Y_t^{(k)})$ is the joint entropy of the k past values of signal Y and the present values of X conditioned to its k past values (Schreiber, 2000). In fact, this transfer entropy measure estimates the mutual information of the present of signal X and the past of signal Y conditioned to the past of signal X.

Transfer entropy can have values $T(Y \rightarrow X) \geq 0$, where $T(Y \rightarrow X) = 0$ if the present of signal X is independent to the past of Y. A positive transfer entropy value, $T(Y \rightarrow X) > 0$,

means that signal X can be predicted by the past values of signal Y.

To compute the transfer entropy $T(X \rightarrow Y)$ in the reverse direction, that is from signal X to signal Y:

$$T(X \rightarrow Y) = H(Y_t | Y_t^{(k)}) - H(Y_t | Y_t^{(k)}, X_t^{(k)}). \tag{2.23}$$

The conditioning to the past of the first signal makes the transfer entropy measure asymmetric and thus indicates the direction of information transfer. Hence, $T(Y \rightarrow X)$ and $T(X \rightarrow Y)$ need not be equal. If $T(Y \rightarrow X) = T(X \rightarrow Y)$, then equal information is transferred from X to Y and from Y to X, that is information flow is bidirectional. If $T(Y \rightarrow X) > T(X \rightarrow Y)$, then signal Y sends more information to signal X than it receives. Similarly, if $T(Y \rightarrow X) < T(X \rightarrow Y)$, then signal X sends more information to signal Y than it receives. If $T(Y \rightarrow X) = 0$ or $T(X \rightarrow Y) = 0$, then no information flows in the corresponding direction.

When implementing this method to analyse electrophysiological signals, the parameter k needs to be defined. Since the number of samples in the past that affect the present value of the signal is not known, a number of possible values for k should be investigated. A large enough value of k could theoretically capture all possible influences on the signals. However, increasing the value of k, would increase exponentially the sampling bias of the conditioned entropies computed from finite data (bias is explained in the next section), and thus an unrealistically large dataset would be required for accurate estimation of transfer entropy. In addition, as the value of k increases, the computational time of estimating transfer entropy increases exponentially making large values of k non-feasible for analysing large datasets. To compensate for these limitation, the parameter k can be set to 1 and a variable time lag τ can be introduced to span the past of the signals so that:

$$T(Y \rightarrow X) = H(X_t | X_{t-\tau}) - H(X_t | X_{t-\tau}, Y_{t-\tau}) \tag{2.24}$$

(Besserve et al., 2010). The time lag can be equal in both signals. Using this approach, a range of time lags can be investigated so as to determine how different points in the past of one signal affect the present value of another signal.

Similarly, t can be kept as the present time of the two signals (X_t and Y_t) but vary τ in the future of predicted signal $X_{t+\tau}$ so that:

$$T(Y \rightarrow X) = H(X_{t+\tau} | X_t) - H(X_{t+\tau} | X_t, Y_t). \tag{2.25}$$

This is illustrated in Fig. 2.6. In this case, the only change is in the interpretation, which

becomes: the present value of Y_t can predict the future value of $X_{t+\tau}$ if the transfer entropy has some positive value.

Computing transfer entropy from experimental data is easier using joint entropies rather than conditional entropies. From Eqs. 2.18 and 2.19, Eq. 2.25 can be written as:

$$T(Y \rightarrow X) = H(X_{t+\tau}, X_t) - H(X_t) - H(X_{t+\tau}, X_t, Y_t) + H(X_t, Y_t). \tag{2.26}$$

Transfer entropy $T(Y \rightarrow X)$ computed with the method described in this section has units of bits per time bin $dt = 5$ ms (bits/dt), where the bin size depends on the sampling rate ($F_s = 200$ Hz) of the LFP signals. Reporting information values in bits/dt would be arbitrary since, in principle, the dt could be of any length. To overcome this, the transfer entropy values were converted to bits/s by multiplying the values obtained from Eq. 6.1 (see section 2.7.3) by the sampling rate. The units of bits/s are a standardised way of reporting information rate and has been used before in other studies (for example Strong et al. (1998); Montemurro et al. (2007a, 2008)).

We implemented this method to achieve the third and fourth aims of this project in Paper 3. The exact details of how this method was used is described in the Methods section of the paper. In addition, a method was used to estimate biases arising from the limited sampling of electrophysiological data used to compute the transfer entropy, as well as mutual information. In the next section, the bias and methods to correct for it are discussed.

2.7 Bias correction

Despite the advantages of information theory, its application was initially limited due to the sampling bias in the information estimates. The development of a number of methods to correct for the bias in the last two decades (reviewed in Panzeri et al. (2007)) allowed for more accurate estimates of information measures and thus paved the way for the wider application of information theory in the field of neuroscience. In this section, the origin of bias and bias correction are explained. Subsequently, the methods used to correct for the bias in the estimates of mutual information in Paper 2 and transfer entropy in Paper 3 are presented.

2.7.1 Bias and methods of bias correction

The estimation of information theoretic measures, such as mutual information and transfer entropy, relies on computing the probabilities of neuronal responses from experimental or simulated data. In order to obtain the true information values, the true probabilities of the responses -calculated from an infinite sample- are required. The empirical probabilities estimated from finite data vary around their true values, that is they contain statistical errors. Consequently, computing information by directly 'plugging in' the empirical probabilities in Eqs. 2.21 or 2.26, results in systematic errors in the entropy and information values. These statistical and systematic errors give rise to the bias in the information estimates which is the discrepancy between the true and empirical information values computed from the true and empirical probabilities, respectively (Panzeri et al., 2007).

In the case of simulated data, one can repeat the simulations enough times to reach a close approximate of the true probabilities and obtain an asymptotic estimate of information. However, in the case of experimental data, there is a limit on the amount of data that can be obtained from a recording session. This limit is set by the limitations of experimental techniques, such as how many neurons can be recorded simultaneously from a set of electrodes, or the experimental setup, such as the realistic duration of recordings from the brain of an animal. Since these constrains are difficult to overcome, a number of bias-correction methods have been developed to improve the accuracy of information theoretic measures computed from finite datasets.

Some of the most widely used methods for estimating and correcting for the sampling bias include the Panzeri-Treves Bayesian estimation (Treves and Panzeri, 1995; Panzeri and Treves, 1996), quadratic extrapolation (Strong et al., 1998), Nemenman entropy estimation (Nemenman et al., 2004), best universal bound (Paninski, 2003) and shuffling (Montemurro et al., 2007c). These methods have been originally developed for correcting the bias in the estimates of mutual information from stimulus-response datasets where the responses are usually spike trains. More recently, bias correction methods have been extended to continuous data such as LFP and EEG (Magri et al., 2009) and can also be applied to correct for the bias in the estimates of transfer entropy (Besserve et al., 2010, 2015).

In this project, we estimated mutual information (Paper 2) and transfer entropy (Paper 3) with different types of data. In the first case, mutual information was computed between bursting neuron firing and ongoing LFP. In the second case, transfer entropy was computed between two LFP signals. In both cases, bootstrapping methods based

on Tovee et al. (1993); Montemurro et al. (2007c,b); Panzeri et al. (2007); Montemurro et al. (2008); Besserve et al. (2010) were used to estimate and correct for the bias in the information estimates. The details of the implementation of these methods is described in the next two sections.

2.7.2 Bias correction of mutual information estimates

Information theory was used in Paper 2 to compare three possible neural codes by which the responses of bursting neurons can encode LFP features. The data comprised simultaneous LFP recordings of at least 20-minute duration and spike trains fired by bursting neurons. The recordings were spontaneous, that is there was no stimulus to the animal or trials. Any information encoded about LFP by bursting neurons should thus depend on correlations between specific LFP feature values and some aspect of the neural activity, such as the burst rate or burst size.

To compute the mutual information between the neural responses and LFP features, the whole duration of the LFP recording was digitised in small time bins to construct a vector X of LFP feature values at each time bin; and the associated neural response for each time bin (with or without some time lag) was constructed in the vector Y of neural responses. As explained in the previous section, computing the mutual information by directly plugging in these data in Eq. 2.20 or 2.21 would result in sampling bias overestimating the information values.

In our dataset, the most prominent source of bias was the limited sampling of bursting neuron responses especially of larger bursts which were generally rare (as it becomes evident by observing the burst size distributions in Fig. 4.2). To overcome this problem, a shuffling procedure based on (Tovee et al., 1993; Montemurro et al., 2007c,b; Panzeri et al., 2007; Montemurro et al., 2008) was used to obtain an estimate of the bias. More specifically, the neural responses in vector Y were shuffled in respect to the LFP feature values in vector X in order to remove the correlations between them. This preserves the marginal probabilities of X and Y, while it eliminates the information that is conveyed by the correlations between X and Y. The shuffled mutual information was computed between Y and the shuffled X by:

$$I_s(X;Y) = H(X) + H(Y) - H_s(X,Y). \tag{2.27}$$

If there were no statistical or systematic errors in computing the entropies, the shuffled mutual information would have been zero. However, due to the sampling bias, the shuffled mutual information takes a positive value. This shuffling procedure was repeated

100 times for each time lag and the shuffled mutual information $I_s(X;Y)$ was computed for each repetition. The mean across these shuffled mutual information values was taken as the estimate of the bias. The bias-corrected mutual information $I_c(X;Y)$ was computed by subtracting the bias estimate from the 'plug-in' mutual information estimate $I(X;Y)$:

$$I_c(X;Y) = I(X;Y) - \langle I_s(X;Y) \rangle \tag{2.28}$$

where $\langle ... \rangle$ indicates mean across repetitions.

More details about the bias correction method and its performance are given in the Methods and Supplementary Methods of Paper 2.

2.7.3 Bias correction of transfer entropy estimates

Transfer entropy was used in Paper 3 to determine how interactions of LFP signals in distinct networks within the hippocampal formation can exchange information. To achieve this, pairs of LFP recordings of approximately 30-minute duration obtained simultaneously from hippocampal area CA1 and the subiculum were used to compute transfer entropy.

The LFP signals were digitised in time bins of length $\delta t = 5$ ms. The whole duration of the signals was used to obtain the probabilities for computing the transfer entropy. Hence, each transfer entropy estimate was obtained from approximately 3.6×10^5 data points. Although this dataset was finite, it was large enough to have small sampling bias (computed with a similar shuffling procedure as in section 2.7.2) compared to the transfer entropy estimates: the bias was less than 0.02 bits/s while transfer entropy ranged from approximately 1 to 60 bits/s. The shuffling method used to estimate the bias was similar to the one used in Besserve et al. (2010).

The pairs of X_t and $X_{t+\tau}$ were shuffled in respect to Y_t, while at each time point t, the pairs of X_t and $X_{t+\tau}$ were the same in respect to each other. This method eliminates the correlations between the future values of signal X and the present values of signal Y but preserves the correlations between present and future values of signal X. The shuffled entropies were computed from the shuffled data. Shuffled transfer entropy was computed from these shuffled entropies by:

$$T_s(Y \to X) = H_s(X_{t+\tau}, X_t) - H_s(X_t) - H_s(X_{t+\tau}, X_t, Y_t) + H_s(X_t, Y_t). \tag{2.29}$$

Bias was estimated by shuffling the data 100 times, calculating the shuffled transfer

entropy for each repetion with Eq. 2.29 and taking the mean of these shuffled transfer entropies. The bias-corrected transfer entropy was then computed by:

$$T_c(Y \rightarrow X) = T(Y \rightarrow X) - \langle T_s(Y \rightarrow X) \rangle \tag{2.30}$$

where $\langle ... \rangle$ indicates mean across repetitions. Since the present values X_t and the future values $X_{t+\tau}$ were the same in respect to each other for both the actual and shuffled data, $H_s(X_{t+\tau}, X_t) = H(X_{t+\tau}, X_t)$. Moreover, $H_s(X_t) = H(X_t)$ since X_t comprises the same values both when shuffled or not. Therefore, Eq. 2.30 simplifies to:

$$T_c(Y \rightarrow X) = H(X_t, Y_t) - H(X_{t+\tau}, X_t, Y_t) - \langle H_s(X_t, Y_t) - H_s(X_{t+\tau}, X_t, Y_t) \rangle. \tag{2.31}$$

Eq. 6.1 was used to compute transfer entropy in Paper 3.

Chapter 3

Paper 1

Phase-locking of bursting neuronal firing to dominant LFP frequency components

Maria Constantinou*, Daniel H. Elijah, Daniel Squirrell, John Gigg, Marcelo A. Montemurro

Faculty of Life Sciences, The University of Manchester, Manchester, M13 9PT, UK

**Corresponding author at: Faculty of Life Sciences, The University of Manchester, Oxford Road, Manchester M13 9PT, UK. E-mail address: maria.constantinou@manchester.ac.uk (M. Constantinou).*

Keywords: Bursting, Local field potential, Phase-locking, Subiculum, Neural coding

3.1 Abstract

Neuronal firing in the hippocampal formation relative to the phase of local field potentials (LFP) has a key role in memory processing and spatial navigation. Firing can be in either tonic or burst mode. Although bursting neurons are common in the hippocampal formation, the characteristics of their locking to LFP phase are not completely understood. We investigated phase-locking properties of bursting neurons using simulations generated by a dual compartmental model of a pyramidal neuron adapted to match the bursting activity in the subiculum of a rat. The model was driven with stochastic input signals containing a power spectral profile consistent with physiologically relevant frequencies observed in LFP. The single spikes and spike bursts fired by the model were locked to a preferred phase of the predominant frequency band where there was a peak in the power of the driving signal. Moreover, the preferred phase of locking shifted with increasing burst size, providing evidence that LFP phase can be encoded by burst size. We also provide initial support of the model results by analysing example data of

spontaneous LFP and spiking activity recorded from the subiculum of a single urethane-anaesthetised rat. Subicular neurons fired single spikes, two-spike bursts and larger bursts that locked to a preferred phase of either dominant slow oscillations or theta rhythms within the LFP, according to the model prediction. Both power-modulated phase-locking and gradual shift in the preferred phase of locking as a function of burst size suggest that neurons can use bursts to encode timing information contained in LFP phase into a spike-count code.

3.2 Introduction

Local field potentials (LFP) are fluctuating extracellular electrical signals that result from the sum of currents across all excitable membranes within a local volume (Logothetis, 2003; Buzsaki et al., 2012). A major contributor to the LFP is the combined synaptic activity of neuronal populations (Einevoll et al., 2007; Pettersen et al., 2008). Neuronal firing relative to the phase of ongoing LFP oscillations in the hippocampal formation has been linked with spatial navigation (O'Keefe and Recce, 1993; Skaggs et al., 1996) and memory processing (Lisman and Idiart, 1995). Moreover, evidence from the monkey sensory cortices suggests that more information about stimuli can be transmitted if the LFP phase at which spikes are fired is taken into account (Montemurro et al., 2008; Kayser et al., 2009). The phase of LFP oscillations has been proposed to be involved in keeping timing information for neural communication (Fell and Axmacher, 2011). Thus, locking of neuronal firing during a preferred phase range can be a mechanism of transmitting information for cognitive processing. Although pyramidal neurons in the hippocampal formation are known to lock their firing to LFP phase, the conditions of this phase-locking are not completely understood.

Two factors that may affect the locking properties of pyramidal neurons are the frequency composition of the LFP and the dynamics of individual neurons. The former is relevant to the hippocampal formation since this area is characterised by well-defined oscillatory states that correlate with cognitive function. Regarding neuronal dynamics, pyramidal neurons can fire in either tonic or bursting modes. The existence of bursting neurons in the hippocampal formation has been long documented (Ranck, 1973). Bursting activity is an important mechanism for neural communication because bursts consisting of different spike counts can provide more basic symbols in the neural code (Kepecs and Lisman, 2003; Samengo et al., 2013). Modelling studies have provided some evidence that bursting pyramidal neurons can lock to different phases of the LFP depending on the burst spike-count (Samengo and Montemurro, 2010), but this has not been tested in specific models based on experimental data. We address this by studying

phase-locking of bursting activity in the subiculum which is known to contain intrinsically bursting neurons (Sharp and Green, 1994; Gigg et al., 2000). The subiculum is the major output structure of the hippocampus (for reviews on the subiculum see O'Mara et al. (2001); Gigg (2006)). Similarly to the hippocampus, neurons in the subiculum encode spatial information (Kim et al., 2012) as for example the boundary vector cells which are neurons that fire when a rat encounters boundaries in space (Lever et al., 2009).

We used a neuron model and example *in-vivo* data from the subiculum of a single rat to investigate how bursting neuronal dynamics and LFP frequency components affect phase-locking. The model predicted that bursting neurons locked their firing to a preferred phase of dominant rhythms irrespective of the frequency of these rhythms and phase preference shifted with increasing spike count. We show that subicular bursting neurons locked their firing to a preferred phase of dominant slow oscillations or theta rhythms within the LFP and the preferred phase of locking to dominant slow oscillations changed depending on the spike count according to model predictions. These results suggest a mechanism of encoding timing information in burst spike-count.

3.3 Materials and Methods

3.3.1 Bursting neuron model

A two-compartment (dendrites and soma) conductance-based model of a bursting pyramidal neuron was used for all simulations (Fig. 4.2A). This model is a reduction of a 19-compartment (Traub et al., 1991) to a two-compartment model of a CA3 hippocampal neuron (Pinsky and Rinzel, 1994) which was simplified by Kepecs and Wang (2000) to include the minimal ionic conductances required to generate bursting. This model has been used to investigate the properties of bursting in response to different stimuli in previous studies (Kepecs et al., 2002; Kepecs and Lisman, 2003; Samengo and Montemurro, 2010). For the purpose of this study, the model was fitted to match its responses to realistic burst firing in the rat subiculum. To achieve this, we used the equations and parameters as described in Samengo and Montemurro (2010) and adjusted four parameters (g_K, g_{NaP}, g_{KS} and C_m) so that the probability of firing bursts of size n, where n is the number of spikes in a burst and $n = 1$ for single spikes, is similar to the firing probability of subicular neurons (Fig. 4.1B, C and 4.2C, E, G, I).

An input current $I(t)$ injected into the dendritic compartment produced bursting activ-

ity in the somatic compartment according to:

$$C_m \frac{dV_d}{dt} = -I_L - I_{KS} - I_{NaP} - g_c \frac{V_d - V_s}{1-p} + I(t) \tag{3.1}$$

$$C_m \frac{dV_s}{dt} = -I_L - I_K - I_{Na} - g_c \frac{V_s - V_d}{p} \tag{3.2}$$

The relative area between the two compartments was $p = 0.15$ and the coupling conductance was $g_c = 1$ mS/cm^2. The somatic compartment included a Na current: $I_{Na} = g_{Na} m_\infty^3 h(V_s - E_{Na})$, where $m_\infty = \alpha_m/(\alpha_m + \beta_m)$, $\alpha_m = -0.1(V_s+31)/(\exp(-0.1(V_s+31))-1)$, $\beta_m = 4\exp(-(V_s+56)/18)$, $\alpha_h = 0.07\exp(-(V_s+47)/20)$ and $\beta_h = 1/\exp(-0.1(V_s+17))+1)$; and a K current: $I_K = g_K n^4(V_s - E_K)$, where $\alpha_n = -0.01(V_s+34)/(\exp(-0.1(V_s+34))-1)$ and $\beta_n = 0.125\exp(-(V_s+44)/80)$. The dendritic compartment included a persistent Na current: $I_{NaP} = g_{NaP} r_\infty^3 (V_d - E_{Na})$, where $r_\infty = 1/(\exp(-(V_d+57.7)/7.7)+1)$; and a slow K current: $I_{KS} = g_{KS} q (V_d - E_K)$, where $q_\infty = 1/(\exp(-(V_d+35)/6.5)+1)$, $\tau_q = \tau_{q_0}/(\exp(-(V_d+55)/30)+\exp((V_d+55)/30))$ and $\tau_{q_0} = 200$. The leak currents were described by $I_L = g_L(V - E_L)$, where V is V_d or V_s. Each gating variable x followed the kinetics equation: $dx/dt = \phi_x(\alpha_x(1-x) - x\beta_x) = \phi_x(x_\infty - x)/\tau_x$. The maximum conductances (in mS/cm^2) were $g_{Na} = 45$, $g_K = 15$, $g_L = 0.18$, $g_{NaP} = 0.08$, $g_{KS} = 0.7$ and the reversal potentials (in mV) were $E_{Na} = 55$, $E_K = -90$, $E_L = -65$. Membrane capacitance was $C_m = 0.6\ \mu$F/cm^2. The temperature scaling factors were $\phi_h = \phi_n = 3.33$ and $\phi_q = 1$. The model was integrated with the 4^{th} order Runge-Kutta method with a time step of 0.01 ms.

3.3.2 Input to the model

LFP are broadband signals containing power spectral peaks within frequency bands which are usually associated with different behavioural states. The input to the model was a time-varying signal which simulated physiologically relevant rhythms present in LFP. To obtain this input, a signal containing one peak at a selected frequency in the power-frequency spectrum was added to a background coloured-noise signal. The background signal simulated low-power oscillations and temporal correlations present in LFP. To generate the background signal, a white-noise process was convolved with an exponential kernel and then high-pass filtered with a 3$^{\text{rd}}$ order Butterworth filter with a cut-off frequency of 1 Hz to remove low frequency components. To create the signal with a peak in power at a given frequency, a white-noise process was narrowband filtered with a Kaiser filter (width of band was 1 Hz) so that the signal contained only a sharp peak centred at either 1, 4, 8 or 12 Hz in the power-frequency spectrum. The

background coloured-noise and frequency peak signals were scaled to have a standard deviation of 0.02 and 0.03, respectively, and then added together. The resulting signal was scaled again to have mean $\mu = 0$ and standard deviation $\sigma = 1.2$ for the 1 Hz peak and $\sigma = 0.8$ for the remaining three peaks. This difference in standard deviations was required to reflect that slow oscillations have higher amplitude compared to higher frequency rhythms. Assuming that the LFP can be simulated by the sum of synaptic inputs to neurons (Mazzoni et al., 2008), the input was injected as current into the dendritic compartment of the model (Eq. 4.5).

3.3.3 *In vivo* electrophysiology

All experimental procedures were carried out in accordance with the Animals (Scientific Procedures) Act UK 1986. Ethical approval was provided by the University of Manchester Ethical Review Panel. *In vivo* electrophysiological recordings of LFP and spiking activity were obtained from an adult male Sprague Dawley rat (Charles River, UK: 332 g, group-housed in a pathogen-free environment with food and water available *ad libitum*, maintained on a 12-h light:dark cycle).

Initial anaesthesia was induced via i.p. injection of urethane (30% w/v in 0.9% saline, 1.5 g/kg) and top-up doses of urethane (between 0.1 and 0.15 ml) were administrated at approximately 30-minute intervals until areflexia was achieved. Body temperature was kept at 37°C using a homeothermic heating pad. The rat was head-fixed in a stereotaxic frame and a 2-mm diameter craniotomy was carried out according to the Paxinos and Watson (2007) rat brain atlas for the subiculum (Bregma: −8.0 mm, ML: 3.5 mm). The dura was excised and a 4×8 multi-electrode array (A4×8-5-50-200-413, NeuroNexusTech, USA) was inserted at a 30° compound angle from the vertical axis to match the main dendritic axis of the subiculum. The electrode array was composed of four shanks, each containing eight 413-μm^2 electrodes with 50 μm vertical and 200 μm horizontal spacing between electrodes/shanks, respectively. The array was attached to an electrode board and headstage (Plexon, USA) with fixed gain of 20× and an AC preamplifier providing a total gain of 2000× (Recorder64, Plexon, USA). The positions of the electrodes were verified from Nissl-stained brain sections (Fig. 4.12) by detecting small electrolytic lesions produced by applying a 30 μA current for 5 seconds (Townsend et al., 2002) at the end of the experiment.

Spontaneous LFP (2 kHz sampling rate, low-pass filtered up to 250 Hz) and spiking activity (40 kHz sampling rate, high-pass filtered above 300 Hz) were recorded simultaneously from the electrodes in subiculum for 1 h. Recordings were ground referenced to the stereotaxic frame. Spikes were detected online by manually setting a threshold for

each electrode and stored as discrete shapes (1.3 ms duration) for offline spike sorting.

3.3.4 Data analysis

3.3.4.1 Spike sorting

To identify spikes fired by individual neurons, the recordings of spike shapes were analysed using Offline Sorter V2.8.8 (Plexon Inc). Different spike shape parameters were clustered until units were distinguished from the 'noise' cluster and manually separated. The separation quality was assessed by visually inspecting the interspike interval (ISI) histogram for each unit to ensure there were no spikes within the 1 ms refractory period. Multiple detections of the same unit on adjacent electrodes were identified by plotting cross-correlograms of each unit versus every other unit and only the unit with the largest waveforms was kept for each duplicate.

3.3.4.2 Spectral analysis and data segmentation

Spectral analysis was done using the Welch's periodogram method with 50% overlapping Hamming windows of length 112.5 s or 450 s for the input signal to the model or LFP signals, respectively. The 1-h LFP signals contained two spectral peaks: at slow oscillations and theta rhythms (Fig. 4.1A). To segment the LFP signals into epochs containing only one dominant rhythm, the power distribution over the frequency ranges 0.5–2.5 Hz for slow oscillations and 2.5–5.0 Hz for theta rhythms was estimated at every time point from the Fourier time-frequency decomposition over Hamming windows of 2.048 s with 50% overlap. The power over these frequency ranges was integrated to compute how much power as a percentage of the total was in each band. The dominant rhythm at a given time point was defined as the one which had at least 10% higher power than the other. That is, the fraction of total power within the dominant band was at least 0.1 greater than the fraction within any other frequency band. The 10% margin was sufficient to identify epochs of LFP with dominant rhythms in our data recorded under urethane anaesthesia as shown in the power spectra of the segmented data in Fig. 4.13.

3.3.4.3 Spike segregation into bursts

The spike times recorded for each unit were separated into two datasets depending on whether spikes were fired when slow oscillations or theta rhythms were dominant. Units were classified as bursting if in the ISI histograms and autocorrelograms of spike times there was a sharp peak within 2–8 ms and this peak was larger than any other

peak within 50 ms. To segregate spikes fired by subicular neurons into bursts, an ISI threshold of 8 ms was chosen because this time point was after the ISI histogram peak which indicated the time interval between spikes within bursts. A spike was considered as part of a burst if the spike occurred within 8 ms from the previous spike in the burst. If the interval between two spikes was greater than 8 ms, the spikes were considered as separate events. For segregating burst spikes fired by the model, as ISI threshold of 10 ms was used because the sharp peak in the ISI histograms and autocorrelograms occurred within 2–10 ms.

3.3.4.4 Filtering and phase extraction

Both the LFP recordings from the rat subiculum and the input signals to the model were downsampled to 500 Hz. Filtering was carried out with a finite impulse response (FIR) digital filter with Kaiser window (sharp transition bandwidth: 1.0 Hz, stopband attenuation: 60 dB, passband ripple: 0.01 dB). The signals were filtered in narrow bands of 1 Hz with 75% overlap, apart from the first band which ranged from 0.1 Hz to 1 Hz. The centres of the narrow bands were at 0.55 Hz, 0.75 Hz and then increased in steps of 0.25 Hz up to 10.25 Hz or 14.25 Hz. Phase was extracted as the argument of the Hilbert transform of the filtered signals. A phase value of 0° corresponded to the peak of an oscillation. For all phase analyses, we used the phase of the filtered signals at the time of spike or burst onset.

3.3.4.5 Phase-locking estimation

Phase-locking was estimated using histograms because this method captures both the strength of locking and the distribution of preferred phases. A waveform cycle from −180° to 180° was separated in either 125 bins of size 2.88° for the simulations or 25 bins of size 14.4° for the experimental data. The difference in the number of bins was because we used the model to simulate enough data to allow for finer binning than was allowed by the finite number of events fired by subicular neurons during the recording session. For the model, phase-locking histograms were constructed by calculating the probability of a spike or burst being fired within each phase bin of the narrowband-filtered input signal. For the experimental data, phase-locking of spikes and bursts was calculated relative to the LFP recorded at the same electrode where the spiking activity of the unit was recorded. Average phase-locking histograms were obtained by averaging the probabilities of firing spikes and bursts within each phase bin of the narrowband-filtered LFP across bursting units in epochs when slow oscillations or theta rhythms were dominant. To accommodate for differences in phase preference of individual units (examples in Fig. 4.14 and 3.8), the phase of 0° was set as the phase of mean maximal

locking of single spikes and phase-locking of spikes and bursts fired by each unit was calculated relative to that phase. Mean and standard deviation of the phase-locking distributions were calculated using the circular statistics toolbox for Matlab (Berens, 2009).

3.4 Results

We investigated bursting activity in relation to LFP using a computational approach. We first present the experimental data which were used to match the firing statistics of the neuron model. We then present results of extensive simulations of the model where we explored the locking properties of spikes and bursts of different spike count. Finally, we provide an example from subicular bursting neurons illustrating that the patterns predicted by the model are also present *in vivo*.

3.4.1 Bursting neurons in subiculum

In order to match the firing statistics of the neuron model to realistic burst firing in the subiculum, we analysed 1-h multi-electrode recordings of simultaneous LFP and spikes from the subiculum of a urethane-anaesthetised rat. The power spectrum of the LFP contained a wide peak around 1–2 Hz and a sharp peak at about 4 Hz (Fig. 4.1A). The first frequency peak is often referred to as slow oscillations or delta rhythms and the latter as theta rhythms. These two states under anaesthesia are analogous to non-REM and REM sleep, respectively (Clement et al., 2008). Since different frequency bands might correspond to different cognitive processes, we analysed epochs of dominant slow oscillations and theta rhythms separately. Out of a total of 26 units identified in the rat subiculum, we identified 13 bursting units firing at a rate of 1.96 ± 1.00 events/s in epochs when slow oscillations were dominant in the LFP. Eleven of these units were also bursting with a firing rate of 3.83 ± 2.68 events/s when theta rhythms were dominant. All bursting units fired single spikes and bursts comprising two or more spikes at a decreasing probability (Fig. 4.1B and C). Bursts consisting of three or more spikes were rare so were grouped together for the following analyses.

3.4.2 Bursting neuron model

To explore the phase-locking properties of bursting neurons, we adapted a dual compartmental model of a bursting pyramidal neuron (Fig. 4.2A). The model was driven with an input comprising time-varying stochastic signals with a peak in the power-

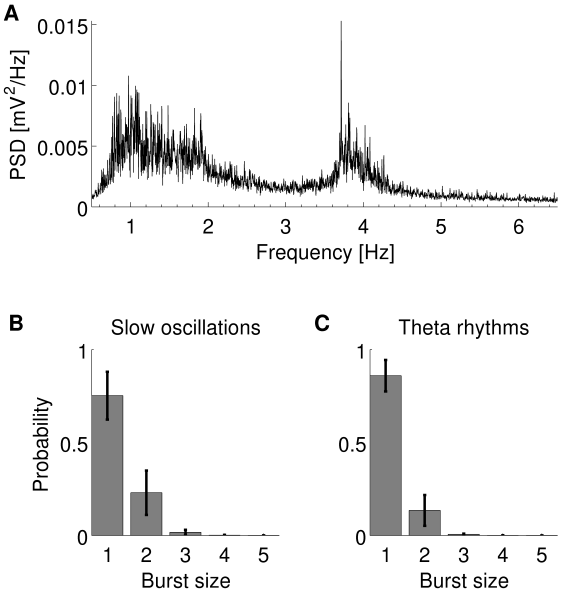

Figure 3.1: (A) Average power-frequency spectrum of LFP recordings in the rat subiculum under urethane anaesthesia. During the 1-h recording, there were two spectral peaks: a wide peak at 1–2 Hz and a sharper peak at about 4 Hz. (B and C) Average probability of a bursting neuron in the subiculum of a urethane-anaesthetised rat firing an *n*-spike burst when slow oscillations (B) or theta rhythms (C) were dominant in the LFP. The errorbars indicate standard deviation.

frequency spectrum in order to simulate similar frequencies occuring in LFP signals when there is only one dominant rhythm. The peaks were centred at 1 Hz (Fig. 4.2B), 4 Hz (Fig. 4.2D), 8 Hz (Fig. 4.2F) and 12 Hz (Fig. 4.2H). The peak at 1 Hz simulated dominant slow oscillations which are characteristic during sleep and anaesthesia. The peak at 4 Hz and 8 Hz simulated dominant low and high theta rhythms, respectively. Low theta rhythms are observed under urethane-anaesthesia and high theta rhythms are prevalent during awake exploratory behaviour. The peak at 12 Hz corresponded to dominant alpha rhythms which are higher than the frequencies usually found to be dominant in the LFP recorded from the rat hippocampal formation *in vivo*. The model fired *n*-spike bursts (Fig. 4.2C, E, G and I) in response to these four input signals with similar positively skewed probability distributions as the bursting units in the rat subiculum (Fig. 4.1B and C).

3.4.3 Spikes and bursts lock to phase of dominant rhythms

Is phase-locking of bursting neuronal firing to LFP rhythms an intrinsic property of bursting neurons regardless of the frequency of these rhythms or is locking restricted to specific frequency bands irrespective of their power? To address this, we used the model to simulate bursting activity in response to broadband signals with spectral

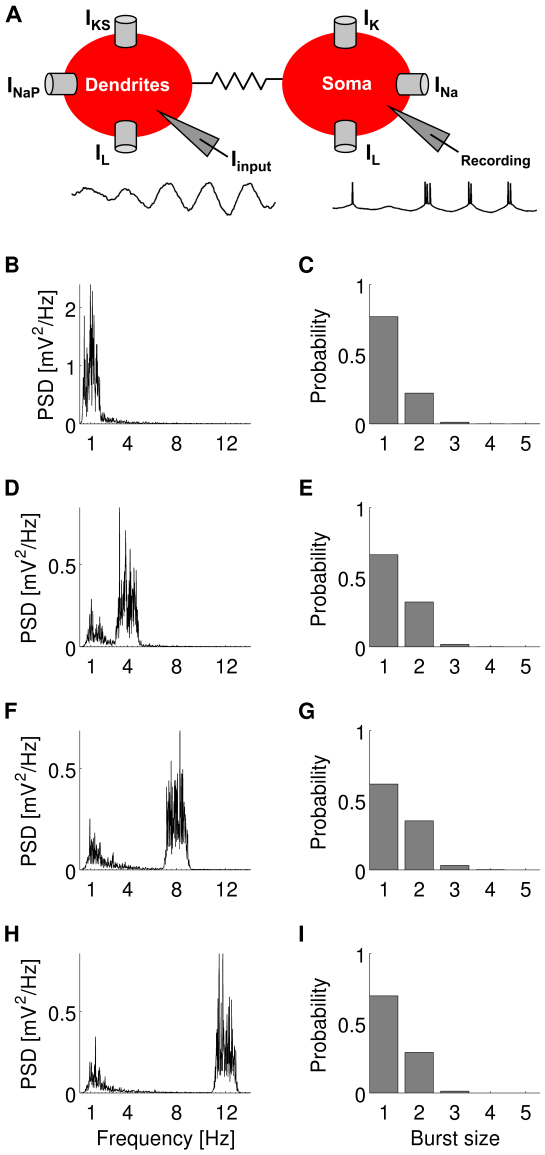

Figure 3.2: (A) Diagram of the two-compartment model of a bursting pyramidal neuron showing the ionic currents. The input signal I_{input} is injected in the dendritic compartment and bursting activity is recorded from the somatic compartment. (B, D, F and H) Power-frequency spectra of input signals to the model. The input signal consists of background coloured noise and a power spectral peak at either 1 Hz (B), 4 Hz (D), 8 Hz (F) or 12 Hz (H). (C, E, G and I) Probability of the model firing an n-spike burst when the input signal comprised the frequencies depicted in the plots at the left.

peaks at different frequencies resembling LFP containing only one dominant rhythm. If neuronal activity is phase-modulated by oscillations within specific frequencies, then neurons should fire with a high probability at a preferred phase of these oscillations. Instead, if neuronal activity is independent of the phase of a specific rhythm, then the firing probability should have a flat distribution relative to the phase of this rhythm. The single spikes ($n = 1$), two-spike bursts ($n = 2$) and larger bursts ($n \geq 3$) fired by

the model were locked to a preferred phase of the dominant rhythm within the input signal (Fig. 3.3). In addition, there was weaker phase-locking of spikes and bursts to the background frequency rhythms present within the input signal (shown as light blue colour in Fig. 3.3). Notably, the probability of firing a spike or burst at a preferred phase of the dominant frequency band within the input signal was consistently greater than the probability of firing relative to the phase of other rhythms. In particular, the probability of firing an n-spike burst at the preferred phase of the dominant rhythm (red colours in Fig. 3.3) was approximately two to four times greater than the firing probability at a preferred phase of background rhythms (light blue colours in Fig. 3.3).

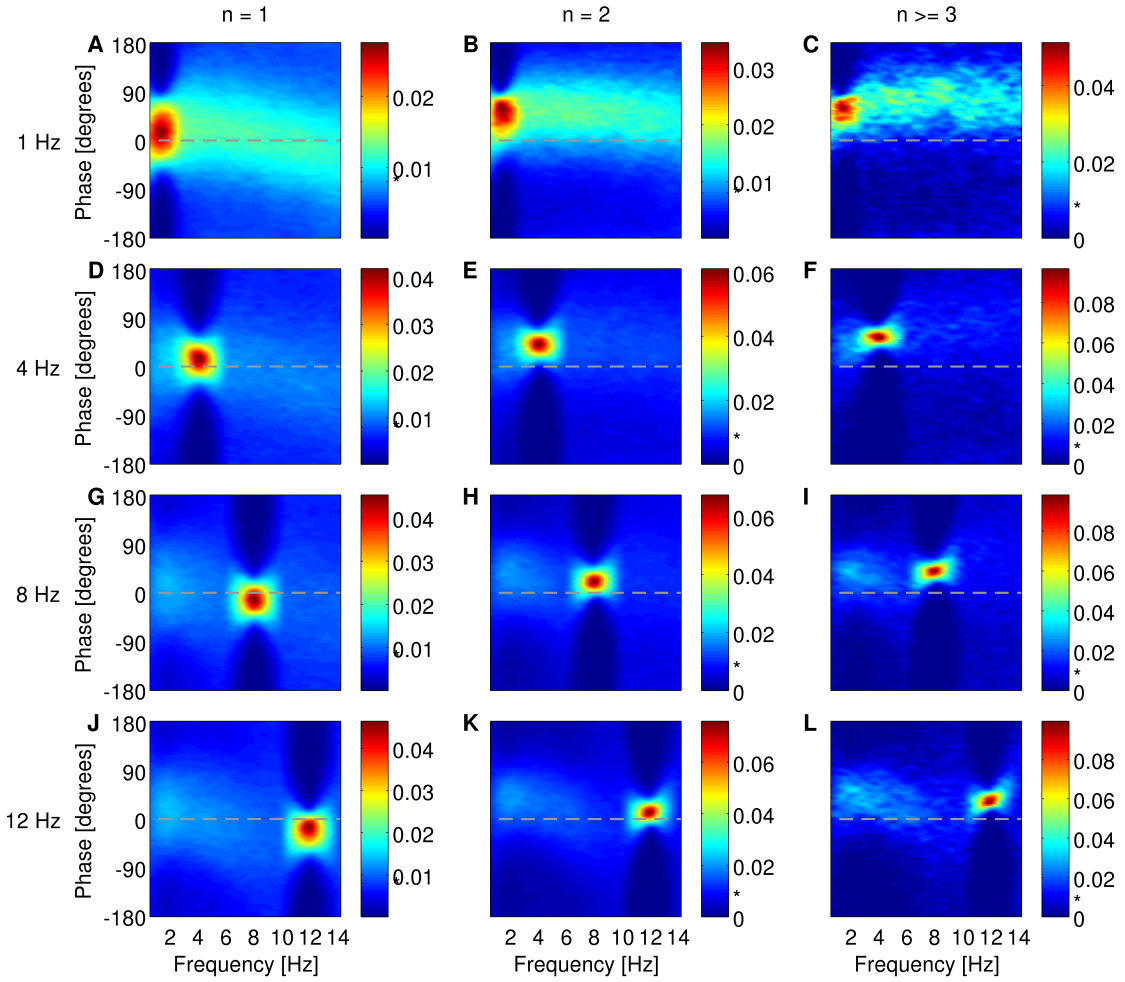

Figure 3.3: Phase-locking histograms of single spikes (A, D, G and J), two-spike bursts (B, E, H and K) and larger bursts (C, F, I and L) fired by the model when the input signal contained a frequency peak at 1 Hz (A–C), 4 Hz (D–F), 8 Hz (G–I) or 12 Hz (J–L). Phase of 0° corresponds to the peak of a waveform as calculated by the Hilbert transform. The colourbar shows the probability of locking to the phase of filtered signal at overlapping steps of 1 Hz. The asterisk (*) in the colourbar indicates chance probability which is equal to 1/125 or 0.008.

In all simulations, there was a shift in phase-locking as a function of burst size n. When the input signal contained a peak at 1 Hz, firing of single spikes relative to the dominant

slow oscillations was concentrated around a preferred phase of $13^\circ \pm 41^\circ$ (Fig. 3.3A). Phase-locking of two-spike bursts and larger bursts advanced by 20° and 30° (preferred phases of $33^\circ \pm 38^\circ$ and $43^\circ \pm 29^\circ$, Fig. 3.3B and C), respectively, relative to the preferred phase of single spikes. When rhythms of 4 Hz were dominant, locking of single spikes relative to low theta rhythms was around a preferred phase of $11^\circ \pm 30^\circ$ (Fig. 3.3D). Two-spike bursts were preferentially fired more advance in phase by 28° (preferred phase of $39^\circ \pm 20^\circ$, Fig. 3.3E) and larger bursts were an additional 15° more advanced (preferred phase of $54^\circ \pm 13^\circ$, Fig. 3.3F). When the input contained a peak at 8 Hz or 12 Hz, single spikes were locked at a preferred phase of $-14^\circ \pm 28^\circ$ of high theta rhythms (Fig. 3.3G) or $-25^\circ \pm 27^\circ$ of alpha rhythms (Fig. 3.3J), respectively. Locking of two-spike bursts was advanced by 36° and 39° (preferred phases of $22^\circ \pm 19^\circ$ and $14^\circ \pm 18^\circ$, Fig. 3.3H and K), respectively, relative to the preferred phase of single spikes. Locking of larger bursts was further advanced by 19° and 23° (preferred phases of $41^\circ \pm 13^\circ$ and $37^\circ \pm 14^\circ$, Fig. 3.3I and L), respectively, relative to the preferred phase of two-spike bursts.

3.4.4 Bursting neuronal firing is phase-locked to dominant LFP rhythms

We tested the model predictions by studying how bursting neurons in the rat subiculum fire spikes and bursts in relation to the phase of LFP recorded at the same electrode where bursting activity was recorded. Figs. 4.14, 3.8 and 3.4 show the probability of firing single spikes ($n = 1$), two-spike bursts ($n = 2$) and larger bursts ($n \geq 3$) at each phase of narrowband filtered LFP. Spikes and bursts were fired at a preferred phase of the dominant rhythm within the LFP signal. This preferred phase varied between individual units as illustrated in the examples in Figs. 4.14 and 3.8. The preferred phase of firing single spikes was set to 0° (Fig. 3.4A and D) and the average phase-locking probabilities of n-spike bursts are presented relative to that phase (Fig. 3.4B–C and 3.4E–F, respectively). When slow oscillations were the dominant rhythms in the LFP, the probability of firing an n-spike burst at the preferred phase of slow oscillations was 20–80% greater than the chance probability (Fig. 3.4A–C). Similarly, when theta rhythms were dominant, the probability of firing an n-spike burst at the preferred phase of theta rhythms was 20–80% greater than the chance probability (Fig. 3.4D–F). There was also some phase preference at frequencies outside the dominant band (yellow colours in Fig. 3.4) but this was substantially weaker than the phase preference at dominant frequencies (red colours in Fig. 3.4). Moreover, there was a shift in phase preference of bursts ($n = 2$ and $n \geq 3$) compared to single spikes ($n = 1$) when slow oscillations were dominant (Fig. 3.4A–C). This shift in phase preference was not observed when n-spike bursts were fired during theta-dominant epochs (Fig. 3.4D–F).

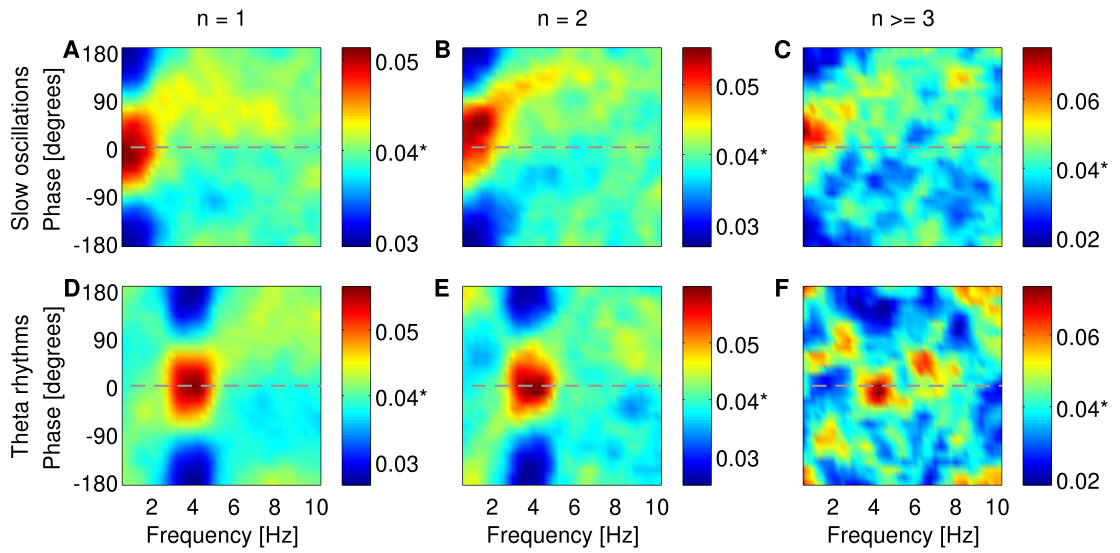

Figure 3.4: Phase-locking histograms of single spikes (A and D), two-spike bursts (B and E) and larger bursts (C and F) fired by subicular neurons. (A–C) Average across 13 units when slow oscillations were dominant in the LFP signals. (D–F) Average across 11 units when theta rhythms were dominant. The phase of maximal locking of single spikes ($n = 1$) was set to 0° and locking of bursts ($n = 2$ and $n \geq 3$) was plotted relative to that phase. The colourbar shows the probability of locking to the phase of filtered LFP at overlapping steps of 1 Hz. The asterisk (*) in the colourbar indicates chance probability which is equal to 1/25 or 0.04.

3.5 Discussion

We studied the phase-locking properties of bursting neurons using a pyramidal neuron model as well as *in-vivo* recordings of LFP and spiking activity from the rat subiculum. We simulated different LFP states with physiologically relevant rhythms to determine how phase-locking of bursting activity depends on frequency composition of LFP. The model predicted that n-spike bursts lock to dominant oscillations in the input signal regardless of the frequency of these oscillations. In particular, the same phase-locking patterns were noticed in simulated states of dominant slow oscillations, low and high theta rhythms, and also persisted when the input signal contained a power spectral peak at 12 Hz which corresponds to the lower boundary of beta rhythms in rodents or upper boundary of alpha rhythms in primates. This suggests that internal cell mechanisms allow bursting pyramidal neurons to lock their firing to dominant LFP rhythms regardless of their specific frequency.

We observed two prominent rhythms within the LFP recorded from the rat subiculum under urethane anaesthesia. These were slow oscillations which are characteristic of slow-wave sleep or non-REM sleep (Wolansky et al., 2006; Clement et al., 2008) and theta rhythms which are present in the hippocampus during REM sleep (Harris et al.,

2002) as well as during exploratory behaviour (O'Keefe and Recce, 1993; Skaggs et al., 1996), although under urethane anaesthesia the theta peak at 4 Hz is lower than the theta peak at 7 Hz during REM sleep (Clement et al., 2008). Since these two rhythms correspond to different cognitive states, we analysed bursting activity during epochs of each dominant rhythm separately.

As predicted by the model, subicular neurons fired single spikes, two-spike bursts and larger bursts which were locked at a preferred phase range of the dominant rhythm within the LFP. The preferred phase range of locking was wider for the subicular neurons than the model. This was possibly a consequence of the lower signal-to-noise in experimental data than the simulated data. Although, some weaker phase preference to background rhythms was also observed, locking to rhythms in the dominant frequency band was at least two times stronger than to any other frequency. These results suggest that the distribution of LFP power modulated the strength of phase-locking of bursting neuronal firing. Modulation of neuronal firing by theta rhythms, which have increased power during behavioural tasks, is a known phenomenon in the hippocampal formation. More specifically, theta phase precession of neuronal firing in the hippocampus has been proposed to be a mechanism to encode spatial position (O'Keefe and Recce, 1993; Skaggs et al., 1996) and a buffer for working memories (Lisman and Idiart, 1995). Theta phase precession has also been reported in the subiculum (Kim et al., 2012). Furthermore, organising neuronal firing by high-power slow oscillations during slow-wave sleep is thought to be important for memory consolidation (Lee and Wilson, 2002; Wolansky et al., 2006; Rasch and Born, 2013).

The model also predicted a gradual shift in phase preference as a function of burst size n supporting a burst spike-count code in which single spikes and bursts of different sizes can provide more symbols to encode timing information conveyed by LFP. A similar shift in phase-locking of subicular bursting neurons was observed during epochs when slow oscillations were dominant under anaesthesia providing evidence that this code occurs *in vivo*. We did not observe a similar shift when theta rhythms were dominant but this could be due to the anesthesia affecting theta rhythms. Firing bursts of spikes can have a number of roles as revealed by studies in various brain systems. Thalamic neurons can fire bursts in response to salient stimuli (Guido and Weyand, 1995; Sherman, 2001; Swadlow and Gusev, 2001). Bursting in the hippocampus improves the reliability of synaptic transmission (Lisman, 1997). Bursts fired by electrosensory cells in the weakly electric fish encode different stimuli to those encoded by tonic spikes (Oswald et al., 2004). Firing bursts with different spike counts also provides a graded signal that allows encoding of different stimuli (Kepecs and Lisman, 2003; Samengo et al., 2013). Theoretical studies suggest burst size can encode the slope (Kepecs et al., 2002) and phase (Samengo and Montemurro, 2010) of input signals. In addition, there

is experimental evidence that burst size can encode orientation of visual stimuli in the primary visual cortex of awake monkeys (Martinez-Conde et al., 2002) and intensity of auditory stimuli in grasshopper auditory receptor neurons (Eyherabide et al., 2008, 2009). The outcome of our study expands understanding about the role of bursting in the subiculum.

3.5.1 Conclusions

The model suggests phase-locking of n-spike bursts is modulated by the power of the rhythms present in the LFP signal, so that locking to dominant rhythms is stronger than to background rhythms. The analysis of experimental data showed that the output of subicular bursting neurons preferentially locked to the phase of slow oscillations and theta rhythms in two distinct states under urethane anaesthesia. Since phase-locking to dominant rhythms was observed regardless of the frequency of these rhythms, locking appears to be a dynamic property of bursting neurons but not a property of the specific frequency at which the locking occurs. This means that burst firing can potentially lock to the dominant frequencies associated with a variety of behaviours. The outcome of this work needs to be explored further in future studies as the present analyses are based on data from one rat. Although we presented example data from the subiculum, the model is more general so can also be applied to understand the properties of bursting in other cortical and subcortical areas containing pyramidal neurons. Similar phase-locking patterns of bursting neuronal firing might occur in other regions of the brain during both sleep and awake states. Therefore, our results suggest that bursting neurons are likely to play a more significant role in the neural code than previously assumed.

3.6 Acknowledgements

MC was supported with a Doctoral Training Partnership PhD Studentship awarded to The University of Manchester by the UK Biotechnology and Biological Sciences Research Council (BBSRC DTP grant code: BB/J014478/1) and with the President's Doctoral Scholar Award by The University of Manchester.

3.7 Appendix A. Supplementary data

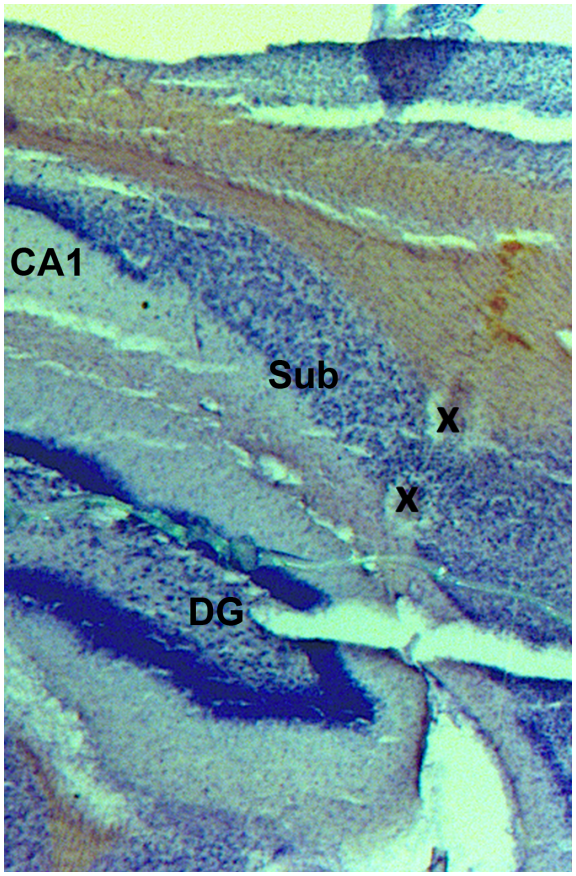

Figure 3.5: Nissl-stained brain section showing the position of electrodes in the subiculum. The electrolytic lesions produced at the end of the experiment are marked with an 'x' and indicate the position of the first shank of the multi-electrode array. The remaining three shanks are located to the left of these lesions. Sub: subiculum; CA1: hippocampal area CA1; DG: dentate gyrus.

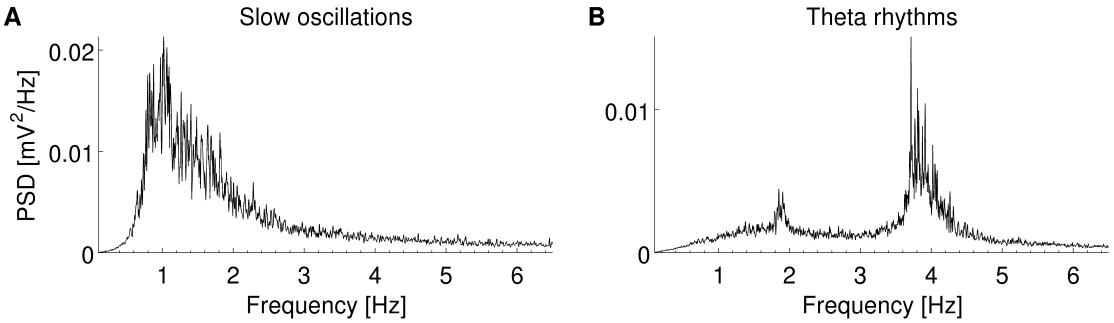

Figure 3.6: Average power-frequency spectra of LFP segments identified as containing dominant slow oscillations (A) or theta rhythms (B) in the rat subiculum under urethane anaesthesia. (A) The spectrum contained only a peak at slow oscillations indicating there was no remnant theta rhythm. (B) The spectrum contained a large peak at theta rhythms and also a small peak at lower frequencies which was due to coexistence of rhythms in the two bands during theta states under urethane anaesthesia. Spectra plotted using the Welch's periodogram method with Hamming windows of length at least 130 s and 50% overlap.

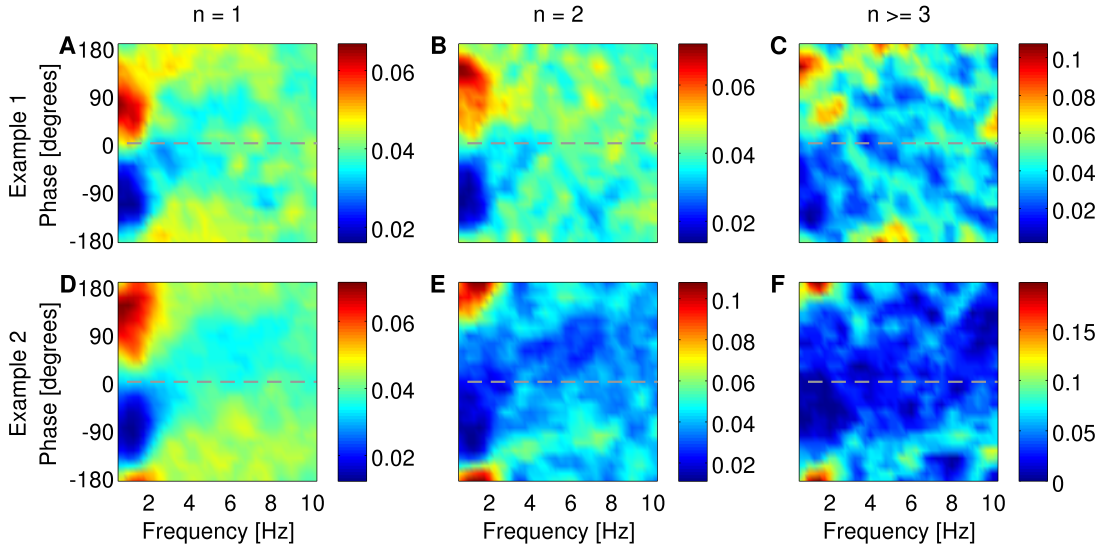

Figure 3.7: Phase-locking histograms of single spikes (A and D), two-spike bursts (B and E) and larger bursts (C and F) fired by two different subicular neurons when slow oscillations were dominant in the LFP signals. The preferred phase range of firing differed for each neuron (A–C and D–F). Phase of 0° corresponds to the peak of a waveform as calculated by the Hilbert transform. The colourbar shows the probability of locking to the phase of filtered LFP at overlapping steps of 1 Hz. Chance probability is equal to 0.04.

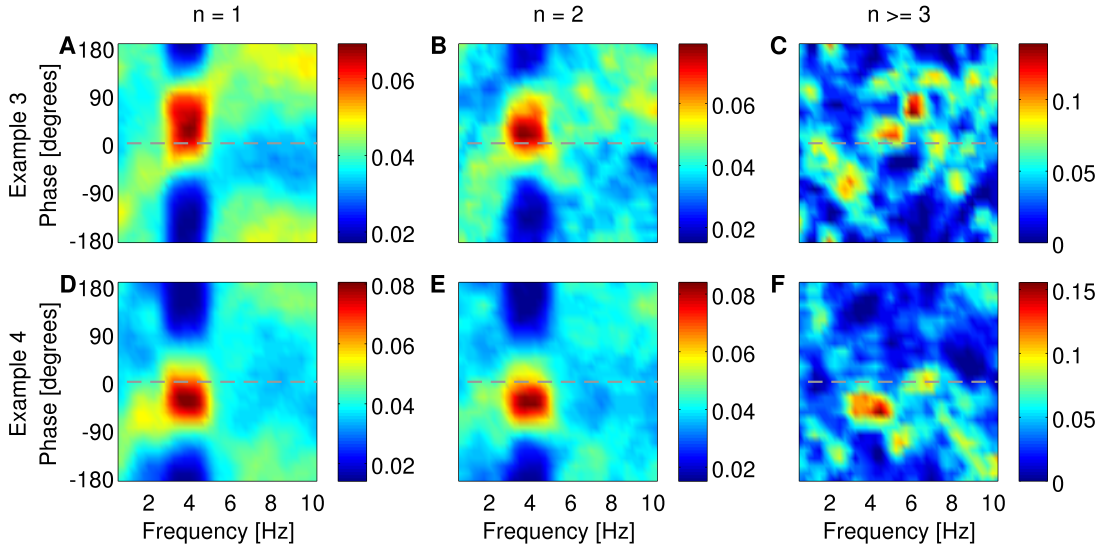

Figure 3.8: Phase-locking histograms of single spikes (A and D), two-spike bursts (B and E) and larger bursts (C and F) fired by two different subicular neurons when theta rhythms were dominant in the LFP signals. The preferred phase range of firing differed for each neuron (A–C and D–F). Phase of 0° corresponds to the peak of a waveform as calculated by the Hilbert transform. The colourbar shows the probability of locking to the phase of filtered LFP at overlapping steps of 1 Hz. Chance probability is equal to 0.04.

Chapter 4

Paper 2

Bursting neurons in the hippocampal formation encode features of LFP rhythms

Maria Constantinou[1,*,#], Soledad Gonzalo Cogno[2,#], Daniel H. Elijah[1], Emilio Kropff[3], John Gigg[1], Inés Samengo[2], Marcelo A. Montemurro[1]

[1] *Faculty of Biology, Medicine and Health, The University of Manchester, Manchester, UK.*
[2] *Centro Atómico Bariloche and Instituto Balseiro, San Carlos de Bariloche, Argentina.*
[3] *Leloir Institute, IIBBA-CONICET, Buenos Aires, Argentina.*
[#] *Equal contribution*

**Corresponding author at: Faculty of Biology, Medicine and Health, The University of Manchester, Oxford Road, Manchester, M13 9PT, UK*
E-mail address: maria.constantinou@manchester.ac.uk

Keywords: Bursting, Local field potential, Subiculum, Entorhinal cortex, Information theory, Neural coding

4.1 Abstract

Burst spike patterns are common in regions of the hippocampal formation such as the subiculum and medial entorhinal cortex (MEC). Neurons in these areas are immersed in extracellular electrical potential fluctuations often recorded as the local field potential (LFP). LFP rhythms within different frequency bands are linked to different behavioral states. For example, delta rhythms are often associated with slow-wave sleep, inactivity and anesthesia; whereas theta rhythms are prominent during awake exploratory behavior and REM sleep. Recent evidence suggests that bursting neurons in the hippocampal formation can encode LFP features. We explored this hypothesis using a two-compartment model of a bursting pyramidal neuron driven by time-varying

input signals containing spectral peaks at either delta or theta rhythms. The model predicted a neural code in which bursts represented the instantaneous value, phase, slope and amplitude of the driving signal both in their timing and size (spike number). To verify whether this code is employed *in vivo*, we examined electrophysiological recordings from the subiculum of anesthetized rats and the MEC of a behaving rat containing prevalent delta or theta rhythms, respectively. In both areas, we found bursting cells that encoded information about the instantaneous voltage, phase, slope and/or amplitude of the dominant LFP rhythm with essentially the same neural code as the simulated neurons. A fraction of the cells encoded part of the information in burst size, in agreement with model predictions. These results provide *in-vivo* evidence that the output of bursting neurons in the mammalian brain is tuned to features of the LFP.

4.2 Introduction

Bursts are groups of high frequency spikes followed by quiescent periods. In the mammalian brain, bursting activity has been observed in the cortex (Connors et al., 1982; McCormick et al., 1985), thalamus (Steriade et al., 1993a; Guido and Weyand, 1995) and hippocampal formation (Kandel and Spencer, 1961; Ranck, 1973) among other regions. However, despite being ubiquitous, little is known about the specific role of bursts in information processing. From a dynamical point of view, bursts are not simply a sequence of individual spikes fired in rapid succession. They rather constitute a single dynamical event triggered and supported by the interplay between slow and fast currents underpinning the cell's membrane excitability (Izhikevich, 2010).

Bursting neurons have been identified in regions of the rodent hippocampal formation such as the subiculum (Sharp and Green, 1994; Gigg et al., 2000) and more recently in the medial entorhinal cortex (MEC) (Latuske et al., 2015). Both of these areas are important for processing hippocampal information (e.g. Hafting et al. (2005); Kim et al. (2012)). The subiculum receives input from area CA1 and projects hippocampal output to cortical and subcortical areas (for reviews see O'Mara et al. (2001); Gigg (2006)) whereas the MEC receives cortical and subcortical input and projects to the hippocampus (Canto et al. (2008); Zhang et al. (2014)).

Neurons are immersed in electrical potential oscillations that can be recorded in the extracellular milieu as the local field potential (LFP). The LFP reflects the sum of all transmembrane currents in the vicinity of the recording electrode (Logothetis, 2003; Buzsaki et al., 2012) with a predominant contribution from synaptic activity of populations of pyramidal neurons within a volume of neural tissue (Einevoll et al., 2007;

Pettersen et al., 2008). Hence, extracellular oscillations usually contain information about the local network activity. Oscillations within specific frequency bands have been associated with a range of cognitive functions (Engel et al., 2001; Ward, 2003; Wang, 2010). For instance, in the hippocampal formation theta and gamma rhythms are involved in memory processing (Lisman and Idiart, 1995; Lisman, 2005) and spatial navigation (O'Keefe and Recce, 1993; Skaggs et al., 1996; McNaughton et al., 2006), whereas delta rhythms and slow oscillations are involved in memory consolidation (Molle and Born, 2011; Rasch and Born, 2013; Buzsaki, 2015). In addition, LFP rhythms have been suggested to provide a time frame for neuronal interactions and organizing neuronal activity (Fries, 2005; Womelsdorf et al., 2007). Moreover, evidence from the monkey visual (Montemurro et al., 2008) and auditory cortices (Kayser et al., 2009) suggests that the instantaneous phase of the LFP can act as an additional channel operating in parallel to the usual firing-rate code and boost the amount of encoded visual and acoustic stimuli, respectively. Thus, the LFP can contain information that is not present in spike firing alone.

However, the precise mechanism by which downstream neurons could read out the information encoded by the LFP still remains elusive. Recent evidence suggests that bursting pyramidal neurons can lock their firing to a preferred phase range of the dominant LFP rhythm and this phase preference can change as a function of burst spike count (Samengo and Montemurro, 2010; Constantinou et al., 2015). Using this idea, computational models have proposed bursting as a mechanism to encode instantaneous features of an oscillating current into a pattern of spikes that can be transmitted to distant areas (Kepecs and Lisman, 2003; Samengo et al., 2013). In particular, models of pyramidal neurons suggested that intra-burst spike counts have the capacity to encode the slope (Kepecs et al., 2002) and phase (Samengo and Montemurro, 2010) of time-varying input signals.

The main hypothesis in our study is that firing single spikes and bursts of different counts can be a feasible mechanism to transmit information about local field oscillations, thus translating information in the LFP into an easily decodable code. We tested this hypothesis by a two-fold approach involving simulations from a two-compartment model of a pyramidal bursting neuron and *in-vivo* data from anesthetized and behaving rats. The model was constructed to fire with the statistics of experimentally recorded neurons and used to quantify the information about features of LFP-like oscillations in their bursting rate and intra-burst spike count. We investigated the encoding of delta and theta-dominated signals, representing LFPs of anesthetized and behaving animals, respectively. The model predicted that the output of bursting cells can indeed encode information about the instantaneous voltage, phase, slope and, to a lesser extent, amplitude of the dominant rhythms. Furthermore, there was an encoding advantage in a

neural code in which single spikes, two-spike bursts and larger bursts are considered as distinct symbols compared to a code in which all these events are indistinguishable. We then tested whether the same result appeared in experimental data that we had access to: from the subiculum of anesthetized rats and the MEC of an awake behaving rat. The corresponding LFPs were dominated by delta and theta bands, respectively. The analysis, hence, allowed us to determine whether the encoding of LFP features was restricted to a specific behavioral state or frequency band, or whether it appeared as a robust mechanism in the temporal lobe. We found that a large fraction of bursting cells in both regions encoded information about LFP features in their bursting rate. In addition, some of these bursting cells also encoded information in burst size according to the model predictions. Our results suggest that LFP features can be encoded in single-cell bursting activity in the hippocampal formation of both awake and anesthetized animals.

4.3 Materials and Methods

4.3.1 *In vivo* electrophysiology under anesthesia

All experiments under anesthesia were performed in accordance with the Animals (Scientific Procedures) Act UK 1986 and were approved by the University of Manchester Ethical Review Panel. Three adult male Sprague Dawley rats and one adult male Wistar rat were used. The experimental procedures for recording from the subiculum have been described before in Constantinou et al. (2015). The rats were anesthetized by intraperitoneal injection of 1.5 g/kg urethane. Their heads were fixed in a stereotaxic frame, a midline incision was made and craniotomies were drilled according to the Paxinos and Watson (2007) rat brain atlas coordinate system for subiculum (Bregma: -8.0 mm and ML: 3.5 mm). Small electrolytic lesions created at the end of the experiment indicated electrode position in Nissl-stained brain sections.

A 4×8 multi-electrode array was inserted at a 30^o compound angle from the vertical axis to align the main axis of the electrode array parallel to the main pyramidal cell axis in the subiculum. The electrode array was attached to an electrode board and headstage and to an AC preamplifier resulting in total gain of ×2000. Simultaneous recordings of spontaneous LFP (lowpass-filtered up to 250 Hz) and spikes (highpass-filtered above 300 Hz) were obtained for an hour. Spikes were detected by setting a threshold manually for each electrode to account for differences in signal amplitude. Discrete spike shapes of 1.3 ms duration and continuous LFP (sampling rates: 40 kHz and 2 kHz, respectively) were stored for offline analysis.

4.3.2 *In vivo* electrophysiology during awake behavior

The data from the MEC during awake behavior were recorded in a previous study (Kropff et al., 2015). All experimental procedures for the awake recordings were performed in accordance with the Norwegian Animal Welfare Act and the European Convention for the Protection of Vertebrate Animals used for Experimental and Other Scientific Purposes. A Long Evans rat was used. The rat was implanted at 3 months and recorded until 9 months.

The experimental procedures for recording from the MEC have been described before in Kropff et al. (2015). The rat was trained to run freely in a 1-m wide square box. The trials lasted at least 20 min and as long as the rat would exhibit active foraging. Tetrodes were constructed from four twisted polyimide-coated platinum-iridium wires and mounted in a group of four into a microdrive. Once the animal was anesthetized, holes were drilled on the dorsal skull anterior to transverse sinus to reach the entorhinal cortex. The coordinates for implants were: 4.5-4.8 mm medio-lateral relative to lambda, 0.7 mm anterior to the border of the sinus and 1.8 mm dorso-ventral relative to the surface of the brain. The rat was connected to the recording equipment via AC-coupled unity-gain operational amplifiers close to its head. To search for new cells, tetrodes were lowered in steps of 50 μm. The cells reported here belong to layers III and V. The LFP (lowpass-filtered up to 500 Hz, sampled at 4800 Hz) was recorded single-ended from one electrode per drive.

4.3.3 Bursting neuron model

Bursting activity was simulated using a two-compartment conductance-based model of a pyramidal neuron which has been used in previous studies (Kamondi et al., 1998; Kepecs et al., 2002; Kepecs and Lisman, 2003; Samengo and Montemurro, 2010; Constantinou et al., 2015). The model contains the minimal ionic conductances required to generate bursting activity (Kepecs and Wang, 2000) after being reduced from a 19-compartment model of a CA3 hippocampal neuron (Traub et al., 1991) to a two-compartment conductance-based model (Pinsky and Rinzel, 1994). The input current $I(t)$ was injected into a dendritic compartment (Supplementary Equation 1) and bursting activity was recorded from a somatic compartment (Supplementary Equation 2). We had previously adjusted the model parameters (Constantinou et al., 2015) so as to produce single spikes and bursts with the same probability as subicular neurons (Figure 4.2A,C). Burst production by entorhinal neurons was governed by a similar distribution, so we only modified the variance of the input current to adapt the model to entorhinal bursting neurons (Figure 4.2B,D). The parameters and equations of the model are listed

in the Supplementary Methods and Supplementary Tables 4.1, 4.2.

The model was used to predict the spiking activity of subicular and entorhinal neurons when immersed in oscillations present in the LFP *in vivo*. We simulated the effect of these oscillations by injecting an input current $I(t)$, which had the same spectral structure as the experimental LFP, into the dendritic compartment of the simulated neuron. Since the LFP recordings had limited duration (1 h for subiculum and 30 min for MEC), we used a method of creating surrogate data that preserves the spectral content of LFP observed *in vivo* and can produce input signals of any desired length from a segment of LFP. To construct the input signals, a 30-min segment of the experimental LFP signal was interpolated to obtain a sampling frequency of 100 kHz and then used to create surrogate oscillatory current signals. The surrogate signals were created from the recorded trace by randomizing the phases of Fourier components and then transforming back to the time representation. Hence, the power spectra of the surrogate signals (Supplementary Figure 4.14A,B) are the same as their real counterpart (Figure 4.1C,D), but the temporal structure is altered (Theiler et al., 1992). The signals were scaled so that the mean was 0 nA and the standard deviation was 0.7 nA or 0.4 nA depending on whether the simulation corresponded to anesthetized or behaving experiments, respectively.

4.3.4 Spike sorting

For the dataset from the subiculum, the spike shapes recorded from each electrode were imported in Offline Sorter V2.8.8 (Plexon Inc.) to isolate spikes from individual neurons. Different combinations of spike shape parameters were chosen for clustering until units were identified and manually separated. Units that were difficult to isolate from the background noise were discarded. The quality of separation was assessed by visual inspection of interspike interval (ISI) histograms to ensure no spikes were present within the neuronal refractory period of 1 ms. To identify multiple detection of the same unit on adjacent electrodes, cross-correlograms were plotted for each unit vs. all the other units. For pairs of units with apparent cross-correlation, indicated by a large peak within 1 ms from zero, only the unit with the largest spike waveforms was used for subsequent analyses.

For the dataset from the MEC, spikes were assigned to individual neurons offline using the graphical cluster-cutting software TINT (Axona Ltd.), as described in Kropff et al. (2015). The procedure was analogous to that for the dataset from the subiculum.

4.3.5 Identification of bursting neurons and spike train segmentation

Bursting units were identified from ISI histograms and autocorrelograms of spike times recorded at each electrode. Units in the subiculum were classified as bursting if the ISI histogram and the autocorrelogram had a sharp peak within 2-8 ms and these peaks were larger than any other peak within 50 ms (Supplementary Figure 4.12A,B). Units in the MEC were classified as bursting if the sharp peak was within 2-5 ms (Supplementary Figure 4.12C,D). These criteria are consistent with previous studies characterizing bursting units as having a peak within 6 ms or 10 ms (Ranck, 1973; Harris et al., 2001; Mizuseki et al., 2009).

Consecutive spikes separated by less than 8 ms or 5 ms (in subiculum and MEC, respectively) were assigned to the same burst. These thresholds were larger than the prominent peak in the ISI histograms (Supplementary Figure 4.12A,C). Changing the 8 ms threshold to 6 ms or 10 ms gave qualitatively similar burst size distributions, phase locking and information patterns (data not shown) so spike segregation in bursts was robust to small differences of threshold.

The time-scale of the response patterns of the simulated neurons was slower, since the prominent peak of the ISI distribution appeared at longer times (Supplementary Figure 4.14C-F). Hence, consecutive spikes were assigned to the same burst when the ISI was below 16 ms.

4.3.6 Spectral analysis and data segmentation

LFP and input signals to the model were resampled to 200 Hz to reduce computation time. Decimation was used in order to prevent the aliasing effect of signal components above the Nyquist frequency in the downsampled signal. To visualize the spectral content of LFP signals, power spectra were plotted using the Welch's periodogram method with Hamming windows of 200 s and 50% overlap (Figure 4.1C,D). To depict how the power of LFP oscillations changed over the duration of the experiment, the Fourier decomposition of the signal across time and frequency was visualized in spectrograms computed with Hamming windows of 2 s and 50% overlap (Figure 4.1A,B). For illustration purposes in Figure 4.1A,B and Supplementary Figure 4.13A only, the spectrograms were smoothed with a 200-ms moving window to overcome excessive pixelation of the image.

In each rat, the power spectra of the LFP recorded from all electrodes in the subiculum or MEC were remarkably similar. During the 1-h recording under urethane-anesthesia,

there was a prevalent peak at ∼1 Hz (example in Figure 4.1A,C) and for three of the four rats there were epochs in which the network shifted transiently to a different dynamical state, dominated by a peak at ∼3-4.5 Hz (example in Supplementary Figure 4.13). The first peak corresponded to delta rhythms and the latter to theta rhythms as recorded under urethane anesthesia. The ∼1 Hz rhythm under similar experimental conditions has also been referred to as hippocampal slow oscillations in the literature (Wolansky et al., 2006; Clement et al., 2008). We isolated the epochs with dominant delta rhythms as described in Constantinou et al. (2015). In summary, based on the power spectra, the frequency bands for delta and theta rhythms were defined as 0.5-2.5 Hz and 2.5-5.0 Hz, respectively. Small changes in the boundaries of these bands did not affect the results in pilot analyses. The dominant rhythm was defined as the band with the highest power at a given time point at which the difference between the power of this band and any other band was at least 10%. The epochs with dominant theta rhythms under anesthesia are discussed in the Supplementary Results and Supplementary Figures 4.19, 4.20. The LFP recordings from the awake rat during foraging activity contained a prominent spectral peak at ∼8 Hz (example in Figure 4.1B,D). This frequency corresponds to the theta rhythm associated with exploratory behavior and was stable throughout the recordings.

4.3.7 LFP filtering and feature extraction

LFPs were filtered using a finite impulse response (FIR) digital filter with Kaiser window (sharp transition bandwidth: 1.0 Hz, stopband attenuation: 60 dB, passband ripple: 0.01 dB). LFPs were bandpass-filtered with cut-off frequencies 0.5 Hz and 3 Hz to extract the delta rhythm in the anesthetized data, or 6 Hz and 12 Hz to extract the theta rhythm in the awake data. For the systematic narrowband analysis of Figures 4.8-4.11 and Supplementary Figures 4.16-4.18,4.20, the LFP signals were filtered in 1 Hz windows with 75% overlap, except for the first frequency window which ranged from 0.1 Hz to 1 Hz.

Features were extracted from the filtered LFP signals. The investigated features were the instantaneous voltage (or input signal for the model), slope, phase and amplitude. Slope was calculated as the derivative of the LFP (experiments) or input signal (simulations). Phase and amplitude were computed as the argument and modulus, respectively, of the complex Hilbert transform of the LFP or input signal. With our angular convention, a phase of 0^o corresponded to a maximum in the oscillatory signal.

4.3.8 Information measures

Information theory (Shannon, 1948) was used to quantify how much information about LFP features can be conveyed by the output of bursting neurons. In the case of simulated neurons, the features of the LFP are replaced by the same features of the input current $I(t)$ injected into the model. Information was defined as the average reduction in uncertainty about a given LFP feature by knowing the neuronal output.

To estimate information measures, time was binned into small intervals of duration $\delta t = 5$ ms. Each interval was associated with a neural response and a LFP feature. The latter could be either synchronous with the neural response (no time lag) or could be located at a fixed time before or after the response. The collection of all the values of a given feature throughout a session defined the feature set X.

We studied three possible ways – referred to as *full burst code*, *burst rate code* and *burst distinction code* – by which bursting neurons encode LFP features. For the full burst code, the set N of all possible neuronal responses consisted of four distinct symbols: no spike ($n = 0$), single spike ($n = 1$), two-spike burst ($n = 2$) and larger burst ($n = 3$). Bursts of three or more spikes were represented by the same symbol because they occurred rarely (Figure 4.2). Each time bin was associated with one such response, located at the time of burst initiation. The burst rate code was obtained from the full burst code by considering all bursts containing one or more spikes ($n \geq 1$) as indistinguishable events. Hence, the 0s of the full burst code were preserved in the burst rate code and a new symbol representing the initiation of a burst replaced all other n values. The burst distinction code differed from the previous two in that only a subset of the time bins was employed: the time bins where a burst was initiated. That is, all the time bins associated with a 0 response were discarded. Neuronal activity was described by a response set $N = \{1,2,3\}$ which distinguished between bursts of different spike count. The information encoded by the burst distinction code quantifies whether bursts of different sizes are useful to discriminate LFP features. The data processing inequality (Cover and Thomas, 2006) ensures that the full burst code cannot encode less information than any of the other codes and equality is only possible if the discarded aspect is irrelevant to information encoding.

When the time bin is sufficiently brief, the information $I(X;N)$ about a LFP feature (X) conveyed by bursts (N) with the full burst code or with the burst rate code can be estimated by adapting the method described in Skaggs et al. (1993) to incorporate the

firing rate of n-spike bursts (Eyherabide et al., 2008) so that:

$$I(X;N) = \delta t \sum_{n\in N}\sum_{x\in X} p(x) r_n(x) \log_2 \frac{r_n(x)}{r_n}, \tag{4.1}$$

where $p(x)$ is the probability of each LFP feature value and $r_n(x)$ is the rate of each n-spike event conditional to a LFP feature of value x. The average rate of each n-spike event r_n is:

$$r_n = \sum_{x\in X} p(x) r_n(x). \tag{4.2}$$

The information values obtained from Equation 4.1 are in units of bits per time bin. The information was converted to bits/burst by dividing the value obtained from Equation 4.1 by the average number of bursts in a time bin, that is, by $\delta t\ r$, where r is the total burst rate.

In the full burst code: $N = \{0,1,2,3\}$, in the burst rate code: $N = \{0, \text{burst}\}$, and in the burst distinction code: $N = \{1,2,3\}$. Applying the chain rule $I(X;Y,Z) = I(X;Y) + I(X;Z|Y)$ to the case $Y = \{0,\text{burst}\}, Z = \{1,2,3\}$, the three codes are related by $I(X;\{0,1,2,3\}) = I(X;\{0,\text{burst}\}) + r\delta t\, I(X;\{1,2,3\})$ (derivation in Supplementary Methods). Therefore, in order to calculate the information per burst encoded in the burst distinction code, one may calculate the difference:

$$I(X;\{1,2,3\}) = \frac{1}{\delta t\ r}\left[I(X;\{0,1,2,3\}) - I(X;\{0,\text{burst}\})\right]. \tag{4.3}$$

Alternatively, the information of the burst distinction code can be computed directly from the Shannon equation $I(X;N) = H(X) - H(X|N)$ with $N = \{1,2,3\}$ and defining X as the set of features associated with the time bins where a burst was fired.

The continuous values of the LFP features were discretized into four symbols to define the set X (a justification of the chosen binning is given in the Supplementary Methods and Supplementary Figure 4.15). The boundary of bins was adjusted such that the distribution of the four symbols was uniform. Hence, the probability of each symbol x was $p(x) = 0.25$.

Due to the finite nature of experimental data, the estimated probabilities used to compute mutual information contain statistical errors, which lead to a sampling bias in the information estimators. The bias is defined as the difference in the information values calculated from the probabilities estimated from experimental data and from the true probabilities (Panzeri et al., 2007). To correct for this bias, a bootstrapping method (Montemurro et al., 2007b,c, 2008) was used. The burst size labels corresponding to each LFP feature value were shuffled and the mutual information $I_s(X;N)$ was calcu-

lated with the shuffled data. Although in principle shuffling eliminates all statistical correspondence between burst size and LFP features, the resulting information value still does not vanish, due to the bias. The procedure was repeated 100 times, and the average of the shuffled information values $\langle I_s(X;N)\rangle$ was taken as an estimation of the sampling bias. Since the output statistics varied across cells, the bias estimation was done individually for each cell.

A given cell was considered to convey a significant amount of information about a given feature when the information obtained with the real data was larger than the maximum value of the 100 shuffled information estimates across time. This maximum value could happen at any point in the time window around burst onset. For significantly encoding cells, the bias-corrected information $I_c(X;N)$ was obtained by subtracting $\langle I_s(X;N)\rangle$ from the mutual information estimate $I(X;N)$. The bias-corrected information is hereafter referred to as information.

4.3.9 Phase-locking estimation

For each cell and n value, phase-locking was estimated by calculating the probability of firing a burst of n spikes conditional to a LFP phase of a specific range. The interval $[-180^o, 180^o]$ was divided into 25 phase ranges, each of size 14.4^o. The phase was computed at the time of burst onset.

4.3.10 Principal component analysis

In order to determine whether pairwise correlations suffice to explain all the structure in the statistics of the information data, we performed a principal component analysis (PCA) of the information transmitted about the four features at the population level. Each cell in either subiculum or MEC was taken as a sample of a 4-dimensional vector $\mathbf{v}_i$, whose components were the values of the mutual information obtained with the full burst code about the four explored LFP features (voltage, slope, phase and amplitude). The 4×4 covariance matrix of each population (subiculum or MEC) is:

$$C = \overline{\left(\mathbf{v}_i - \overline{\mathbf{v}_i}\right)\ \left(\mathbf{v}_i - \overline{\mathbf{v}_i}\right)^T}, \tag{4.4}$$

where the horizontal bar represents a population average on all the bursting cells i of each brain area, and the supra-script T stands for vector transposition. The eigenvectors of C are orthogonal, and indicate the directions in which information vectors are uncorrelated. The associated eigenvalues are always non-negative and equal to the variance

of the population data along the direction of the corresponding eigenvector. If one of the eigenvalues is much larger than the other three, then the information about the different features is strongly correlated throughout the population and all information vectors are essentially proportional to the principal eigenvector (the one associated with the largest eigenvalue). The eigenvector associated to the second eigenvalue indicates an additional direction of variability which, although less important, implies fluctuations in information values that are uncorrelated with those in the principal direction.

4.4 Results

We investigated how bursting neurons encode information about LFP features in the hippocampal formation using both a bursting neuron model and electrophysiological data recorded *in-vivo* from the subiculum and the MEC. Three possible ways of transmitting information were explored: the full burst code, burst rate code and burst distinction code (see Materials and Methods). Each code corresponds to a different representation of the bursting responses. The full burst code considers both the timing and the spike count of each burst, representing the *when* and *what* of the encoded features, respectively (Eyherabide and Samengo, 2010a,b). In the burst rate code, only the timing of bursts is represented; and in the burst distinction code, only the spike count.

For shortage of notation, we employ the word *burst* to all spike patterns including not only sequences of two or more spikes, but also single spikes, which are considered as one-spike bursts. In all cases, the statistical correspondence between LFPs and bursting responses was explored using the LFP recorded at the same electrode where the single-cell activity was registered.

4.4.1 Information encoded by simulated bursting neurons

In order to mimic the effect of the fluctuating extracellular medium on neuronal excitability, we used variations of the LFP recorded in the experimental data as the input signal driving a simulated neuron (see Methods for input signal construction and computational model). The LFPs recorded in anesthetized and behaving animals contained markedly different spectral characteristics (Figure 4.1). Therefore, each of these conditions was simulated independently using a driving signal with the corresponding spectral profile (Supplementary Figure 4.14). The firing statistics of the simulated neuron were similar to the *in-vivo* recorded cells (Figure 4.2).

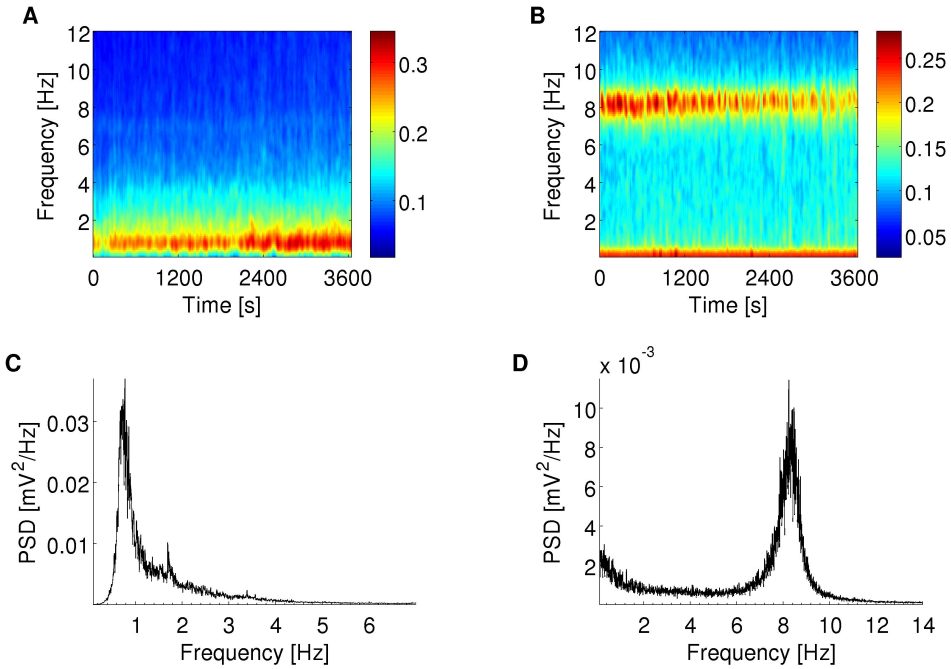

Figure 4.1: Spectral content of LFP. Example of spectrograms **(A,B)** and power-frequency spectra **(C,D)** of LFP recorded by an electrode in the subiculum of an anesthetized rat **(A,C)** and the MEC of an awake behaving rat **(B,D)**. **(A,C):** LFP show a peak in spectral power at ∼1 Hz throughout the recording session. **(B,D):** LFP show a peak in spectral power at ∼8 Hz throughout the recording session. There is also a smaller peak at frequencies <1 Hz. **(A,B):** Color scale in $(\mathrm{mV}^2/\mathrm{Hz})^{0.25}$. Warmer colors indicate higher power spectral density.

Neurons integrate information over time and, at a certain moment, fire a response (or not). Therefore, responses are not only sensitive to the instantaneous properties of the input signal, they also depend on its past history. Moreover, if the signal contains temporal correlations, the past values of the signal are correlated with its future values. Hence, a given event in the neural response may predict a future signal feature. Indeed, neuronal bursting was not only modulated by features occurring at the time of burst initiation, but also, to a lesser extent, by features appearing up to 200 ms before or after (Figures 4.3A-C and 4.4A-C). Out of the four tested features (instantaneous value of the input signal $I(t)$ and the associated slope, phase and amplitude), the best encoded features were the instantaneous value, phase and slope. The information about $I(t)$ and slope oscillated with a frequency that doubled the frequency of the dominant rhythm, both for delta and theta-dominated inputs (Figures 4.3A-C and 4.4A-C). This effect is explained at the end of section 3.4.

A full burst code, in which all n-spike bursts –where n indicates the intra-burst spike count and $n = 0$ for time bins where there is no event fired– corresponding to each instantaneous LFP feature are distinct symbols, encoded slightly more information than

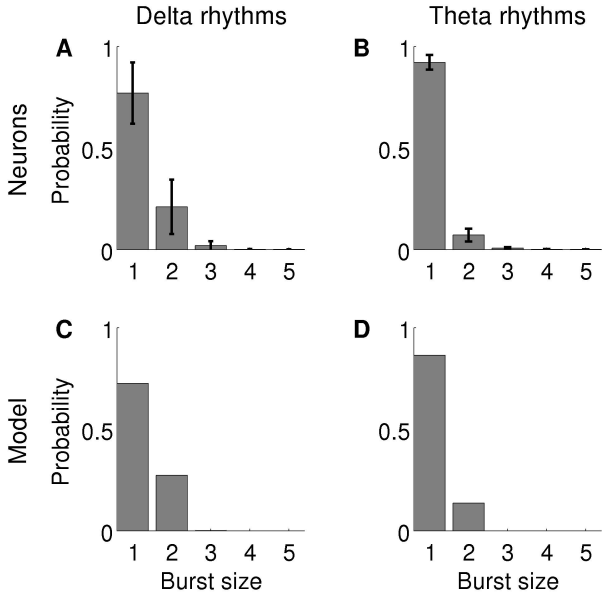

Figure 4.2: Probability of firing n-spike events by bursting neurons in the subiculum when delta rhythms were dominant in the LFP under anesthesia **(A)** and in the MEC when theta rhythms were dominant in the LFP during awake behavior **(B)**. Bars show the average probability across 28 units in subiculum **(A)** and 42 units in MEC **(B)**; error bars indicate standard deviation. **(C,D):** Probability of the model firing n-spike bursts when delta **(C)** or theta rhythms **(D)** were dominant in the input signal.

a burst rate code, in which the size of bursts was indistinguishable (Figures 4.3A,B and 4.4A,B). The information obtained with the burst distinction code, which considers the spike count n only in the time bins where a burst was registered, was approximately 10-20 times smaller than with the other two codes (Figures 4.3C and 4.4C). These results imply that most of the encoded information was temporal. In other words, the simulated neuron mainly detected *when* a given feature fell within a specific range and, to a lesser extent, encoded finer distinctions in the intra-burst spike count.

Bursting neurons *in-vivo* exhibited a range of patterns of information encoding, often resembling the simulated neuron. Figures 4.3D-I and 4.4D-I show examples in the subiculum under anesthesia and the MEC during awake behavior, respectively.

4.4.2 Population analysis of subicular neurons

We identified 28 bursting units in the subiculum of anesthetized rats during states with predominant delta rhythms. The probability of firing n-spike bursts decreased with the intra-burst spike count (Figure 4.2A). The population distributions of information values obtained with the full burst code are displayed in Figure 4.5A. For each cell

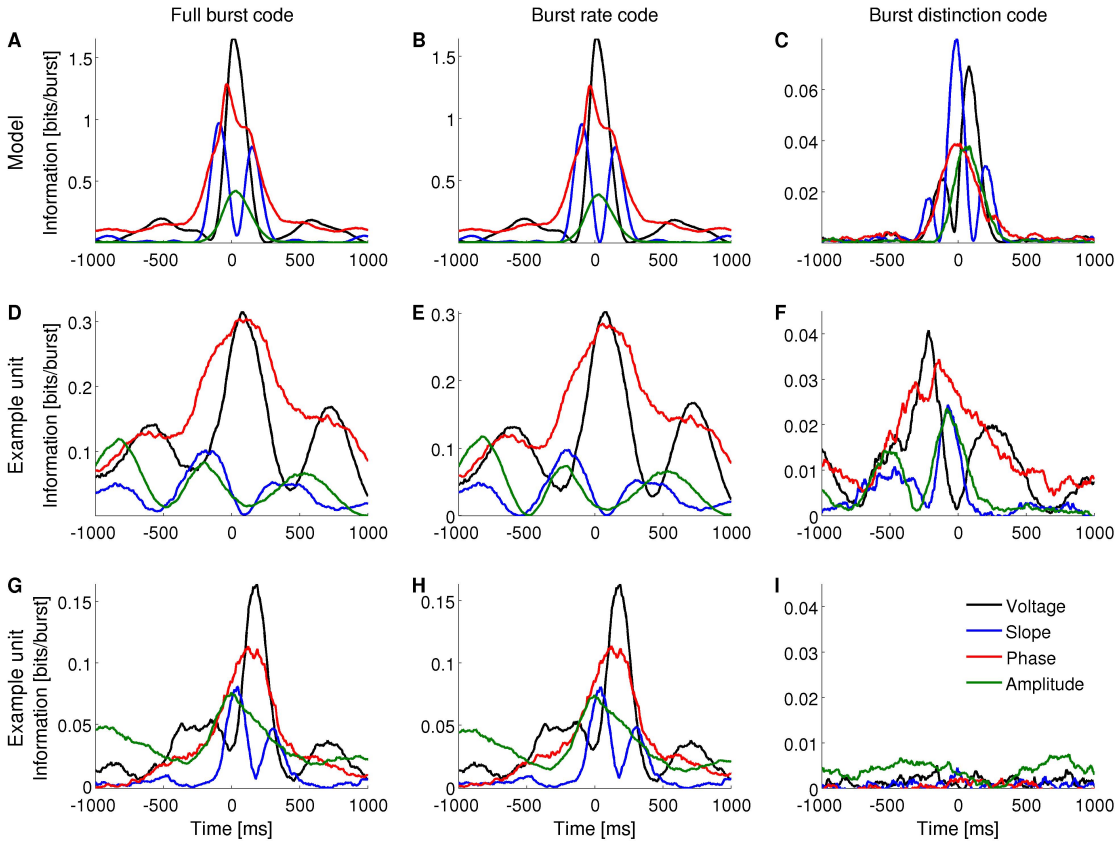

Figure 4.3: Information encoded by bursting neurons about the instantaneous voltage, slope, phase and amplitude of the delta-filtered LFP. **(A-C):** Mutual information obtained with the computational model when the input signal contains dominant delta rhythms. **(D-F)** and **(G-I):** Mutual information obtained for two different subicular cells under anesthesia. Both cells encode information about the voltage, slope, phase and amplitude of delta-filtered LFP by the full burst code **(D,G)** and burst rate code **(E,H)**. One of the cells encodes information about LFP features in the distinction between different burst sizes **(F)** whereas the second does not **(I)**.

in the population and each feature, the reported information values correspond to features evaluated at the time where information was maximal. The dark bars show significant information values, and the light bars show non-significant information values (information values below threshold). There were cells that encoded up to 0.4 bits/burst about voltage and phase, whereas the values corresponding to slope and amplitude were typically lower. The fraction of cells encoding significant information of at least 0.1 bits/burst about the voltage, slope, phase and amplitude were 50.0%, 32.1%, 50.0% and 35.7%, respectively (Figure 4.5B).

The information encoded by subicular cells about each LFP feature reached its maximum value for features occurring synchronously, before or after burst onset (examples in Figure 4.3). The distributions of times at which information was maximized with the full burst code are summarized in Figure 4.5C. Most subicular neurons encoded

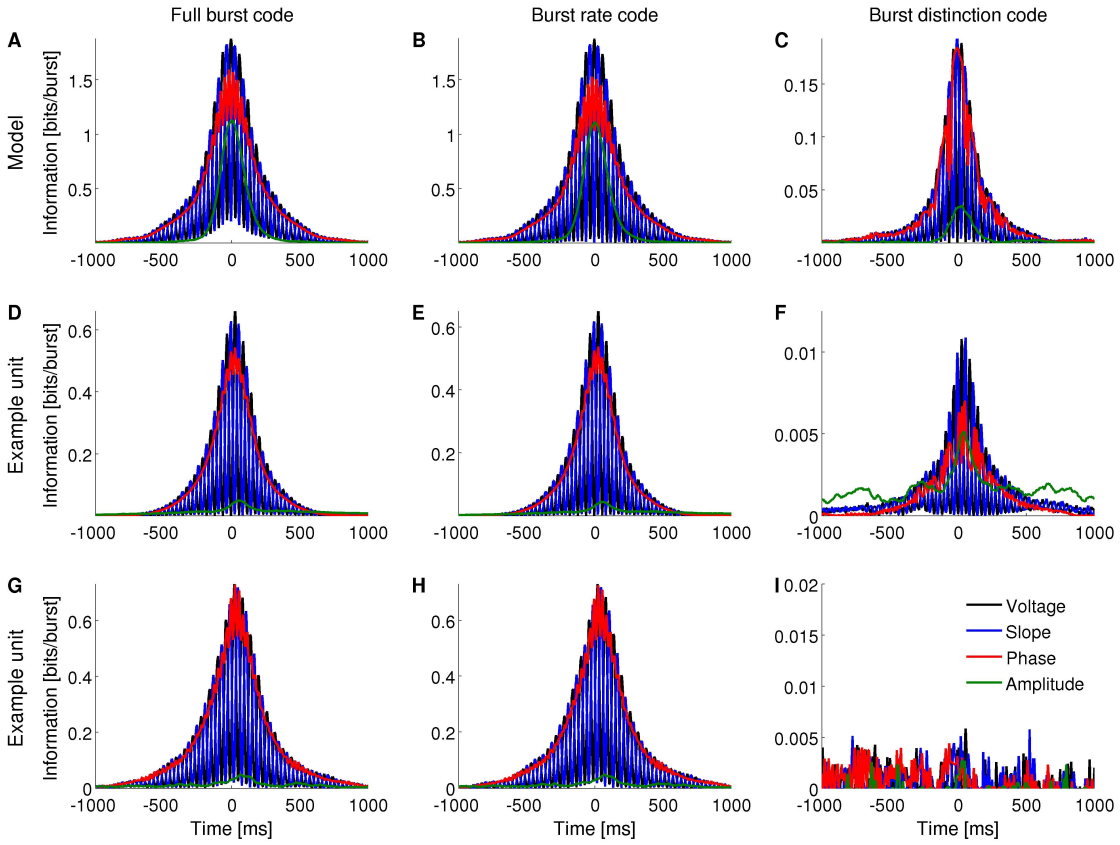

Figure 4.4: Information encoded by bursting neurons about the instantaneous voltage, slope, phase and amplitude of the theta-filtered LFP. **(A-C):** Mutual information obtained with the computational model when the input signal contains dominant theta rhythms. **(D-F)** and **(G-I):** Mutual information obtained for two different entorhinal cells during foraging behavior. Both cells encode information about the voltage, slope and phase of theta-filtered LFP by the full burst code **(D,G)** and burst rate code **(E,H)**. One of the cells encodes information about LFP features in the distinction between different burst sizes **(F)** whereas the second does not **(I)**.

maximal information about features occurring approximately 200–300 ms before or after burst onset. At the population level, the timing of maximal information about voltage and amplitude swept a wider range than for slope and phase. For 81.3% of the cells encoding significant information about phase, the timing of the maximal information corresponded to future phase values. For 82.4% of the cells encoding significant information about amplitude, the timing of the maximal information corresponded to past amplitude values. Therefore, bursting neurons can encode information about both past and future features of the delta-filtered LFP.

The distributions of significant information values for the full burst code are summarized in Figure 4.5D. Some of the four distributions had significantly different medians (Kruskal-Wallis test: $\chi^2 = 18.57$, $df = 67$, $p = 0.0003$; followed by Tukey-Kramer multiple comparisons test of the averaged group ranks). In particular, at the population

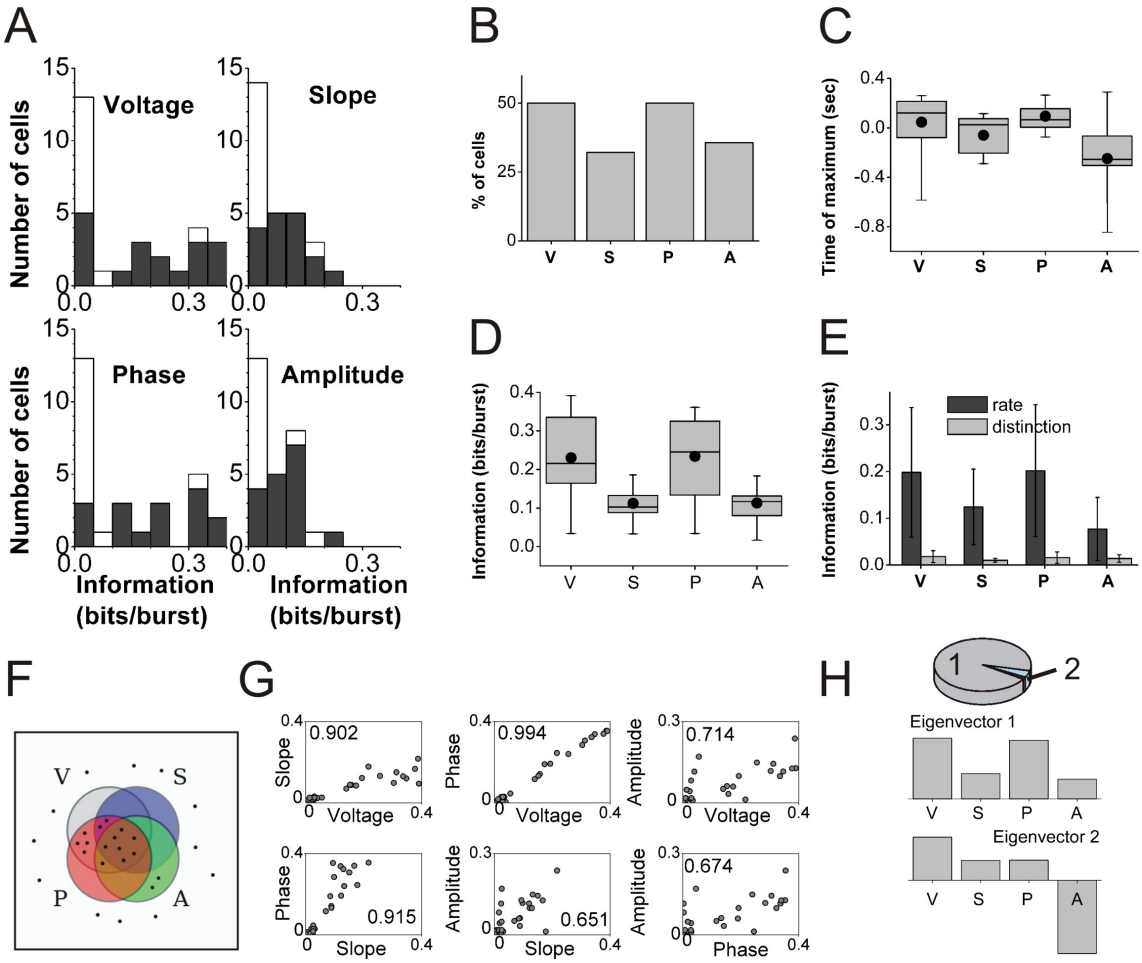

Figure 4.5: Population analysis of the information encoded by subicular bursting neurons about the delta-filtered LFP. **(A):** Histograms displaying the information encoded by different cells in the population about the four explored features. Black and white areas represent cells with significant and non-significant amounts of information, respectively. **(B):** Fraction of cells encoding significant information of at least 0.1 bits/burst. **(C):** Population statistics of the time relative to burst onset at which the information encoded by the full burst code reached its maximum value (only significant values included). Black dot: mean; horizontal bar: median; upper and lower borders of the box: 25^{th} and 75^{th} percentiles; thin lines: maximum and minimum values. **(D):** Population statistics of the maximal information encoded by the full burst code. Box representation same as in **(C)** (significant values only). **(E):** Comparison of the mean maximal information encoded by the burst rate and burst distinction codes (significant values only). Error bars report standard deviation. **(F):** Schematic representation of which features are encoded by each cell in the population. Each cell is indicated as a dot, and each set encloses only the cells that encoded at least 0.1 bits/burst about voltage (V), slope (S), phase (P) or amplitude (A). **(G):** Pearson correlation coefficients between the maximal information encoded by each bursting neuron (shown as a dot) about all pairs of features. **(H):** Principal component analysis (PCA) in which each cell is taken as a sample vector, and each feature as a dimension. Top: 98% of the variance is explained by only two eigenvectors, 94% and 4% respectively. Middle and bottom: First two eigenvectors obtained by PCA.

level, the median information about voltage and phase was not significantly different, nor was the information about slope and amplitude. However, the median information about voltage was significantly different from slope and amplitude, and also the median information about phase was significantly different from slope and amplitude.

The comparison between the population averages of the information encoded in the burst rate and burst distinction codes is summarized in Figure 4.5E. The population averages of the ratio $I_{\text{distinction}}/I_{\text{full}}$ were 13.8 %, 12.6 %, 13.1 % and 21.2% for voltage, slope, phase and amplitude, respectively. This indicates that most information was encoded in the timing of bursts and a smaller fraction in the distinction between burst sizes.

Figure 4.5F depicts the population profile of feature representation. Each neuron is indicated as a dot, and the set of each feature includes the neurons that encoded significant information of at least 0.1 bits/burst. More than half of the cells (57.1%) encoded at least one of the four features and thus appear inside of at least one of the sets. Out of all cells, 25.0% encoded all four features and thus appear in the intersection of the four sets; 14.3% encoded only voltage and phase; 7.1% encoded voltage, slope and phase but not amplitude; 7.1% encoded only amplitude; and 3.6% encoded voltage, phase and amplitude but not slope.

Figure 4.5G shows that the information about the four LFP features was typically pairwise correlated, most notably between phase and voltage. Amplitude was the most independently encoded feature. PCA indicated that most of the variance (94%, Figure 4.5H, top) in the distribution of information values was captured by an eigenvector whose predominant components included voltage and phase, and to a minor extent, slope and amplitude (Figure 4.5H, middle). An additional 4% of the variance was captured by a second eigenvector that had a large component in the direction of amplitude (Figure 4.5H, bottom). These results underscore that a large fraction of cells encoded the four features simultaneously, with more information encoded about phase and voltage, and less about slope and amplitude. An independent subset of cells encoded predominantly the amplitude as indicated by the second eigenvector.

4.4.3 Population analysis of entorhinal neurons

We identified 42 bursting units in the MEC of the awake behaving rat during theta rhythms. Burst firing probability decreased as the intra-burst spike count increased (Figure 4.2B). The population distributions of information values obtained with the full burst code are displayed in Figure 4.6A. The histograms corresponding to voltage

and slope are remarkably similar, and all but amplitude contain long tails with high-information values. There were cells that encoded more than 0.9 bits/burst about voltage and slope, and more than 0.8 bits/bursts about phase. The maximal information about amplitude was notably lower (0.13 bits/burst). The fraction of cells encoding significant information of at least 0.1 bits/burst about the voltage, slope, phase and amplitude were 38.1%, 38.1%, 28.6% and 4.8%, respectively (Figure 4.6B).

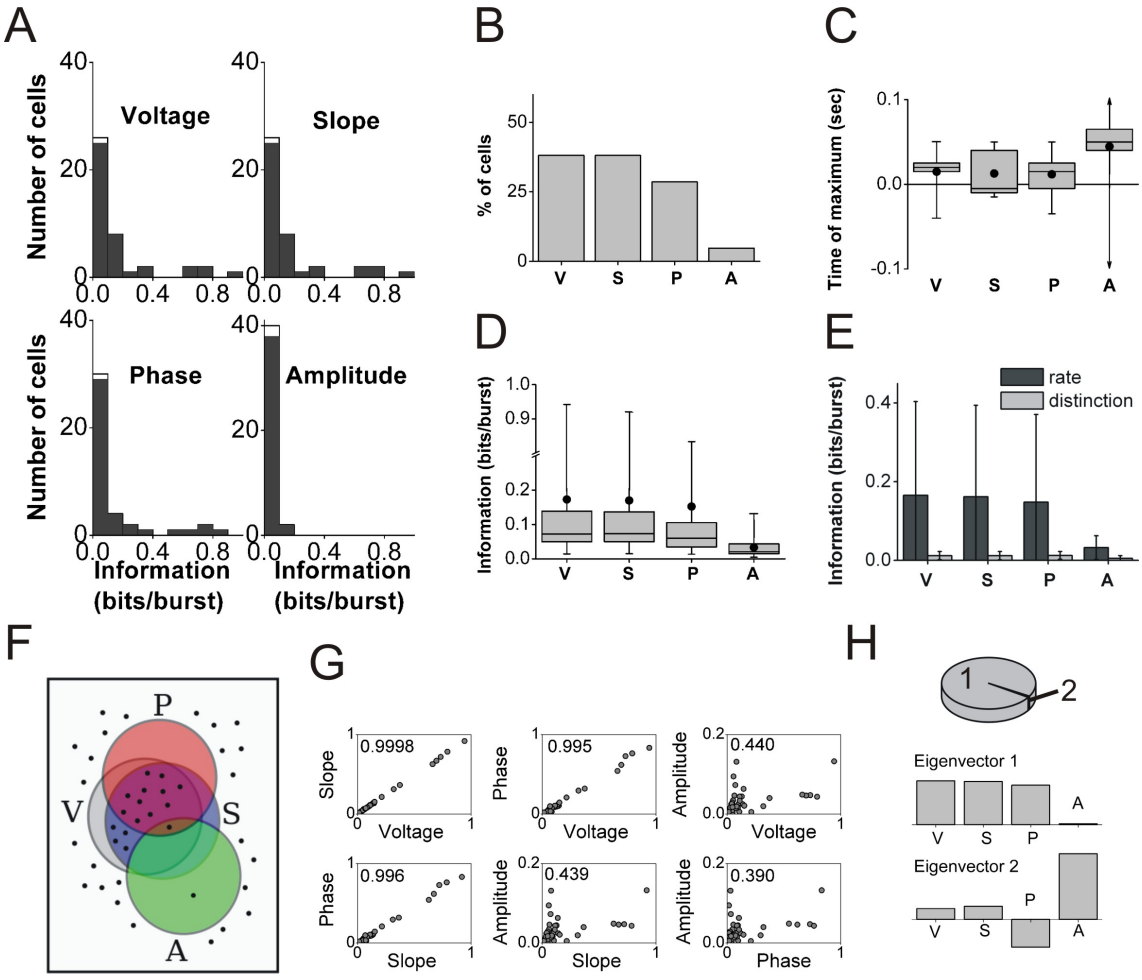

Figure 4.6: Population analysis of the information encoded by entorhinal bursting neurons about the theta-filtered LFP. Panels same as in Figure 4.5. **(C):** The largest and smallest times of maximal information about amplitude were +780 and −880 ms (out of scale). **(D):** Note the break in the y-axis. **(H):** 99.7% of the variance is explained by only two eigenvectors: 99% and 0.7% respectively.

Similarly to subicular neurons, the maximal information encoded by bursting cells in the MEC could correspond to features occurring synchronously, before or after burst onset (examples in Figure 4.4). The distributions of times of maximal information for the full burst code are summarized in Figure 4.6C. At the population level, entorhinal neurons encoded maximal information about the instantaneous voltage, slope and phase within 50 ms before or after burst onset; whereas maximal information about

amplitude could be up to approximately 800–900 ms around burst onset. Maximal information tended to correspond to future feature values of the theta-filtered LFP, in particular, 87.8% of the encoding cells conveyed maximal information for future voltage values.

The distributions of significant information values for the full burst code are summarized in Figure 4.6D. The long tails obtained for voltage, slope and phase produced mean information values that were notably larger than the medians. At the population level, the median information about voltage, slope and phase was not significantly different, but the median information about amplitude was different from the other three (Kruskal-Wallis test: $\chi^2 = 42.5$, $df = 161$, $p = 3 \times 10^{-9}$; followed by Tukey-Kramer multiple comparisons test of the averaged group ranks).

The comparison between the population averages of the information encoded in the burst rate and burst distinction codes is summarized in Figure 4.6E. The population averages of the ratio $I_{\text{distinction}}/I_{\text{full}}$ were 16 %, 16 %, 23 % and 13 % for voltage, slope, phase and amplitude, respectively. Thus, the timing of bursts encoded most of the information, and intra-burst spike counts encoded a smaller fraction of the information.

Figure 4.6F illustrates that 40% of the entorhinal bursting cells encoded at least 0.1 bits/burst of one or more of the four features and thus appear inside at least one of the feature sets. Out of all cells, 26% encoded at least 0.1 bits/burst of information about voltage, slope and phase but not amplitude; 10% only voltage and slope; 2% only amplitude; and 2% all four features.

The information about the four different features was typically pairwise correlated, most notably, between voltage, slope and phase (Figure 4.6G). Amplitude was the most independently encoded feature. The PCA indicated that 99% of the variance (Figure 4.6H, top) was captured by an eigenvector with predominant components along voltage, slope and phase (Figure 4.6H, middle). An additional 0.7% of the variance was captured by a second eigenvector that had a large component in the direction of amplitude (Figure 4.6H, bottom). Hence, most cells encoded voltage, slope and phase simultaneously, and an independent subset of cells encoded a small amount of information about amplitude.

4.4.4 Burst-triggered averages

In order to gain insight about how bursting neurons encode LFP features, for each cell and n value, we calculated the n-burst triggered average (n-BTA), that is, the average

bandpass-filtered LFP around n-spike bursts. In both subiculum and MEC, the n-BTA revealed that specific n values were predominantly associated with specific LFP features and the code varied from cell to cell. To illustrate these variations, two example units from each area are shown in Figure 4.7.

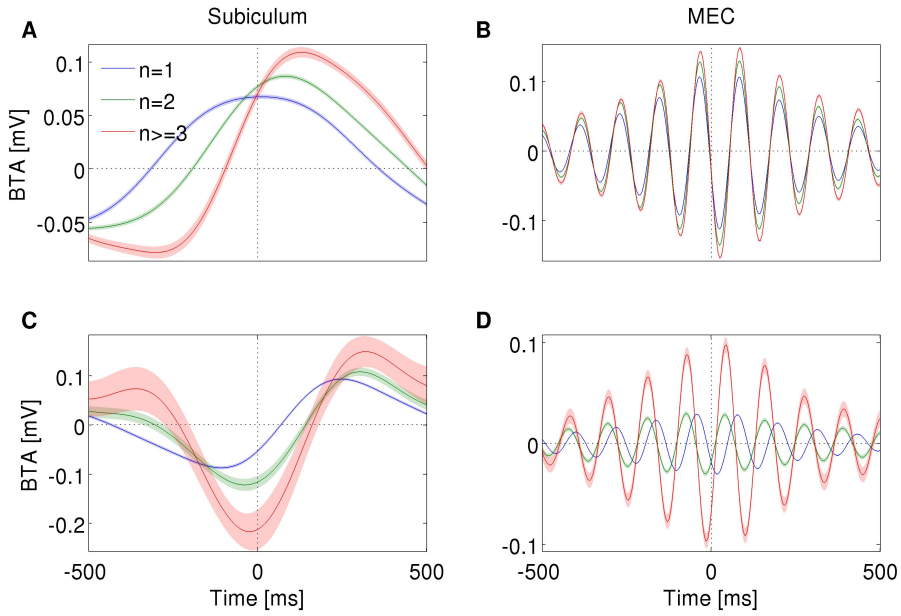

Figure 4.7: n-BTA of LFP around single spikes (blue), two-spike bursts (green) and larger bursts (red) fired by subicular neurons during epochs with dominant delta rhythms in the LFP **(A,C)** or entorhinal neurons during dominant theta rhythms **(B,D)**. Each example is from a different bursting unit. LFP was filtered within 0.5-3 Hz **(A,C)** or 6-12 Hz **(B,D)**. Shade shows standard error of mean. Spike or burst onset is at time = 0 ms.

The subicular unit of Figure 4.7A fired bursts near a maximum of the LFP, whereas the one in Figure 4.7C fired near the trough. In both examples, the slope and amplitude of the LFP around burst initiation ($t = 0$) changed with increasing spike count n. Instantaneous phase changed with n only for the cell in Figure 4.7A, whereas in Figure 4.7C, all bursts were triggered at the minimum of the LFP, irrespective of n. At the time of burst onset, voltage varied with n in Figure 4.7C but not in Figure 4.7A. The information encoded by the cell of Figure 4.7A is shown in Figure 4.3D-F.

The entorhinal unit of Figure 4.7B encoded LFP features both in the burst rate (Figure 4.4D,E) and, to a much smaller extent, in the distinction between bursts of different spike-count (Figure 4.4F). Accordingly, the n-BTAs of Figure 4.7B are all similar, implying that bursts of different sizes hardly discriminate between LFP features. The cell in Figure 4.7D shows a different case, where the instantaneous voltage, slope, phase and amplitude vary with n. Hence, the distinction between bursts of different size provides

information about the four features.

Figure 4.7 is useful to understand why the information plots in Figures 4.3, 4.4 display oscillating patterns for voltage and slope (but not for phase and amplitude) and why the frequency of the oscillations doubled the dominant frequency of the LFP. The LFP typically remains coherent during several cycles. The voltage therefore displays a rather regular oscillatory pattern. Whenever the BTAs corresponding to different n values cross each other, the distinction between these n values cannot convey information about voltage. The crossings occur at twice the dominant frequency, so this is the frequency at which information necessarily drops significantly. If all the n-BTAs cross simultaneously, information drops down to zero. If only some of the n-BTAs cross at a given time, the information decreases, but does not necessarily vanish. The same argument can be constructed for the slope of the LFP, since the slope is also an oscillatory signal and crossings occur at twice the dominant frequency. The case of instantaneous phase and amplitude is different, since they are not constrained to oscillate, and if they do, their frequency is not fixed.

4.4.5 Burst generation and phase locking

For a neuron to transmit information about the phase of the LFP, bursting probability (with or without distinction of different n-values) must be modulated by the phase of the LFP. Under anesthesia, 61% of bursting units in subiculum locked their firing to a preferred phase of the delta-filtered LFP (examples in Figure 4.8). Sometimes, the preferred phase of locking shifted to more advanced or earlier phases as intra-burst spike count increased (36% and 4% of all bursting units, respectively). Figure 4.8A-C shows an example where the preferred phase of locking shifted from 0° to 90° with increasing burst size. This is the same cell as in Figures 4.3D-F, 4.7A. Not all cells displayed shifts, see for example Figure 4.8D-F. Two additional examples from the same dataset are shown in the supplementary data of Constantinou et al. (2015). Cells that are locked to a specific phase value for all burst sizes encode information about phase in the burst rate. Instead, cells whose preferred phase depends on n also encode information in the distinction between different n-values. In MEC, 59 % of bursting units locked their firing to a preferred phase of the theta rhythm; 12% of neurons exhibited a phase locking that shifted to more advanced phases, whereas 21% shifted to earlier phases. Two examples from the MEC are shown in Figure 4.9. Both cells locked to a preferred phase range of the theta-filtered LFP. For the first cell (Figure 4.9A-C), the preferred phase of locking shifted with increasing burst size. This shift was not observed in the second example (Figure 4.9D-F; same unit as in Figure 4.7B), implying that the phase was hardly encoded in burst size.

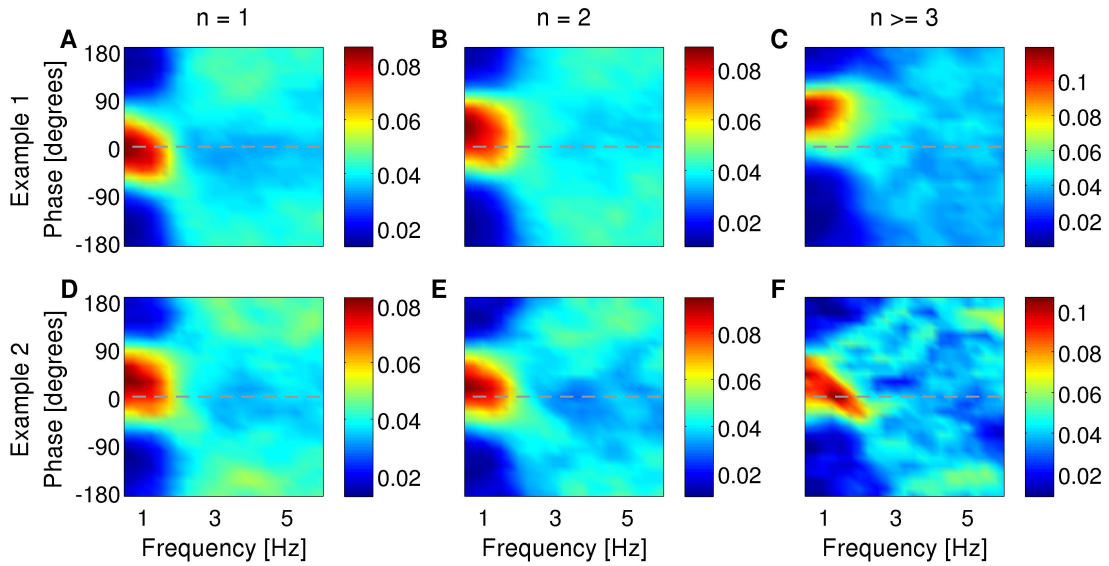

Figure 4.8: Examples of phase locking of two bursting units **(A-C)** and **(D-F)** identified in the subiculum of anesthetized rats when delta rhythms were dominant in the LFP. Phase-locking histograms of single spikes **(A,D)**, two-spike bursts **(B,E)** and larger bursts **(C,F)** fired by the example bursting units. Phase of 0^o indicates the peak of an oscillation. Colorbar: probability of firing n-spike bursts within a phase bin of narrowband-filtered LFP. Chance probability is equal to 0.04.

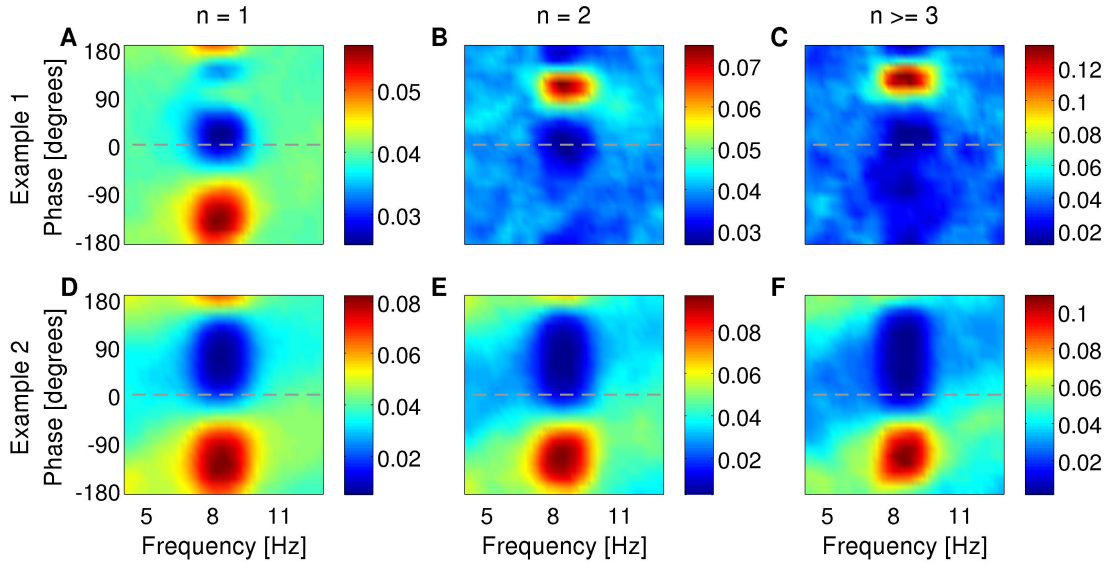

Figure 4.9: Examples of phase locking of two bursting units **(A-C)** and **(D-F)** identified in the MEC of an awake behaving rat when theta rhythms were dominant in the LFP. Phase-locking histograms of single spikes **(A,D)**, two-spike bursts **(B,E)** and larger bursts **(C,F)** fired by the example bursting units. Phase of 0^o indicates the peak of an oscillation. Colorbar: probability of firing n-spike bursts within a phase bin of narrowband-filtered LFP. Chance probability is equal to 0.04.

4.4.6 Bursting neurons encode features of dominant LFP rhythm

So far, we have examined the ability of bursting neurons to encode features of the dominant frequency band within the LFP: the delta band in the anesthetized animals and the theta band during exploratory behavior. However, neurons are immersed in a broadband LFP, so in principle, they could also encode features of more than a single frequency band. To verify whether such is the case, we narrowband-filtered the LFP over a range of frequencies and repeated the information analysis for each band.

In agreement with model prediction (Supplementary Figures 4.16, 4.17), most subicular and all entorhinal neurons that encoded features of the band-filtered LFP showed maximal information encoding in the frequency band with highest power but not other frequencies (examples in Figures 4.10, 4.11). Five of the encoding subicular cells also showed information encoding of the instantaneous amplitude of LFP at frequencies higher than ∼6 Hz (example in Supplementary Figure 4.18). The information about voltage and slope exhibited the same oscillatory patterns observed in Figures 4.3, 4.4 with the frequency of the oscillations being twice the frequency at which the signal was filtered. The oscillations in information therefore became narrower as the frequency increased. The information encoded by the burst rate code was very similar to that of the full burst code.

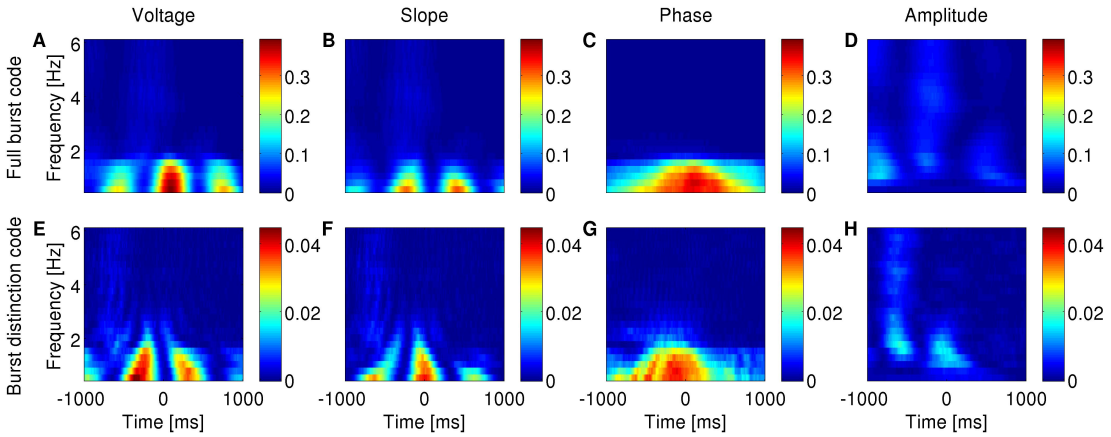

Figure 4.10: Information encoded by bursting neuron output about LFP features as a function of LFP frequency and time around burst onset. Example from a bursting unit in the rat subiculum during dominant delta rhythms under anesthesia. Information about the instantaneous voltage **(A,E)**, slope **(B,F)**, phase **(C,G)** and amplitude **(D,H)** of narrowband-filtered LFP conveyed by the full burst code **(A-D)** and burst distinction code **(E-H)**. Colorbar: mutual information in bits/burst.

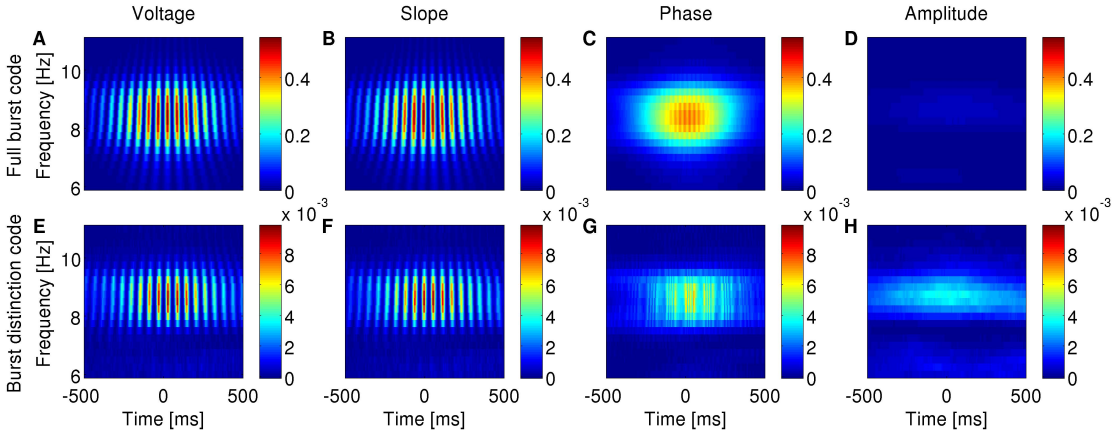

Figure 4.11: Information encoded by bursting neuron output about LFP features as a function of LFP frequency and time around burst onset. Example from a bursting unit in the rat MEC during awake behavior when theta rhythms were prevalent in the LFP. Information about the instantaneous voltage **(A,E)**, slope **(B,F)**, phase **(C,G)** and amplitude **(D,H)** of narrowband-filtered LFP conveyed by the full burst code **(A-D)** and burst distinction code **(E-H)**. Colorbar: mutual information in bits/burst.

4.5 Discussion

Bursts encode behaviorally-relevant information in several systems (Guido and Weyand, 1995; Sherman, 2001; Swadlow and Gusev, 2001; Chacron et al., 2004; Lesica and Stanley, 2004; Oswald et al., 2004; Marsat and Pollack, 2006; Sabourin and Pollack, 2009). In particular, temporally-structured neural codes have been found to encode information both in the timing and the spike count of bursts (DeBusk et al., 1997; Martinez-Conde et al., 2002; Arganda et al., 2007; Eyherabide et al., 2008, 2009; Marsat and Pollack, 2010). Neurons in the hippocampal formation are equipped with the endogenous mechanisms required for bursting (Hablitz and Johnston, 1981; Taube, 1993) and are tightly regulated by inhibitory networks that modulate bursting (Royer et al., 2012). Moreover, neurons are immersed in strongly oscillating fields that may favor temporally structured outputs such as bursting (Mizuseki et al., 2009). Therefore, bursts are likely to subserve a number of computational functions. For example, bursts generated at different frequencies induce long-term potentiation involving different ionic mechanisms and lasting different time intervals (Grover et al., 2009). Bursts are also involved in replay sequences during slow wave sleep (Lee and Wilson, 2002) and REM sleep (Louie and Wilson, 2001). It is therefore important to determine the contextual conditions in which bursts are generated, in particular, the statistical relation between the surrounding LFP and burst initiation.

We found that the probability of generating a burst of n spikes decreased with n, showing

a steeper decay for the awake data. A large fraction of bursting cells encoded significant amounts of information about at least one of the tested features (instantaneous voltage, slope, phase and amplitude), even though cells were only selected according to their ISI histogram. No criterion regarding neuronal type was used to exclude cells. In the MEC, the number of informative neurons was smaller than in the subiculum, but the informative neurons encoded more information. Spikes belonging to the same burst often decrease progressively in amplitude (Kandel and Spencer, 1961; Ranck, 1973), and could thus be assigned to different cells by typical spike sorting techniques (Harris et al., 2000). Therefore, our experimental results constitute a lower bound to the burst-mediated code, since there are potentially more bursts in the data than the ones we detected.

In the codes we studied, all bursts of n spikes were described by the same symbol (indicating the spike count in the full burst and burst distinction codes or the occurrence of a burst in the burst rate code) assuming that small differences in the ISI inside the burst are uninformative. As a result, the space of all possible spike patterns is reduced to a much smaller space, in which only burst-like patterns matter. The reduction could, in principle, discard information, because the neural code is not guaranteed to occur by means of a discrete alphabet (Eyherabide and Samengo, 2010a,b). The advantage, however, is that information measures do not require the study of long response windows, and by studying a small number of BTAs, the neural code is revealed.

The timing of each burst was defined as the time of the first spike in the burst. In principle, other choices could have been considered, such as the last spike or the mid-point. Since the investigated burst codes only make sense if all bursts of the same duration are taken as the same symbol (fluctuations in the duration are neglected), shifting the time assigned to each burst is an invertible transformation, so the data processing inequality reduces to an equality. Therefore, the mutual information values remain unchanged. The only difference is that the value of information, which we now assign to time t, would be assigned to time $t - t_{\text{shift}}$, and the same would happen to BTAs. The shift would therefore displace the graphs, but the conclusions of the paper would still be valid.

We found that most of the information about the LFP was encoded in the timing of burst initiation, implying that the code mainly represented temporal information. Burst onset punctuated LFP features falling within a specific range. Some cells also encoded 10–15% of additional information in the differentiation between bursts of different spike counts. The additional information represented fine-grained distinctions between the encoded feature values.

In the MEC, most cells encoded voltage, phase and slope simultaneously, and an independent subset of cells encoded amplitude. In the subiculum, most cells encoded a large amount of information about voltage and phase, and approximately half that amount about slope and amplitude. In order to understand these correlations, it is important to notice that the four tested features are not independent from one another. The LFP contains temporal correlations, and therefore induces a certain amount of statistical dependence between voltage, slope, phase and amplitude. Both in the theta and the delta-dominated LFPs, phase was correlated with voltage. The mutual information between the two features was approximately 0.8–1 bit (out of a maximum of 2 bits, given the employed binning). Phase and slope were less correlated and the mutual information between them was approximately 0.5 bits out of 2. Amplitude was mildly correlated with voltage in the delta-dominated LFP (mutual information was 0.3 bits out of 2), and even less in the theta-dominated LFP (mutual information was 0.1 bits out of 2). Importantly, slope was not correlated with voltage (mutual information was less than 0.1 bit out of 2), and by construction, phase and amplitude were independent. Therefore, the high correlation between the information encoded by bursting neurons about voltage, phase and slope found in the MEC could be potentially explained by an encoding mechanism mainly focused on representing phase, the other two features being no more than residual epiphenomena. There is no single feature whose encoding can explain the results found in the subiculum, so we must either conclude that at least two features are encoded (for example, voltage and slope, or phase and amplitude), or that a yet unexplored feature plays the protagonist role.

Although there is no complete understanding of the mechanisms through which the LFP arises, many authors agree that the main contribution is provided by the extracellular currents produced by synaptic input to a given brain region (Logothetis, 2003; Buzsaki et al., 2012; Einevoll et al., 2013). Hence, LFP fluctuations mainly reflect fluctuations in the input, the output activity of the local neurons playing only a minor role. It may therefore be puzzling to find that bursts also encode future LFP values, which seems to violate causality. It should be noticed, however, that such future encoding is also found in the simulations, where by construction, neural activity is the consequence (and not the cause) of the driving signal. As discussed in Samengo et al. (2013), encoding of future input features only takes place in signals that contain temporal correlations themselves. One can only expect a burst to encode future stimulus values if the burst is driven by input currents whose present value contains information about how they will evolve in the near future. Therefore, predictive encoding is only expected to occur up to time windows that are within the range of the temporal correlations of the signal itself. Indeed, we found that when the LFP is dominated by theta, bursts can predict features that extend up to 250 ms into the future, that is 1–2 theta cycles. Instead, for delta-dominated LFPs, the encoding goes as far as 500 ms, again, 1–2 cycles of the much

slower delta.

The computational model used to simulate bursting neurons was able to reproduce the main results obtained with the experimental data. The model contained the minimal ionic conductances required for inducing bursting and thus, by construction, does not represent every biophysical detail that generates bursts in all real neurons. Even so, the simulations are useful to show that the differences observed in the neural code of behaving and anesthetized animals can be obtained by simply changing the frequency content and the amplitude of the driving signal, rather than the specific biophysical mechanisms of a particular bursting neuron.

In summary, we have combined computational modeling with analysis of *in-vivo* data from awake and anesthetized rats with the aim to determine the code by which burst firing in the hippocampal formation can convey information about features of ongoing LFP oscillations. Our results confirm that the burst code represents the temporal features of the predominant frequency band of the extracellular oscillations, and that most of the information is encoded in the timing of burst onset. A more complex code, in which the different burst sizes are distinguished, added a further 10–15% of information. These findings suggest that bursts may have an important role in relaying information encoded in the LFP to downstream neurons.

We interpret the term 'information' in the technical sense defined by Shannon: the reduction in uncertainty about the value of a LFP feature by observing the response of the bursting neuron. This interpretation of the word information follows the line of the classical studies in the topic, as for example by Rieke et al. (1997); Borst and Theunissen (1999); Quian Quiroga and Panzeri (2009). We do not, however, address the issue of whether or how this encoding is further exploited by the brain. However, this does not preclude us to hypothesize about its possible function. Theta and delta rhythms are known to be involved in processing information related to declarative memory. In addition, previous studies demonstrated that the information carried by spikes is boosted by knowledge of LFP features (Montemurro et al., 2008; Kayser et al., 2009). After Samengo and Montemurro (2010), the hypothesis that bursting could be involved in making such information available to downstream neurons became more credible. Our current paper, then, is the first to actually show that the hippocampal formation is indeed endowed with the mechanisms to do so. We hope to motivate other scientists to search for evidence relating to the decoding of this information by downstream neurons and also whether these mechanisms are present in other regions.

4.6 Disclosure/Conflict-of-Interest Statement

The authors declare that the research was conducted in the absence of any commercial or financial relationships that could be construed as a potential conflict of interest.

4.7 Author Contributions

MC, SGC and IS analyzed data. MC, SGC, IS and MM wrote code. MC and DE programmed the simulations. EK and JG collected the data. IS and MM designed the study. MC, SGC, IS and MM wrote the paper. MC wrote the supplementary material. All authors proofread the manuscript.

4.8 Acknowledgments

We would like to thank Edvard and May-Britt Moser for agreeing in the use of data that EK collected as a postdoc in their lab. We also thank Daniel Squirrell and Claire Scofield for their help in collecting the data from anesthetized rats. MC wishes to thank Juan F Ramirez-Villegas for comments on the manuscript.

Funding: MC was funded by a Doctoral Training Partnership PhD Studentship awarded to the University of Manchester by the UK Biotechnology and Biological Sciences Research Council (BBSRC DTP grant code: BB/J014478/1) and a President's Doctoral Scholar Award by the University of Manchester. SGC and IS were supported by Consejo Nacional de Investigaciones Científicas y Técnicas (grant code: PIP 11220090100738) and Universidad Nacional de Cuyo. SGC, EK, IS and MM were supported by Proyecto Raíces Siembra of Agencia Nacional de Promoción Científica y Tecnológica.

4.9 Supplementary Material

4.9.1 Supplementary Methods

4.9.1.1 Bursting neuron model

The equations and parameters of the bursting neuron model have been published before in Constantinou et al. (2015) and are included here for completion. The model

consisted of two compartments: dendrites and soma. The input signal $I(t)$ was injected in the dendritic compartment and bursting activity was recorded from the somatic compartment as described in Supplementary Equations 4.5 and 4.6, respectively.

$$C_m \frac{dV_d}{dt} = -I_L - I_{KS} - I_{NaP} - g_c \frac{V_d - V_s}{1-p} + I(t) \tag{4.5}$$

$$C_m \frac{dV_s}{dt} = -I_L - I_K - I_{Na} - g_c \frac{V_s - V_d}{p} \tag{4.6}$$

The equations of the ionic currents and the model parameters are listed in Supplementary Tables 4.1 and 4.2, respectively. The 4^{th} order Runge-Kutta method with 0.01 ms time step was used for numerical integration of the model.

4.9.1.2 Discretization of LFP feature signals

LFP features (voltage, slope, phase and amplitude) vary continuously. However, estimating the probability of continuous LFP features from a finite sample would result in an enormous bias. Hence, the continuous signal was discretized into a finite number of bins M chosen by optimizing the trade-off between being large enough to preserve most of the information and, at the same time, small enough to reduce the bias, as in Elijah et al. (2015). In short, we varied M and, for each value, obtained the feature set X, from which we computed the mutual information $I(X;N) = I(X) - I(X|N)$, the bias estimate $I_s(X;N) = \langle I(X) - I(X|N_s) \rangle$ (where $\langle ... \rangle$ indicates average over 100 repetitions), and the bias-corrected information $I_c(X;N) = I(X;N) - I_s(X;N)$. We computed these measures for the burst distinction code with no time lag, so that $N = \{1,2,3\}$ and X comprised the features occurring at the time of burst onset.

The results were similar for all bursting neurons (example in Supplementary Figure 4.15). When $M < 2^2$, the information measures were underestimated; whereas when $M > 2^3$, there was considerable bias in the information estimate $I(X;N)$ as depicted by the diverging lines of $I(X;N)$ and the bias-corrected information estimate $I_c(X;N)$. The bias correction method we used was sufficient to correct for this as indicated by the plateau of $I_c(X;N)$ (Supplementary Figure 4.15). Since there was no considerable gain in information by using $M > 2^2$, LFP features were discretized with $M = 4$.

4.9.1.3 Relation between the three burst codes

This section explains how we used the chain rule for mutual information to derive the equation $I(X;\{0,1,2,3\}) = I(X;\{0,\text{burst}\}) + r\delta t\, I(X;\{1,2,3\})$ which relates the three codes we investigated.

In the full burst code: $N=\{0,1,2,3\}$, in the burst rate code: $N=\{0,\text{burst}\}$, and in the burst distinction code: $N=\{1,2,3\}$. We define the variables

$$\begin{aligned} W &= \{0,1,2,3\}, \\ Y &= \{0,\text{burst}\}, \\ Z &= \{1,2,3\}. \end{aligned} \tag{4.7}$$

Since the three variables arise from the same neural response, Y is a deterministic function of W,

$$Y(W)=\begin{cases} 0 & \text{if } W=0, \\ \text{burst} & \text{if } W\neq 0. \end{cases} \tag{4.8}$$

When $Y=\text{burst}$, the variable Z is also a deterministic function of W,

$$Z(W)=\begin{cases} W & \text{if } W>0, \\ \text{not defined} & \text{if } W=0. \end{cases} \tag{4.9}$$

The chain rule states that for any three variables X, A, B,

$$I(X;A,B)=I(X;A)+I(X;B|A). \tag{4.10}$$

If we take $A=W$ and $B=Y$, the chain rule becomes

$$I(X;W,Y)=I(X;W)+I(X;Y|W). \tag{4.11}$$

The deterministic rule of Supplementary Equation 4.8 implies that $H(Y|W)=0$, so Y cannot transmit information about any variable, when conditioned on W. That is, $I(X;Y|W)=0$. Hence, Supplementary Equation 4.11 reduces to

$$I(X;W,Y)=I(X;W). \tag{4.12}$$

If we now take $A=Y$ and $B=W$, the chain rule becomes

$$I(X;Y,W)=I(X;Y)+I(X;W|Y). \tag{4.13}$$

In addition,

$$\begin{aligned} I(X;W|Y) &= P(y=0)\sum_{x\in X}\sum_{w\in W}P(x,w|y=0)\log\frac{P(x,w|y=0)}{P(x|y=0)P(w|y=0)}+ \\ &+ P(y=\text{burst})\sum_{x\in X}\sum_{w\in W}P(x,w|y=\text{burst})\log\frac{P(x,w|y=\text{burst})}{P(x|y=\text{burst})P(w|y=\text{burst})} \end{aligned} \tag{4.14}$$

Supplementary Equation 4.8 implies that when $y=0$, there is no alternative but to have $w=0$. Therefore, in the first term of Supplementary Equation 4.14, only the

term with $w = 0$ appears, for all others, $P(x, w|y = 0)$ vanishes. Moreover, $P(x, w = 0|y = 0) = P(x|y = 0)$, so the first term vanishes. Similarly, Supplementary Equation 4.9 implies that when $y = \text{burst}$, w is equal to z, and $P(x, w|y = \text{burst}) = P(x, z)$. Therefore, Supplementary Equation 4.13 becomes

$$I(X; Y, W) = I(X; Y) + P(Y = \text{burst})I(X; Z). \tag{4.15}$$

Given that $P(Y = \text{burst}) = r\delta t$, and taking Supplementary Equation 4.12 into account, we get

$$I(X; W) = I(X; Y) + r\delta t \; I(X; Z). \tag{4.16}$$

4.9.2 Supplementary Results

Theta rhythms can be separated in two types based on their sensitivity to atropine (Kramis et al., 1975). Urethane preserves the atropine-sensitive theta (3-7 Hz) but eliminates the atropine-resistant theta (7-12 Hz) (Kramis et al., 1975; Clement et al., 2008). We observed that, under urethane anesthesia, the LFP of three rats exhibited shifts in which either delta (∼1 Hz) or theta rhythms (∼4 Hz) were dominant (example in Supplementary Figure 4.13). We identified 13 bursting units during the epochs containing dominant theta rhythms under anesthesia. These units were also bursting during epochs of dominant delta rhythms. We analyzed these data separately for the theta-dominant epochs and present the results here.

We investigated whether these cells encoded features of theta rhythms in their bursting output. Eleven cells showed evidence of encoding the instantaneous voltage, slope and phase of theta rhythms by the full burst code and the burst rate code (examples in Supplementary Figures 4.19A-B,D-E and 4.20A-D); and five of these cells also encoded the instantaneous amplitude. For the latter cells, the information encoded for voltage, slope and phase was twice to ten times higher than of amplitude. Four of the encoding cells also showed evidence of feature encoding by the burst distinction code (example in Supplementary Figures 4.19C and 4.20E-H). One cell encoded most information about the instantaneous amplitude of theta rhythms, and less about the voltage and slope, by the full burst code and burst rate code. These results suggest that bursting neurons can encode information conveyed by atropine-sensitive theta rhythms during anesthesia.

4.9.3 Supplementary Tables and Figures

Table 4.1: Equations describing the ionic currents of the two-compartment model. The last row shows the kinetics equation of the gating variables for the Na, K and slow K currents.

Na current	$I_{Na} = g_{Na} m_\infty^3 h(V_s - E_{Na})$
	$m_\infty = \alpha_m/(\alpha_m + \beta_m)$
	$\alpha_m = -0.1(V_s+31)/(\exp(-0.1(V_s+31))-1)$
	$\beta_m = 4\exp(-(V_s+56)/18)$
	$\alpha_h = 0.07\exp(-(V_s+47)/20)$
	$\beta_h = 1/\exp(-0.1(V_s+17))+1)$
K current	$I_K = g_K n^4(V_s - E_K)$
	$\alpha_n = -0.01(V_s+34)/(\exp(-0.1(V_s+34))-1)$
	$\beta_n = 0.125\exp(-(V_s+44)/80)$
Persistent Na current	$I_{NaP} = g_{NaP} r_\infty^3(V_d - E_{Na})$
	$r_\infty = 1/(\exp(-(V_d+57.7)/7.7)+1)$
Slow K current	$I_{KS} = g_{KS} q(V_d - E_K)$
	$q_\infty = 1/(\exp(-(V_d+35)/6.5)+1)$
	$\tau_q = \tau_{q_0}/(\exp(-(V_d+55)/30)+\exp((V_d+55)/30))$, $\tau_{q_0} = 200$
Leak currents	$I_L = g_L(V - E_L)$, where $V = V_d$ or V_s
Kinetics of gating variables	$dx/dt = \phi_x(\alpha_x(1-x) - x\beta_x) = \phi_x(x_\infty - x)/\tau_x$, where $x = h$, n or q

Table 4.2: Parameters of the two-compartment model.

Reversal potentials (mV)	E_{Na}	55
	E_K	-90
	E_L	-65
Maximum conductances (mS/cm^2)	g_{Na}	45
	g_K	15
	g_L	0.18
	g_{NaP}	0.08
	g_{KS}	0.7
Coupling conductance (mS/cm^2)	g_c	1
Membrane capacitance (μF/cm^2)	C_m	0.6
Relative area between compartments	p	0.15
Temperature scaling factors	ϕ_h	3.33
	ϕ_n	3.33
	ϕ_q	1

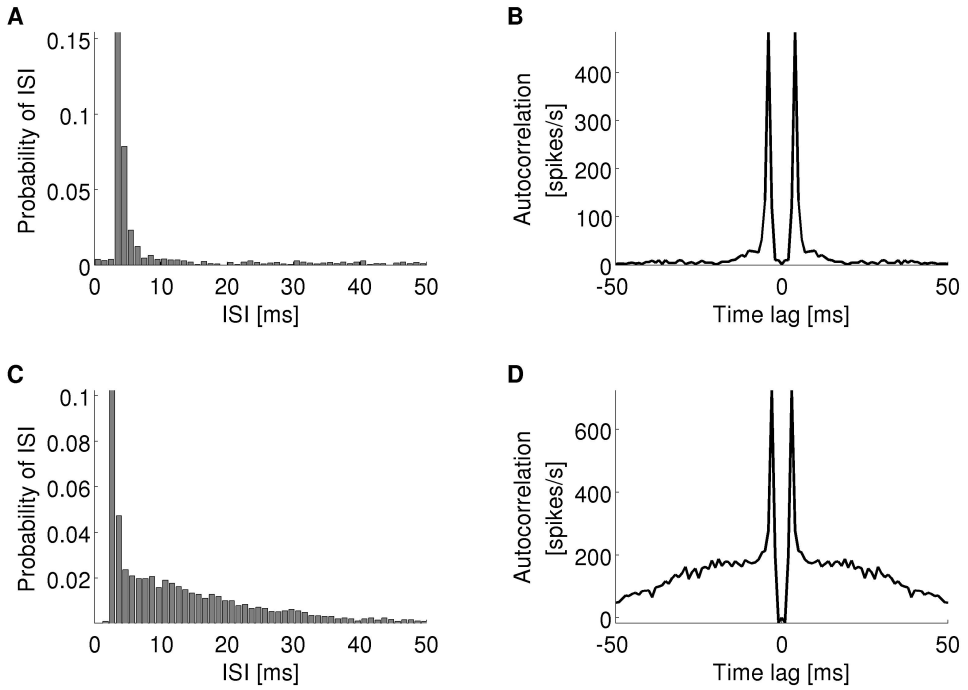

Figure 4.12: Example of ISI histograms **(A,C)** and autocorrelograms **(B,D)** of a busting unit in the subiculum **(A,B)** and the MEC **(C,D)**. A unit was classified as bursting if there was a sharp peak within 2-8 ms for subiculum **(A,B)** or 2-5 ms for MEC **(C,D)** in the autocorrelogram and ISI histogram but not another peak within 50 ms.

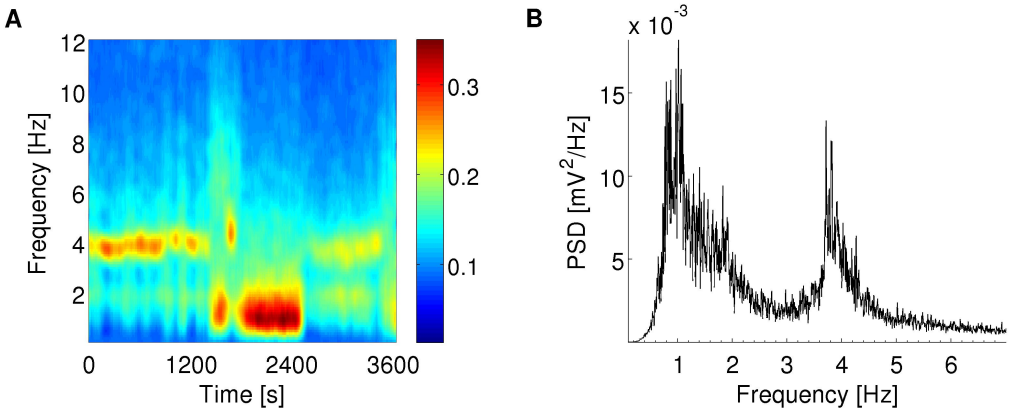

Figure 4.13: Example of spectrogram **(A)** and power spectrum **(B)** of the LFP recorded by an electrode in the subiculum of a urethane-anesthetized rat. The LFP shifts between states in which there is a spectral peak at either ∼1 Hz or ∼4 Hz. [**A**: The color scale is in $(\mathrm{mV}^2/\mathrm{Hz})^{0.25}$. Warmer colors indicate higher power spectral density.]

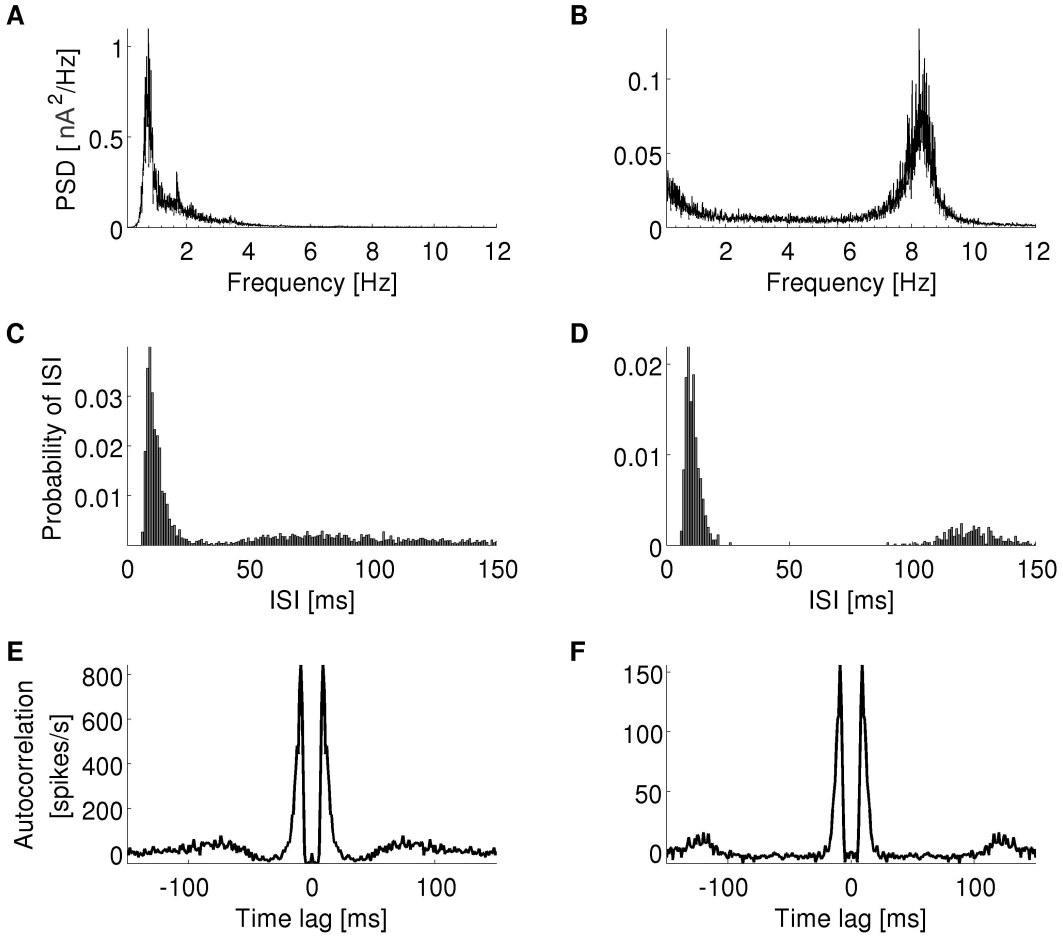

Figure 4.14: Power spectra of input signals to the model containing peaks at delta rhythms **(A)** or theta rhythms **(B)**. ISI histograms **(C,D)** and autocorrelograms **(E,F)** of the spiking output of the model when the input had the corresponding spectra in **A,B**.

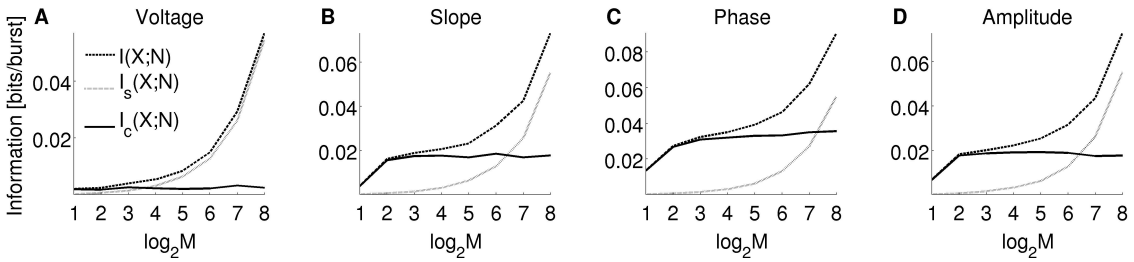

Figure 4.15: Information and bias estimates as a function of the number of bins M used to discretize the instantaneous voltage **(A)**, slope **(B)**, phase **(C)** and amplitude **(D)** of the LFP. Information measures were estimated for the burst distinction code at the time of burst onset. This example is for the same unit as in Figure 4.3D-F.

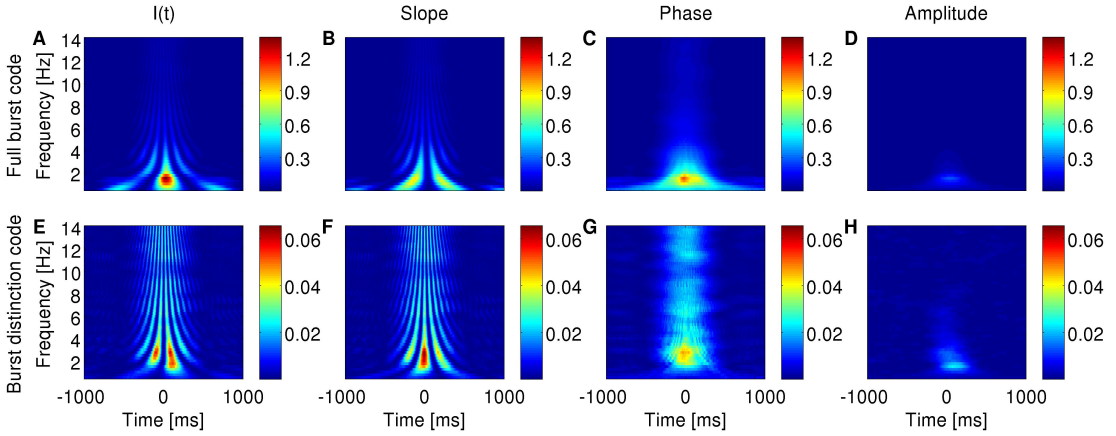

Figure 4.16: Information encoded by the bursting neuron model about features of the input signal $I(t)$ as a function of frequency and time around burst onset. For these simulations, $I(t)$ contained dominant delta rhythms to mimic the LFP rhythms present during anesthesia. Information about the instantaneous $I(t)$ **(A,E)**, slope **(B,F)**, phase **(C,G)** and amplitude **(D,H)** of narrowband-filtered $I(t)$ conveyed by the full burst code **(A-D)** and burst distinction code **(E-H)**. Colorbar: mutual information in bits/burst.

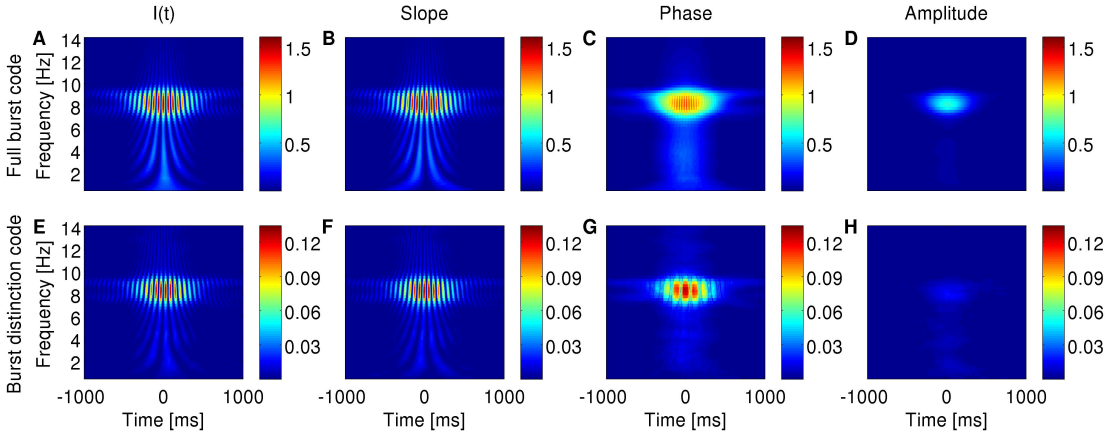

Figure 4.17: Information encoded by the bursting neuron model about features of the input signal $I(t)$ as a function of frequency and time around burst onset. For these simulations, $I(t)$ contained dominant theta rhythms to mimic the LFP rhythms present during exploratory behavior. Information about the instantaneous $I(t)$ **(A,E)**, slope **(B,F)**, phase **(C,G)** and amplitude **(D,H)** of narrowband-filtered $I(t)$ conveyed by the full burst code **(A-D)** and burst distinction code **(E-H)**. Colorbar: mutual information in bits/burst.

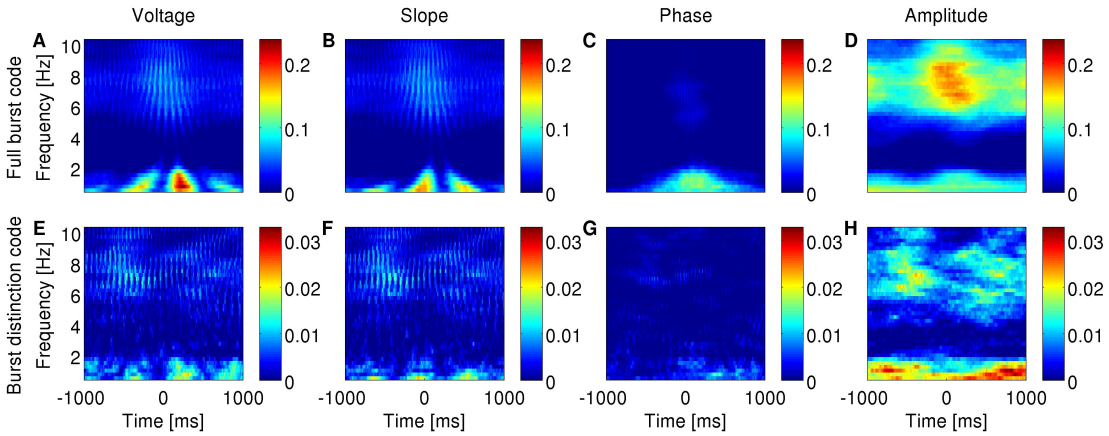

Figure 4.18: Information encoded by bursting neuron output about LFP features as a function of LFP frequency and time around burst onset. Example from a bursting unit in the rat subiculum during dominant delta rhythms under urethane-anesthesia. Information about the instantaneous voltage **(A,E)**, slope **(B,F)**, phase **(C,G)** and amplitude **(D,H)** of narrowband-filtered LFP conveyed by the full burst code **(A-D)** and burst distinction code **(E-H)**. Colorbar: mutual information in bits/burst.

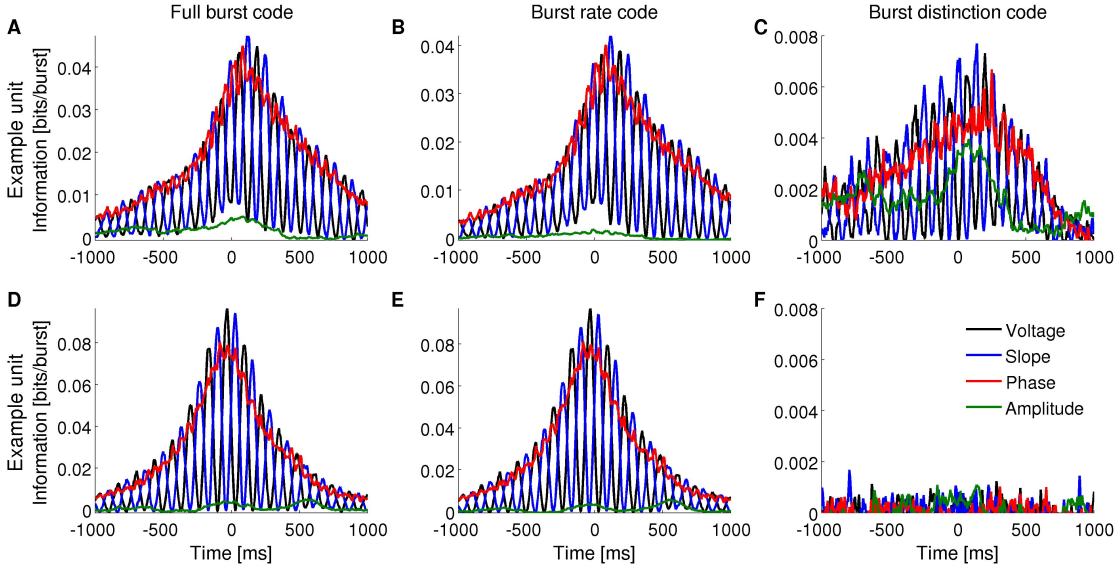

Figure 4.19: Information encoded by bursting output of two different subicular cells **(A-C** and **D-F)** about the voltage, slope, phase and amplitude of theta rhythms in the LFP during urethane-anesthesia. Both cells encode information about the voltage, slope and phase of theta-filtered LFP by the full burst code **(A,D)** and burst rate code **(B,E)**. One of the cells encodes information about LFP features in the distinction between different burst sizes **(C)** whereas the second does not **(F)**. LFPs were filtered within 2.5-5 Hz. x-axis: time relative to burst onset defined at 0 ms.

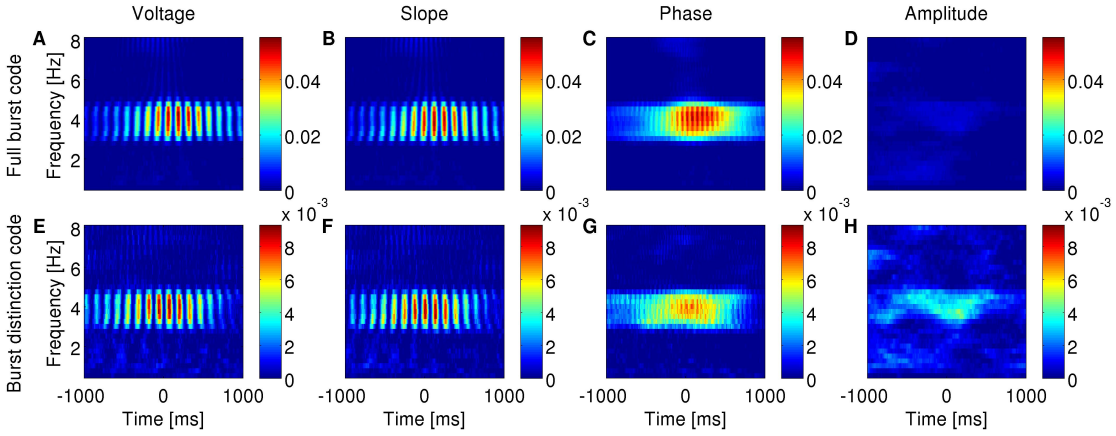

Figure 4.20: Information encoded by bursting neuron output about LFP features as a function of LFP frequency and time around burst onset. Example from a bursting unit in the rat subiculum during dominant theta rhythms under urethane-anesthesia. Information about the instantaneous voltage **(A,E)**, slope **(B,F)**, phase **(C,G)** and amplitude **(D,H)** of narrowband-filtered LFP conveyed by the full burst code **(A-D)** and burst distinction code **(E-H)**. Colorbar: mutual information in bits/burst.

Chapter 5

Paper 3

Information transfer by LFP rhythms within the hippocampal formation

Maria Constantinou*, Daniel Squirrell, John Gigg, Marcelo A. Montemurro

Faculty of Biology, Medicine and Health, The University of Manchester, Manchester, M13 9PT, UK

**Corresponding author at: Faculty of Biology, Medicine and Health, The University of Manchester, Oxford Road, Manchester M13 9PT, UK.*
E-mail address: maria.constantinou@manchester.ac.uk (M. Constantinou).

Keywords: Local field potential, Hippocampus, Subiculum, Delta rhythm, Theta rhythm, Information transfer

5.1 Abstract

The hippocampal formation is vital for declarative memory. Increasing evidence suggests that rhythms in the electrical potential recorded from the extracellular medium as the local field potential (LFP) are involved in exchanging information for this cognitive processing. However, the mechanisms by which LFP can transfer information are still not clear. We addressed this question by investigating how interactions of LFP rhythms can transfer information between hippocampal area CA1 and subiculum. These structures form the last processing point before projecting hippocampal output to cortical and subcortical areas. We analysed simultaneous LFPs recorded from multiple electrodes positioned along the depth of area CA1 and subiculum in anaesthetised mice. We used information theoretic methods to quantify how much information can be transmitted by LFP rhythms as well as to determine the direction of information flow within the CA1-subicular circuit. We show that delta and theta rhythms can act as two

independent channels that transmit segregated information. Most of the information is conveyed by linear correlations in the LFP signals. In particular, interactions of the phase of delta or theta rhythms transmit most of the information, and a smaller fraction of information is transmitted by the amplitude of these rhythms. Moreover, we show that information transfer is bidirectional comprising both feedforward and feedback connections. These results agree with the anatomical connectivity between area CA1 and subiculum and suggest that information is dynamically processed in bidirectional loops.

5.2 Introduction

The hippocampal formation is a compound structure which is essential for memory formation (Scoville and Milner, 1957; Squire, 2009) and spatial navigation (O'Keefe and Dostrovsky, 1971; O'Keefe and Nadel, 1978). The anatomy of this system has been well studied (reviewed in Amaral and Witter (1989); O'Mara et al. (2001)). The hippocampus receives input from the entorhinal cortex and projects to the subiculum which, in turn, projects the hippocampal output to cortical and subcortical areas. Reciprocal projections between these structures also provide feedback at each stage of information processing (O'Mara et al., 2001). The anatomical connectivity within the hippocampal formation is non-homogeneous suggesting that information is processed in interconnected loops (Gigg, 2006).

Cognitive functions are dynamic, occurring at millisecond timescales during which the anatomical connections are fixed. At these timescales, firing of action potentials, which last for ∼1 ms, can transmit neural messages along anatomical projections (Hodgkin and Huxley, 1939). However, neural networks might process information about a number of cognitive functions simultaneously which may result in unwanted interference by ongoing unrelated information processes. This implies the existence of a mechanism by which relevant information about a cognitive task is effectively routed along anatomical connections without interference by unrelated processes. However, such a mechanism of dynamically routing information remains an open question.

Increasing evidence suggests that electrical potential fluctuations in the extracellular medium of the brain, often recorded as the local field potential (LFP), are involved in this dynamic information processing. LFP rhythms have been proposed to 'bind' information from distant networks for cognitive processing including working memory, attention and perception (Engel and Singer, 2001). LFP rhythms can provide a timeframe for neuronal interactions (reviewed in Fries (2005); Sirota and Buzsaki (2005); Panzeri

et al. (2010)). In particular, LFP rhythms allow for temporal windows during which coherent activity can exchange information whereas absence of coherence can block information flow (Fries, 2005). According to this, synchronised rhythms (indicated by high correlations) between distant neural networks are thought to allow for the exchange of information, whereas desynchronised rhythms (uncorrelated) prevent information exchange (Fries, 2005). Computational studies have provided evidence that LFP interactions can dynamically route information along fixed anatomical connnections (Battaglia et al., 2012). However, the exact details of how LFP interactions effectively connect neural networks in the mammalian brain *in-vivo* is still not known.

LFP in the hippocampal formation have been associated with several cognitive functions. For instance, theta and gamma rhythms are associated with memory retention (Lisman and Idiart, 1995) and spatial navigation (O'Keefe and Recce, 1993; Skaggs et al., 1996), and delta rhythms with memory consolidation (Molle and Born, 2011; Rasch and Born, 2013). Despite the importance of the information processing by the output part of the hippocampal formation, little is known about how LFP rhythms in area CA1 and subiculum interact to exchange information.

We sought to determine the intrinsic dynamics by which LFP rhythms route information among the two networks by analysing LFP recordings from area CA1 and subiculum of anaesthetised mice. We show that delta and theta rhythms can act as two separate channels to transmit information from area CA1 to subiculum and vice versa. Most of the information was transmitted by linear correlations in the rhythms and more specifically by the phase of delta and theta rhythms. Our results suggest that interactions in the phase of LFP rhythms can dynamically route information along anatomical connections.

5.3 Methods

5.3.1 *In vivo* electrophysiology

All experimental procedures were carried out in accordance with the Animals (Scientific Procedures) Act UK 1986. Ethical approval was provided by the University of Manchester Ethical Review Panel. Seven male 3-4 month-old C57/129sv mice (LaFerla lab, University of California, USA) were used. Mice were group-housed in a pathogen-free environment with food and water available *ad libitum* and kept on a 12-h light:dark cycle.

Anaesthesia was induced with urethane (30% w/v in 0.9% saline, i.p., 1.5-1.7 g/kg) followed by additional doses (10% w/v in 0.9% saline, 50 μl) if required after approximately

30-minute intervals to achieve areflexia. Tracheotomy (Moldestad et al., 2009) was performed to sustain breathing and survival. Body temperature was kept at 37°C using a homeothermic blanket and monitored with a rectal thermometer. Mice were head-fixed in a stereotaxic frame (Kopf 1430, USA) and 2-mm diameter craniotomies were carried out with a high-speed hand held drill (Foredom, USA) and 0.9-mm drill bit (Fine Science Tools, Germany) at B: -1.5 mm, ML: 1.7 mm for hippocampal area CA1 and B: -2.8 mm, ML: 1.7 mm for subiculum based on the Franklin and Paxinos (2007) mouse brain atlas coordinate system.

Two 2×16 electrode probes (A2×16-10-100-500-413, NeuroNexusTech, USA) were inserted at 20° and 25° compound angles from the vertical axis in area CA1 and subiculum, respectively, so as to align with the main dendritic axis of pyramidal neurons. Each probe comprised two shanks containing sixteen 413 μm^2 recording sites with 100 μm vertical and 500 μm horizontal distance between sites. The probes were attached to an electrode board and headstage (Plexon, USA) with fixed gain of 20× and an AC preamplifier giving a total gain of 2000× (Recorder64, Plexon, USA) and recordings were ground referenced to the stereotaxic frame. Electrode positions were verified by histological examination of CM-DiI labelling with fluorescence microscopy.

Spontaneous LFP (2 kHz sampling rate, low-pass filtered up to 250 Hz) were recorded simultaneously from the electrodes in area CA1 and subiculum for at least 25 minutes.

5.3.2 Spectral analysis

The frequency composition of the LFP recorded at each electrode in hippocampal area CA1 and subiculum was computed by Welch's periodograms with 50% overlapping Hamming windows of 180 s. Spectrograms with 50% overlapping Hamming windows of 2 s were used to identify changes in the power of LFP rhythms over time. The spectrograms presented here were smoothed with a moving window of 200 ms to avoid excessive pixelation of the printed images.

5.3.3 LFP filtering

LFP were resampled to 200 Hz to improve computation time. Decimation was used to prevent aliasing. LFP were bandpass-filtered using a finite impulse response (FIR) digital filter with Kaiser window (sharp transition bandwidth: 1.0 Hz, stopband attenuation: 60 dB, passband ripple: 0.01 dB). On the basis of spectral analysis, the cutoff frequencies were 0.5 Hz and 2.0 Hz for the delta rhythm or 2.5 Hz and 4.5 Hz for the theta rhythm.

Phase and amplitude were extracted as the angle and modulus, respectively, of the Hilbert transform of the bandpass-filtered LFP.

5.3.4 Multiple surrogates method

Surrogate LFP signals were created for each pair of LFP signals from area CA1 and the subiculum as described in Prichard and Theiler (1994) so that the surrogates contained only linear temporal correlations but no non-linear correlations. To construct these surrogates: (1) the LFP time series of a pair of recordings were transformed in the frequency domain by the Fourier transform so that the phase and amplitude could be decomposed, (2) the phases were 'randomised' by rotating each phase of each Fourier component by a random variable phase which was the same for the two signals, and (3) the signals were converted back to the time representation by the inverse Fourier transform. The resulting pairs of surrogate signals had linear autocorrelations and cross-correlations but no non-linear correlations.

5.3.5 Transfer entropy

Transfer entropy (TE) is a directional information theoretic measure based on the Wiener-Granger causality principle (Schreiber, 2000). This measure can be used to quantify the information transfer between two LFP signals and also reveal the direction of this information flow because it incorporates past values of the signals. To compute the TE, we implemented a similar procedure to Besserve et al. (2010). The LFP signals were discretised so that all possible values of LFP belonged in one of four equipopulated bins.

For a pair of LFP signals X and Y recorded simultaneously, the TE from Y to X is given by:

$$T(Y \rightarrow X) = H(X_{t+\tau}|X_t) - H(X_{t+\tau}|X_t, Y_t) \tag{5.1}$$

where t indicates a given time point and τ is a variable time lag between the two signals. $H(X_{t+\tau}|X_t)$ is the conditional entropy of the future value $X_{t+\tau}$ conditioned to the present value X_t, and $H(X_{t+\tau}|X_t, Y_t)$ is the joint entropy of the present value Y_t and the future value $X_{t+\tau}$ conditioned to the present value X_t. If no information is transferred from Y to X at a given time lag, the TE value will be zero. A positive TE indicates the amount of information that can be predicted about signal X by only observing the present values of signal Y.

Computing the entropies from finite data can give rise to sampling bias in the estima-

tions (reviewed in Panzeri et al. (2007)). To correct for this bias, a shuffling method similar to Besserve et al. (2010) and Constantinou et al. (2016) was implemented. For a given time point t, the pairs of X_t and $X_{t+\tau}$ were shuffled relative to Y_t, while X_t and $X_{t+\tau}$ were kept the same relative to each other. This method destroyed the correlations between the future values $X_{t+\tau}$ and the present values Y_t, and at the same time preserved the correlations between the present X_t and past $X_{t+\tau}$. Shuffling was repeated 100 times for each time lag τ. For each repetition, the shuffled TE was computed from the shuffled data by Equation 5.1. The bias was estimated as the average of the shuffled TE for all repetitions. The bias-corrected TE for a pair of LFP signals was then computed by subtracting the bias estimate for that given pair from the TE estimate computed from the actual data.

TE estimates for a pair of LFP signals were considered statistically significant if they were greater than all 100 estimates of shuffled transfer entropy for that pair of LFP signals. With this criterion, transfer entropy estimates from all pairs of recordings were statistically significant and thus were included in the population analyses.

5.4 Results

We investigated how LFP transmit information between the hippocampus and the subiculum. We analysed LFPs recorded from six equidistant electrodes spanning 500 μm along the depth of hippocampal area CA1 and subiculum of seven mice. The LFP recordings were from two parallel shanks of electrodes placed 500 μm apart in area CA1 of six mice and in the subiculum of five mice, or from one shank in area CA1 and subiculum of the other one and two mice, respectively.

5.4.1 Spontaneous shifts in brain state

The LFPs in area CA1 and subiculum of each mouse exhibited two prominent rhythms which either coexisted or shifted between each other. For each mouse, the LFP rhythms were very similar across the whole span of area CA1 and subiculum from which the recordings were obtained. Three example cases are shown in Figure 5.1. In one of the mice, there was a prevalent peak at ∼1–2 Hz (Figure 5.1A) which was persistent during most of the recording. There were also transient changes in the network state in which rhythms of ∼2.5-4 Hz became prevalent (Figure 5.1B). In the second case, there was a strong rhythm at ∼3.5 Hz which also co-occured with a weaker ∼1–2 Hz rhythm (Figure 5.1C-D). This pattern was observed in three mice. In the third case, both rhythms co-existed (Figure 5.1E-F), and this was observed in three mice. The slower rhythm

corresponds to delta rhythms or slow oscillations, and the higher band corresponds to theta rhythms under urethane anaesthesia (Pagliardini et al., 2013b). The two bands are hereafter referred to as delta and theta rhythms. These two rhythms were extracted from the LFP by bandpass-filtering within 0.5-2 Hz or 2.5-4.5 Hz and analysed separately to determine their role in information transmission within the CA1-subicular circuit.

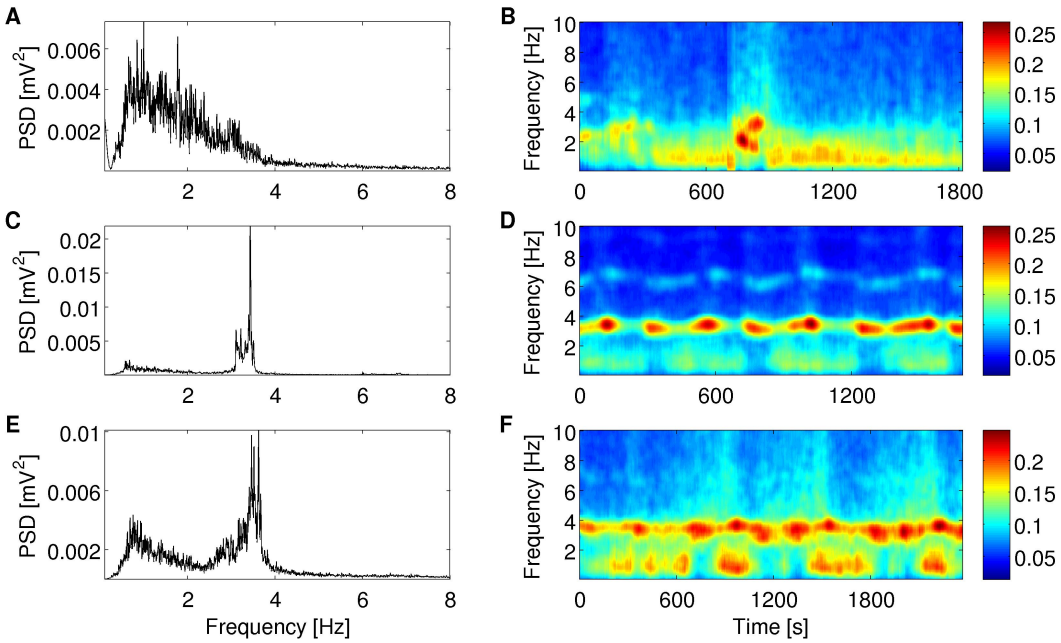

Figure 5.1: Examples of power spectra (A, C and E) and spectrograms (B, D and F) of LFP recorded by an electrode in hippocampal area CA1 of three different anaesthetised mice (A-B, C-D and E-F). B, D and F: Color scale in $(mV^2/Hz)^{0.25}$. Warmer colors indicate higher power spectral density (PSD).

5.4.2 Information transfer by LFP rhythms

We investigated whether interactions of delta or theta rhythms can communicate information between hippocampal area CA1 and subiculum. We quantified the amount of information that can be transmitted between pairs of electrodes in area CA1 and subiculum using the TE measure, which also reveals the direction of information flow. To capture the temporal extent by which these interactions take place we computed the TE for different time lags between the signals. Examples from three pairs of electrodes in area CA1 and subiculum of three different mice are shown in Figure 5.2. These examples are from the same mice as the examples presented in Figure 5.1.

The information exchange by delta and theta rhythms was bidirectional. That is, information was transferred from area CA1 to subiculum and vice versa. The amount of information transferred between area CA1 and subiculum oscillated with varying time

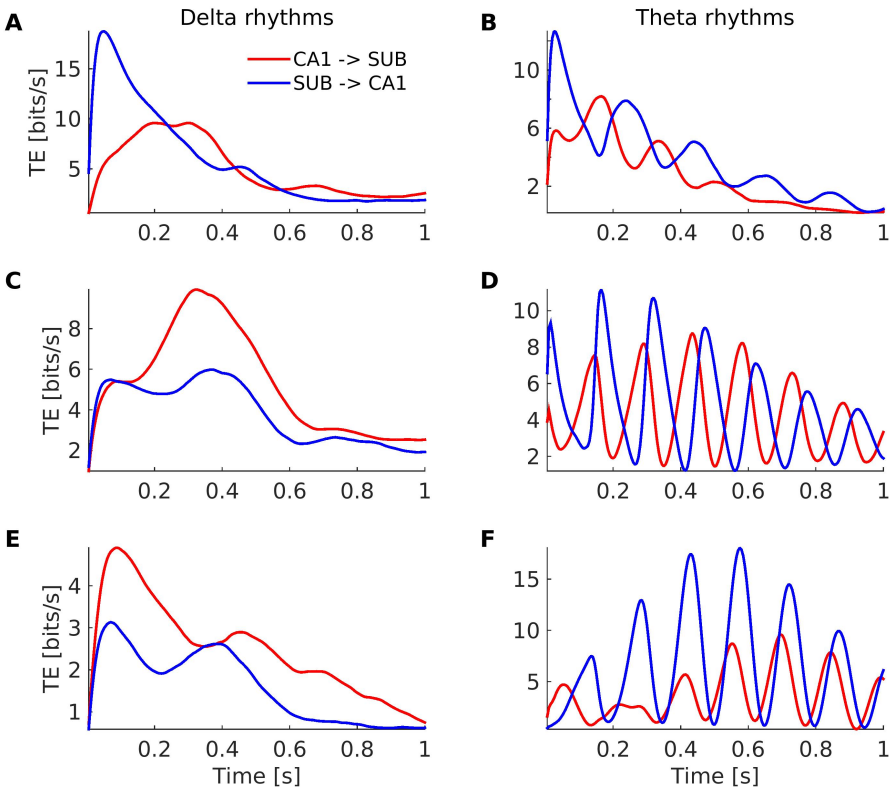

Figure 5.2: Examples of information transfer between hippocampal area CA1 and subiculum (Sub) by delta-filtered (A, C and E) and theta-filtered LFP (B, D and F). Each row (A-B, C-D and E-F) shows an example from a different mouse. Each example is from the same pair of LFP signals recorded in area CA1 and subiculum.

lag between the LFP signals of the two regions. The peaks and troughs in TE occurred at slightly different time delays (in the range of a few milliseconds) for each direction (Figure 5.2).

For all pairs of LFP signals, the frequency of TE oscillations depended on the frequency of the LFP rhythms. For delta rhythms, the TE oscillated across the time lag with a frequency of ∼1-2 Hz (Figure 5.2A, C and E); whereas for theta rhythms, the TE oscillations were ∼5-7 Hz (Figure 5.2B, D and F), that is almost double the investigated theta band frequency. These oscillations could arise because of the correlations within each LFP rhythm. That is for a rhythm with a given frequency, the instantaneous LFP value at a present time point depends on its past and future values.

The TE oscillations were synchronous for all pairs of electrodes within each animal. The average TE across all pairs in each mouse were computed and example averages from three mice are shown in Figure 5.3. These examples are for the same mice shown in Figure 5.2. The TE oscillations were preserved in the averages across LFP pairs in

an animal (Figures 5.2 and 5.3). This result indicates that the timing of TE peaks and troughs is consistent for all LFP pairs suggesting that information flow from area CA1 to subiculum, or vice versa, is homogeneous along the span of the recorded regions. However, the TE oscillations across time lag differed between animals (Figure 5.3).

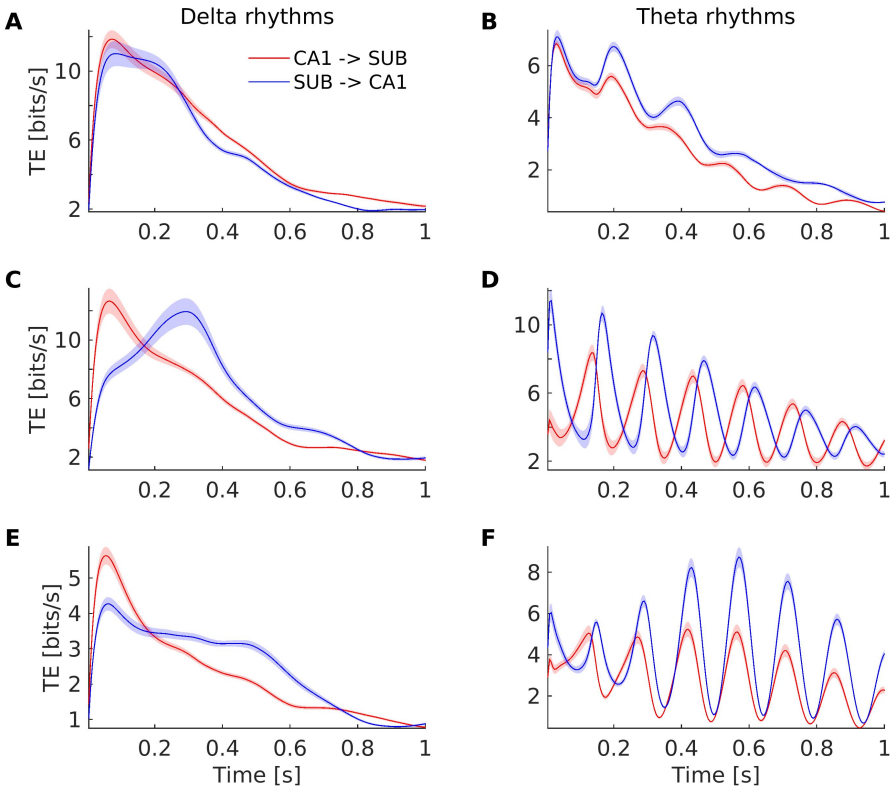

Figure 5.3: Average information transfer between hippocampal area CA1 and subiculum (Sub) by delta-filtered (A, C and E) and theta-filtered LFP (B, D and F). Each row (A-B, C-D and E-F) shows the averages across all pairs of electrodes in a different mouse (corresponding to the mice in Figure 5.2). Shadow shows the standard error of mean (SEM).

5.4.3 Information transfer by LFP phase and amplitude

What interactions between LFP rhythms mediate the information exchange in the CA1-subicular circuit? The information could be transmitted by phase-phase or amplitude-amplitude interactions of rhythms having the same frequency. To quantitatively compare the contribution of phase and amplitude in information transfer, we decomposed the bandpass-filtered LFP into its phase and amplitude and computed the information transferred by either phase-phase (Figure 5.4) or amplitude-amplitude (Figure 5.5) interactions in the LFP signals.

On average, the amount of information transferred by interactions in delta phase or

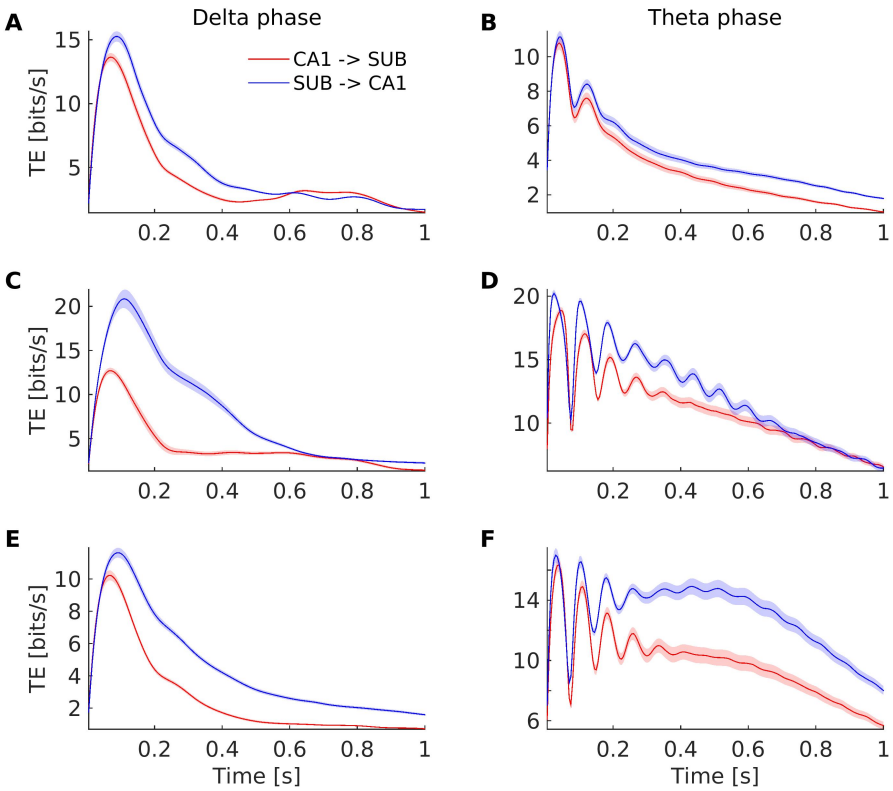

Figure 5.4: Average information transfer between hippocampal area CA1 and subiculum (Sub) by the phase of delta (A, C and E) and theta rhythms (B, D and F). Each row (A-B, C-D and E-F) shows the averages across all pairs of electrodes in a different mouse (corresponding to the mice in Figure 5.2). Shadow shows the SEM.

theta phase (Figure 5.4) was almost double than the information transferred by the instantaneous voltage of the bandpass-filtered LFP (Figure 5.3). In contrast, delta amplitude and theta amplitude interactions (Figure 5.5) conveyed either similar or less amount of information than the instantaneous voltage (Figure 5.3).

5.4.4 Information transfer by linear correlations in LFP

We further investigated how much information can be conveyed only by linear interactions in the LFP signals. To achieve this, we created surrogates from the pairs of LFP signals that preserved the linear cross-correlations in the signals but removed all non-linear interactions. TE analysis revealed that the surrogate signals conveyed almost the same amount of information as the LFP signals (Figures 5.6, 5.3 and 5.7). This result suggests that linear correlations in the LFP signals are sufficient to transmit information between neural networks.

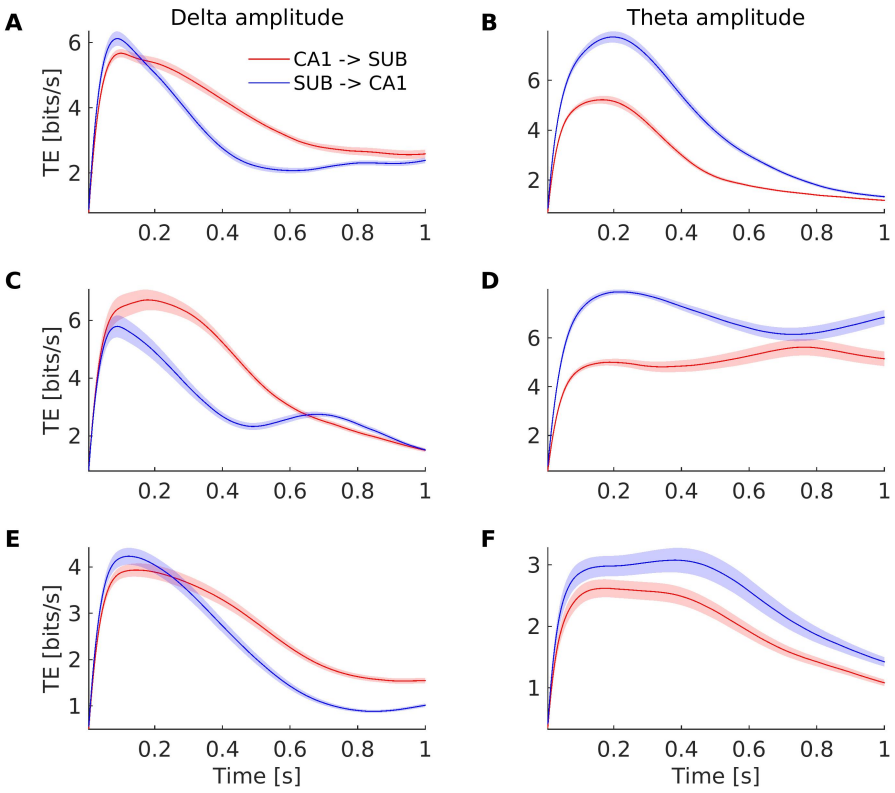

Figure 5.5: Average information transfer between hippocampal area CA1 and subiculum (Sub) by the amplitude of delta (A, C and E) and theta rhythms (B, D and F). Each row (A-B, C-D and E-F) shows the averages across all pairs of electrodes in a different mouse (corresponding to the mice in Figure 5.2). Shadow shows the SEM.

5.4.5 Population analysis of information transfer

As already mentioned, information transfer between different pairs of electrodes in area CA1 and subiculum varied considerably across animals. Since the TE across time had an oscillatory pattern, averaging across animals by parametric statistics (computing the mean and standard deviation or standard error of mean) would not be an appropriate method to represent these results. Instead, the data from all pairs were pooled and non-parametric statistics were used to represent the important aspects of the results.

For each rhythm and each pair of electrodes, we identified the time delay at which information transfer was maximal for each direction and the associated maximal information transferred. These quantities are summarised in box plots shown in Figures 5.7 and 5.8. The distributions of maximal information transferred in either direction (area CA1 to subiculum or subiculum to area CA1) by each of the four components of the LFP rhythm signals (instantaneous voltage, phase, amplitude and linear component) were compared to determine statistically significant differences.

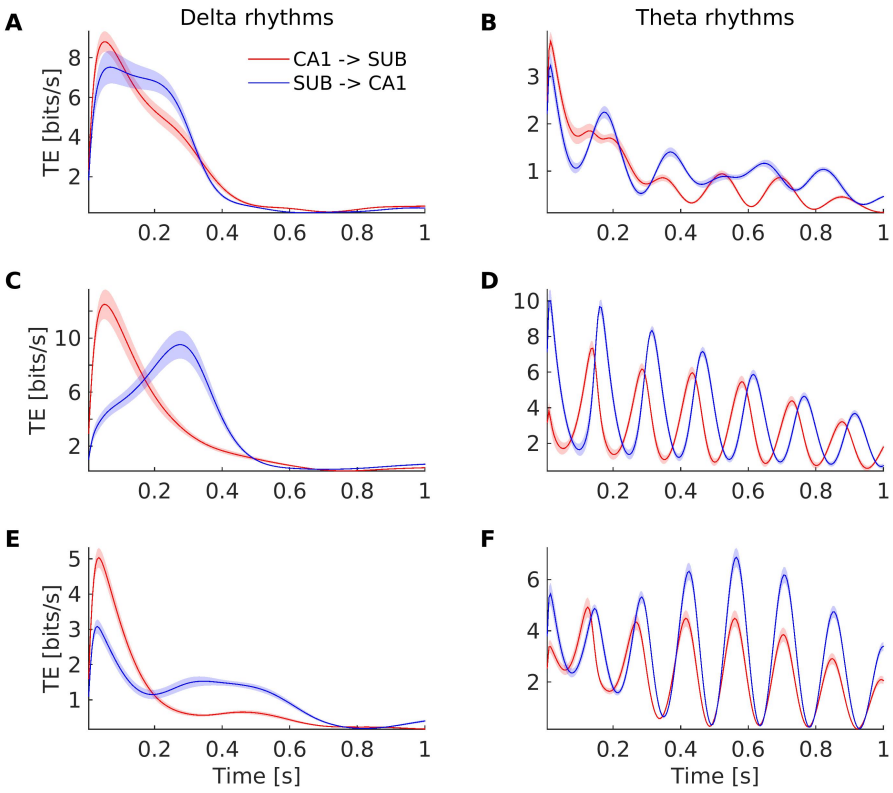

Figure 5.6: Average information transfer between hippocampal area CA1 and subiculum (Sub) by linear correlations in delta (A, C and E) and theta rhythms (B, D and F). Each row (A-B, C-D and E-F) shows the averages across all pairs of electrodes in a different mouse (corresponding to the mice in Figure 5.2). Shadow shows the SEM.

Delta rhythms conveyed significantly more information in both directions than their linear component (Figure 5.7A and D). Delta phase transferred significantly more information than all other signal components; and delta amplitude transferred significantly less information (Figure 5.7A-D). The information transferred by phase or amplitude was equally bidirectional; whereas information transfer by the delta rhythm and its linear component was greater in one direction than the other (Kruskal-Wallis test: $\chi^2 = 1858$, $df = 6143$, $p = 0$, followed by Tukey-Kramer multiple comparisons test of the averaged group ranks to identify the distributions with different medians). The information transferred by theta rhythms, linear component and amplitude were significantly different for either direction and all other signal components; whereas the information conveyed by phase was not different between the two directions (Figure 5.7E-H, Kruskal-Wallis test: $\chi^2 = 3042$, $df = 6143$, $p = 0$, Tukey-Kramer multiple comparisons test of the averaged group ranks).

On average, the time lags at which these maximal transfer entropies occurred in either direction were significantly different for the delta rhythm, phase and linear component,

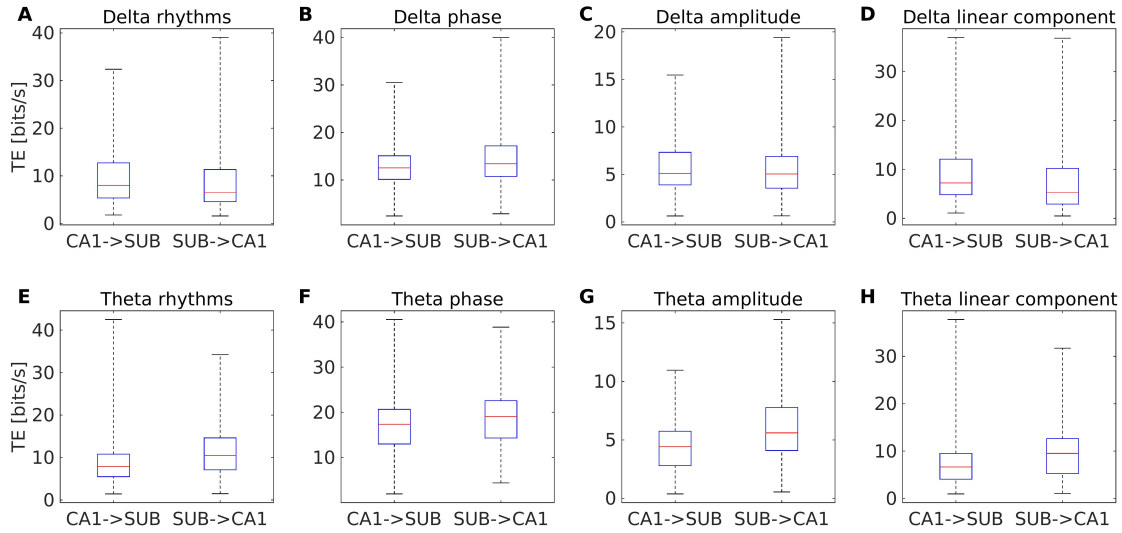

Figure 5.7: Population statistics of the maximum information transfer between area CA1 and subiculum by delta (A-D) and theta rhythms (E-H) of seven mice. Red horizontal bar: median; upper and lower borders of the box: 25$^{\text{th}}$ and 75$^{\text{th}}$ percentiles; dashed lines: maximum and minimum values.

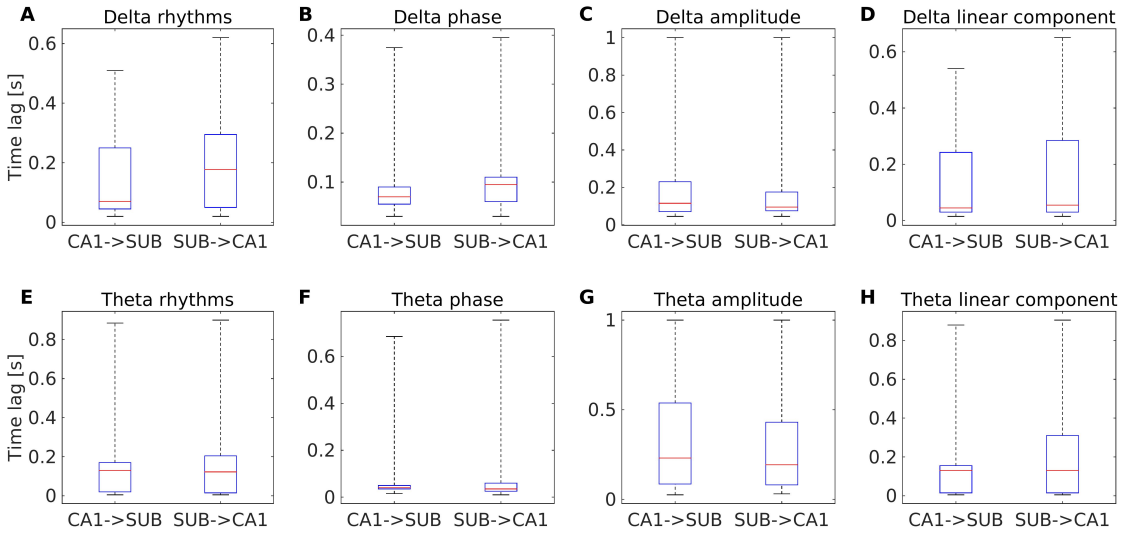

Figure 5.8: Population statistics of the time lags of maximal information transfer between area CA1 and subiculum by delta (A-D) and theta rhythms (E-H) of seven mice. Red horizontal bar: median; upper and lower borders of the box: 25$^{\text{th}}$ and 75$^{\text{th}}$ percentiles; dashed lines: maximum and minimum values.

but not amplitude (Figure 5.8A-D, Kruskal-Wallis test: $\chi^2 = 510$, $df = 6143$, $p \approx 0$, Tukey-Kramer multiple comparisons test of the averaged group ranks). For the theta rhythm and linear component, the median time lags were not statistically different in either direction or between the two signal components. For the other two signal components (phase and amplitude) the time lags were not different in either direction,

but were different between them and the first two components (Figure 5.8E-H, Kruskal-Wallis test: $\chi^2 = 910$, $df = 6143$, $p \approx 0$, Tukey-Kramer multiple comparisons test of the averaged group ranks).

This analysis suggests that on average different components of delta rhythms (e.g. phase, amplitude, linear component) convey information between area CA1 and subiculum in both directions with different time delays. An application of this methodology for quantifying information transfer in the study of neurological disease is also presented in the Supplementary Material.

5.5 Discussion

We investigated how LFP interactions can transfer information between hippocampal area CA1 and the subiculum of anaesthetised mice. We show that interactions of delta or theta rhythms in these regions can transmit information bidirectionally with a time delay between the two directions: from area CA1 to subiculum and vice versa. This agrees with the anatomical connections between area CA1 and the subiculum which comprise both direct and indirect projections (O'Mara et al., 2001; Gigg, 2006). The directionality in the information flow extends the idea of coherence/synchronisation for communicating information (Fries, 2005; Womelsdorf et al., 2007) by adding the notion of effective connectivity, that is a causal relationship between the activities (Friston, 1994, 2011). According to this idea, activity in area CA1 could drive activity in subiculum to transmit information and vice versa. However, this does not exclude the possibility of another region, e.g. the entorhinal cortex, driving both regions with a different time delay.

We further show that phase-phase interactions can transmit most of the information; whereas amplitude-amplitude interactions can transmit less than half the amount transmitted by phase-phase interactions. Indeed, studies in monkeys have shown quantitatively that LFP phase can convey information about sensory stimuli not present in spike firing alone (Montemurro et al., 2008; Kayser et al., 2009). Moreover, we show that linear correlations in delta and theta rhythms transmit most of the information conveyed by LFP interactions. This is consistent with the findings of studies that use linear methods, such as Granger causality and Granger causality inferences, to quantify LFP interactions (e.g. Cadotte et al. (2010) and Bosman et al. (2012), respectively).

The frequency ranges of the two rhythms we identified under anaesthesia were consistent with other studies in mice under similar experimental conditions (Pagliardini et al.,

2013a,b). The lower band corresponded to delta rhythms (or slow oscillations) which are common under anaesthesia (Sharma et al., 2010). The higher band corresponded to atropine-resistant theta (Kramis et al., 1975). Urethane, which is a long-acting (8-10 hours) anaesthetic routinely used in rodent studies, preserves REM-like and non-REM-like states in rats (Wolansky et al., 2006; Clement et al., 2008) and mice (Pagliardini et al., 2013a,b). Thus, similar patterns of information transfer might be mediated by delta and theta rhythm interactions during naturalistic sleep. However, further research with non-anaesthetised animals is required to address this.

Routing of information by LFP rhythms has been reported in awake rodents. More specifically, coherence of sub-bands of gamma rhythms (slow and fast) were found to couple areas CA3 and CA1 or medial entorhinal cortex and CA1, respectively, allowing segregate information flow (Colgin et al., 2009). Moreover, slow and fast gamma rhythms were locked to different theta phases in area CA1 (Colgin et al., 2009) supporting model predictions of these interactions as a mechanism to segregate information for memory encoding and memory retrieval (Hasselmo et al., 2002). In addition, information transfer by gamma rhythm interactions has been described in the monkey primary visual cortex (Besserve et al., 2010, 2015).

To conclude, our results provide evidence for a mechanism by which LFP rhythms mediate dynamic effective connectivity to route information at millisecond timescales along anatomically fixed connections. Delta and theta rhythms can act as two separate channels by which segregate information can be routed bidirectinally between the hippocampus and the subiculum in parallel.

5.6 Supplementary Material

5.6.1 Supplementary Background

In this supplementary section, we applied the same methodology used in the main paper in the context of investigating information transfer in a neurological disease affecting the hippocampal formation. More specifically, we quantified information transfer by LFP at early stages of Alzheimer's disease-like pathology in the 3xTg-AD mouse model and compare this to the information transfer in the healthy controls presented in the main paper.

Alzheimer's disease (AD), which is the most common form of dementia, is a neurodegenerative disease with increased prevalence among the aging population and is char-

acterised by cognitive and memory impairments (reviewed in Querfurth and LaFerla (2010); Ittner and Gotz (2011)). The pathology of AD involves the formation of β-amyloid plaques and neurofibrillary tangles of hyperphosphorylated protein tau and synaptic and neuronal loss in the hippocampal formation (Braak and Braak, 1991; West et al., 1994).

The study of AD pathology and cognitive deficits is facilitated by the availability of rodent models expressing mutations linked to AD pathology (reviewed in Hall and Roberson (2012)). A useful model, resembling both the β-amyloid and tangle pathology of AD is the 3xTg-AD mouse. The 3xTg-AD mouse model co-expresses three mutations: $PS1_{M146V}$, APP_{Swe}, and tau_{P301L}. The first two are involved in the pathways producing β-amyloid plaques and the latter in forming neurofibrillary tangles (Oddo et al., 2003).

5.6.2 Supplementary Results

We investigated whether early stages of Alzheimer's disease-like pathology in mice can affect information transfer by LFP rhythms between the hippocampus and the subiculum. We analysed LFP recordings from equidistant electrodes spanning 500 μm along the depth of hippocampal area CA1 and subiculum of seven 3-month-old 3xTg-AD mice and seven age-matched control mice. The LFP recordings were from either one electrode shank or two parallel ones placed 500 μm apart in area CA1 and subiculum of each mouse.

5.6.2.1 Spectral content of LFP in young 3xTg-AD and control mice

The spectral content of LFP recorded from the hippocampal formation of 3xTg-AD mice appeared similar to the LFP spectra observed for the control mice (described in Methods section 5.4.1). Two examples from either phenotype are displayed in Figure 5.9. Therefore, all analyses of information transfer in 3xTg-AD mice were performed for the same frequency bands as for the control mice, that is 0.5-2 Hz for delta and 2.5-4.5 Hz for theta.

5.6.2.2 Information transfer in CA1-subicular circuit of young 3xTg-AD and control mice

We quantified information transfer from hippocampal area CA1 to subiculum and vice versa from each pair of electrodes in the corresponding regions in the 3xTg-AD mice. In the example shown in Figure 5.10, the average information flow by delta rhythms from area CA1 to subiculum and vice versa appears similar among the two phenotype (Figure 5.10A and B). In the case of theta rhythms, average information flow appears

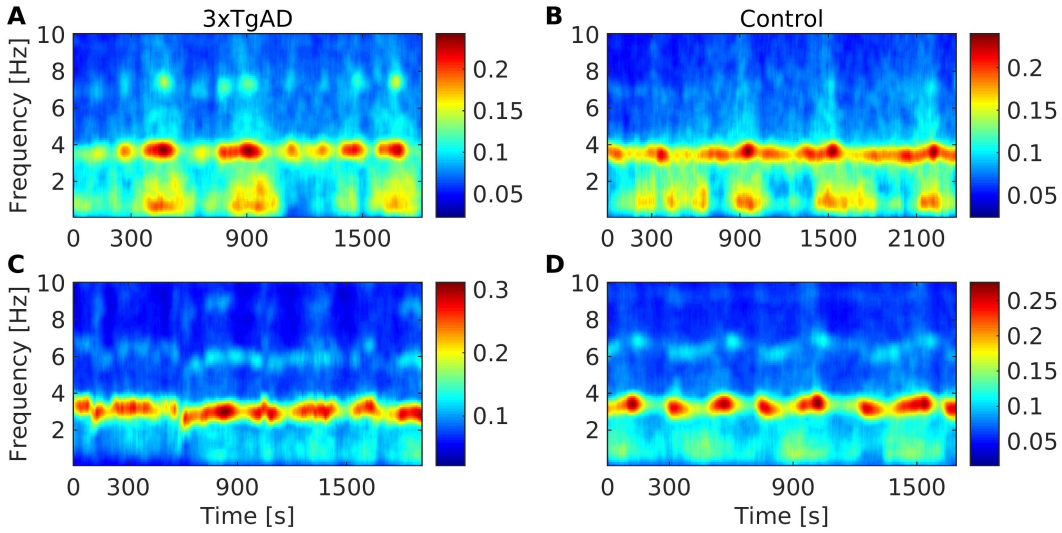

Figure 5.9: Examples of spectrograms of spontaneous LFP recorded by an electrode in the subiculum of two young 3xTg-AD mice (A and C) and two age-matched control mice (B and D) under anaesthesia. Color scale in $(mV^2/Hz)^{0.25}$. Warmer colors indicate higher power spectral density (PSD).

to be greater towards the subiculum than towards area CA1 in the example transgenic mouse (Figure 5.10C) but the reverse pattern is observed in the example control mouse (Figure 5.10D). Moreover, transfer entropy oscillated across time lag in both phenotypes. Notably, the delay at which information by theta rhythms peaked in the transgenic example differed by ∼400 ms (Figure 5.10C), whereas in the control example the peaks lagged by a few milliseconds (Figure 5.10D). Similarly to the controls, the information transfer between area CA1 and subiculum varied across 3xTg-AD mice.

5.6.3 Population analysis of information transfer

In addition to computing TE for the delta-filtered and theta-filtered LFP, we also computed TE for the phase, amplitude and linear component of these rhythms. To gain an insight into how the results for all animals compare, scatter plots were plotted. For each rhythm and each pair of electrode, the maximal transfer entropy and the time delay at which it corresponded was plotted as a point in the scatter plot (Figure 5.11). The two directions of TE for each phenotype are marked with different colours. The patterns of information transfer in the CA1-subicular circuit of young 3xTg-AD and control mice appeared very similar as indicated by the overlap of data points in the scatter plots (Figure 5.11). Notably, an oscillatory pattern (suggested by gaps across time lag) was evident in the plots.

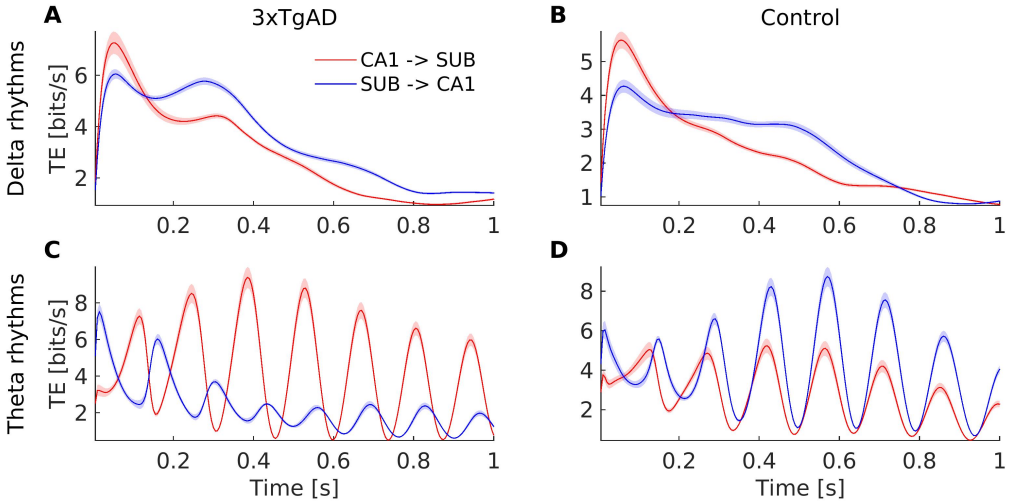

Figure 5.10: Average information transfer between hippocampal area CA1 and subiculum (Sub) by delta-filtered (A and B) and theta-filtered LFP (C and D). Averages across all pairs of electrodes in a control (A and C) and 3xTg-AD mouse (B and D). Shadow shows the SEM.

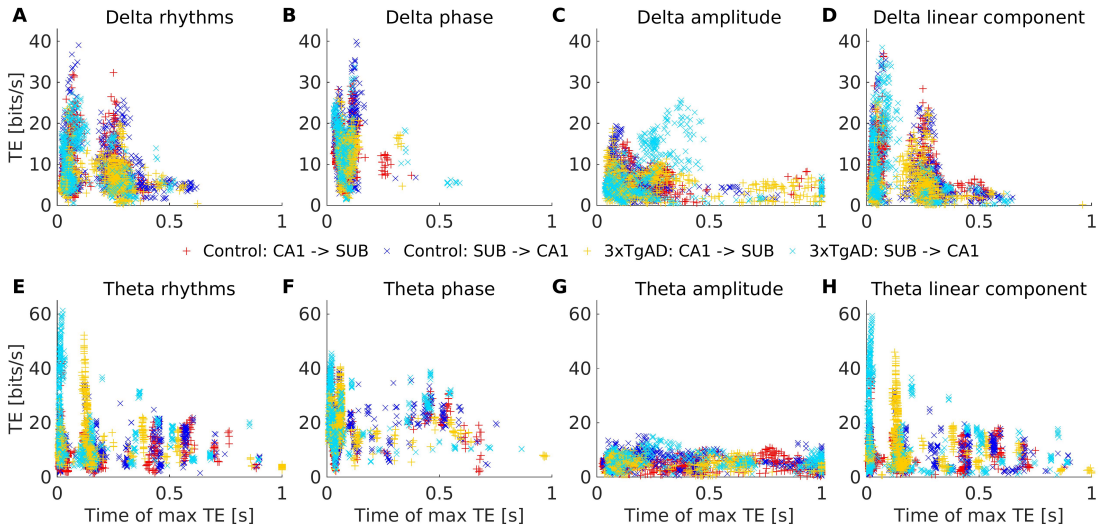

Figure 5.11: Scatter plots of maximum transfer entropy versus time lag at which transfer entropy reached this maximal value for control and 3xTg-AD mice (seven mice for each phenotype). The transfer entropy of each pair of electrodes is marked by a symbol (+ or x) and colour-coded for each phenotype according to the legend in the middle of the figure. Each cross (+) indicates the maximal transfer entropy from an LFP recorded from an electrode in area CA1 to another LFP recorded from an electrode in the subiculum. Each chi (x) indicates the maximal transfer entropy from the subiculum to area CA1 for a pair of electrodes. Transfer entropy conveyed by the LFP (A and E), phase (B and F), amplitude (C and G) and linear components (D and H) of delta (A-D) and theta rhythms (E-H).

Population analysis was carried out as in the main text, to determine whether there were differences in the distributions of maximal TE (Figure 5.12) or time lags (Figure

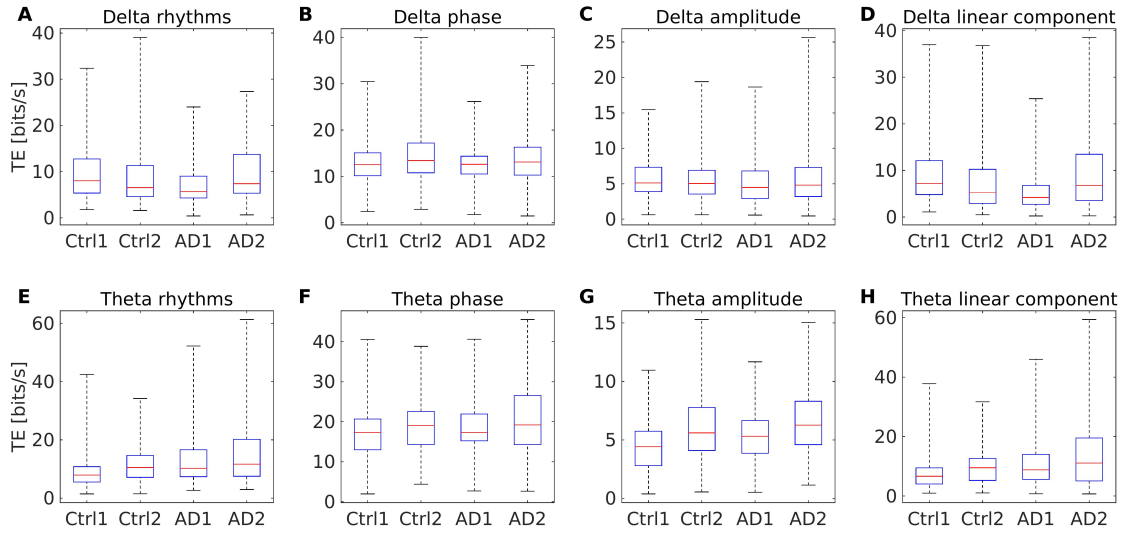

Figure 5.12: Population statistics of the maximum information transfer between area CA1 and subiculum by delta (A-D) and theta rhythms (E-H). Red horizontal bar: median; upper and lower borders of the box: 25th and 75th percentiles; thin lines: maximum and minimum values; Ctrl: control mice; AD: 3xTg-AD mice; 1: CA1->subiculum; 2: subiculum->CA1. Seven mice for each phenotype.

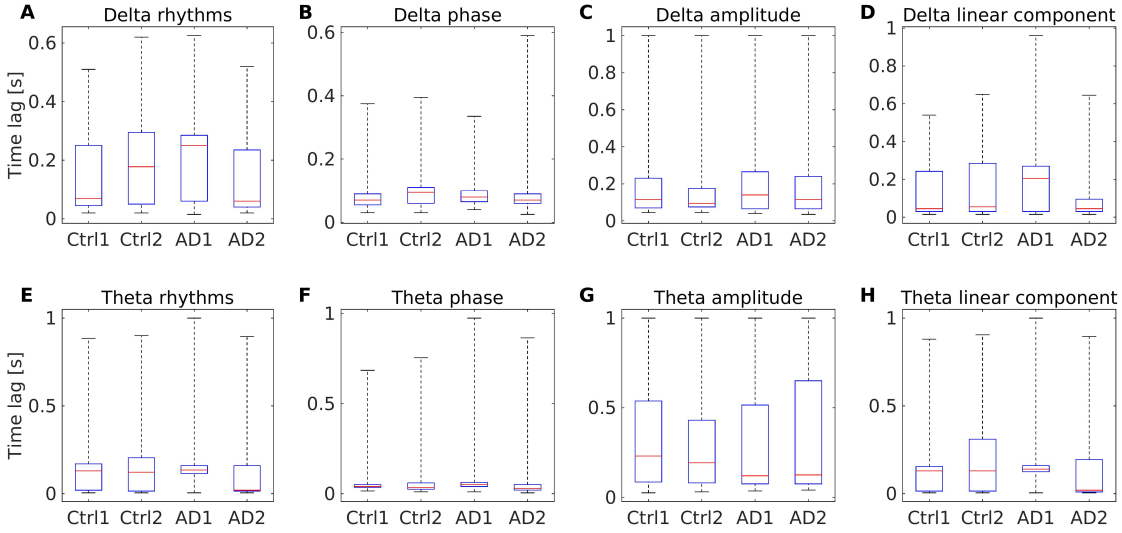

Figure 5.13: Population statistics of the time lags of maximal information transfer between area CA1 and subiculum by delta (A-D) and theta rhythms (E-H). Red horizontal bar: median; upper and lower borders of the box: 25th and 75th percentiles; thin lines: maximum and minimum values; Ctrl: control mice; AD: 3xTg-AD mice; 1: CA1->subiculum; 2: subiculum->CA1. Seven mice for each phenotype.

5.13) across direction or phenotypes. The observed differences in the medians of the distributions of maximal transfer entropy across directions and phenotypes were statistically significant for the delta-filtered (Figure 5.12A-D, Kruskal-Wallis test: $\chi^2 =$

3807, $df = 12479$, $p = 0$, Tukey-Kramer multiple comparisons test of the averaged group ranks) and theta-filtered LFP (Figure 5.12E-H, Kruskal-Wallis test: $\chi^2 = 5701$, $df = 12479$, $p = 0$, Tukey-Kramer multiple comparisons test of the averaged group ranks). Similarly, the observed differences in the medians of the distributions of time lags were statistically significant for the delta-filtered (Figure 5.13A-D, Kruskal-Wallis test: $\chi^2 = 1281$, $df = 12479$, $p \approx 0$, Tukey-Kramer multiple comparisons test of the averaged group ranks) and theta-filtered LFP (Figure 5.13E-H, Kruskal-Wallis test: $\chi^2 = 2172$, $df = 12479$, $p0$, Tukey-Kramer multiple comparisons test of the averaged group ranks). These results suggest that information flow within the CA1-subicular circuit was bidirectional but the amount of information transferred in each direction by different types of signals (instantaneous voltage, phase, amplitude, linear component) varied across direction and phenotype.

Chapter 6

Discussion

This PhD project aimed to unravel how brain rhythms can be encoded in spike trains, as well as to quantify how interactions of brain rhythms can transmit information between neural networks. The first two papers addressed the first question and the last paper the second one. The outcome of each is discussed in the Discussion section of the papers. In this section, the contribution of each outcome and how it relates to current knowledge in the field is discussed. Moreover, additional explanations and interpretations of the results, not already covered in the text of the papers, are included here. A final summary and outlook is presented in the conclusions followed by future directions arising from the outcomes of the project.

6.1 Bursting neurons lock their firing to the phase of dominant LFP rhythms

In Paper 1, the model predicted that bursting neurons lock their firing to the phase of dominant rhythms irrespective of the specific frequency of this LFP-like rhythm. This prediction was confirmed by the analysis of *in-vivo* recordings in the rat subiculum showing that bursting neuron activity was phase-locked to dominant delta or theta rhythms. Moreover, the model and subicular bursting neurons fired bursts of increasing spike count that locked to more advance phase of the dominant rhythms in the input signals or dominant delta rhythms under anaesthesia, respectively. These results provided evidence for a neural code in which the firing rate and burst size can encode LFP phase. This motivated the quantitative analysis in Paper 2.

In the subiculum, bursting neurons are distributed unevenly along the proximodistal axis so that bursting neurons are more common in the distal portion whereas regular spiking neurons are more common in the proximal portion (Staff et al., 2000; Jarsky et al., 2008). Moreover, bursting neurons and regular spiking neurons appear to project to distinct target areas (Kim and Spruston, 2012) suggesting that they process separate information. Although in our studies we did not specifically investigate the distribution

of regular spiking and bursting cells in the span of subiculum, we observed more bursting cells in the distal than proximal portion which agrees with the literature. The uneven distribution of the two cell types suggests that other mechanisms, such as spike rate, spike time and sparse codes (explained in the Introduction section 1.2), might be employed by non-bursting neurons and also co-exist with a burst code.

6.2 Bursting neurons encode LFP features in firing rate and spike count

In Paper 2, we showed that bursting neurons in the rat subiculum and MEC encode LFP features both in their firing rate and intra-burst spike counts. Similar burst codes have also been identified in sensory systems. Experimental evidence suggests that primary visual cortical neurons encode the orientation of visual stimuli in burst rate and size in anaesthetised cats (DeBusk et al., 1997) and burst size in awake monkeys (Martinez-Conde et al., 2002). Burst coding has also been identified in the non-mammalian brain. For instance, sensory neurons in the leech encode tactile stimulus variance in burst rate and size (Arganda et al., 2007). Moreover, grasshopper auditory receptor neurons encode the intensity of acoustic stimuli in burst spike counts (Eyherabide et al., 2008, 2009). Therefore, bursting is an important part of the neural code for stimulus representation.

Our study differs in that bursting neurons in the hippocampal formation do not receive direct stimulation from the external environment. Instead, subicular and entorhinal bursting neurons can encode information about the ongoing LFPs in the surrounding milieu. This finding is important because the LFP mainly reflects the synaptic activity of pyramidal cells and contains information about subthreshold and integrative processes in the local network (Logothetis, 2003; Buzsaki et al., 2012; Einevoll et al., 2013). Therefore, although the LFP does not directly cause spiking, it reflects the activity (synaptic input) that ultimately causes the spiking. One might say that the information we computed reflects the contribution of local spikes to the LFP. However, the contribution of spiking activity in the LFP is at higher frequencies (>100 Hz) (Schomburg et al., 2012; Scheffer-Teixeira et al., 2013) than the delta and theta rhythms investigated in our study. The results obtained with the simulations support the idea that the LFP rhythms we investigated are not a consequence of spiking activity because by construction in the model we can be sure that the bursting output is the consequence (and not the cause) of the LFP features. To conclude, our results extend the role of bursting from merely sensory encoding to the ability of encoding neural network activity in the mammalian brain.

Furthermore, apart from an encoding role, bursting can affect behavioural responses. This is the case in the auditory system of crickets where the timing of bursts encodes features of the ultrasound stimulus and burst size is associated with the avoidance response of the cricket (Marsat and Pollack, 2010). This provides evidence that a burst code is read by postsynaptic neurons in order to mediate a behavioural response. Whether something similar applies for the burst code in the mammalian brain is still to be investigated.

The number of spikes in bursts is not the only factor that adjusts burst size. The interspike interval (ISI) also changes the length of the burst. Some studies have shown that the ISI of bursts is also important in information encoding. For example, in the weakly electric fish, an interval code has been proposed in which the burst ISI encodes stimulus intensity (Oswald et al., 2007). In addition, in the cricket auditory system, bursts might encode stimuli in both the burst ISI and spike count (Marsat and Pollack, 2010). In our studies we focused on the number of spikes in the burst. Further studies should also determine the role of burst ISI in LFP feature encoding.

The burst code we present in this thesis does not exclude other mechanisms of LFP encoding. Another mechanism to transmit information about the phase of oscillatory signals, such as LFP rhythms, has been proposed by a theoretical study (Masquelier et al., 2009). According to this study, the phase-of-firing code (Montemurro et al., 2008) can be decoded by spike-timing dependent plasticity which occurs when the postsynaptic neurons detect spikes arriving repeatedly over some time interval, that is at a specific phase of an oscillation (Masquelier et al., 2009). This mechanism might appear contradicting to a burst code, however, the burst code does not exclude any other possible codes to transmit LFP information. Both mechanisms can coexist or used by different types of neurons. Further research is required to clarify this.

Bursting cells have also been recorded in the hippocampal formation of monkeys (Skaggs et al., 2007). The presence of bursting neurons in the primate hippocampus suggests that our finding of a burst code is not only relevant to rodent research but might also be applicable in the primate brain. Whether this code is also used by bursting neurons in the primate and more specifically in the human hippocampal formation to transmit information about LFP still needs to be investigated in future studies.

6.3 Interpretation of information encoded by burst code

The capacity of a communication channel (or code) is the maximum rate at which it can transmit an input X and retrieve the information at the output Y. This capacity C is defined as the maximum mutual information between X and Y, that is $C = \max I(X;Y)$ (Shannon, 1948). Similarly, we assume that the capacity of the burst codes investigated equals the estimated information values $C = \max I(X;N)$, where X denotes the set of LFP features and N the set of responses of bursting neurons as defined for each burst code in Paper 2. However, this does not necessarily mean that downstream neurons actually obtain this maximal information since decoding could not be investigated by the datasets used. This is because in our datasets there were no recordings from the downstream neurons where bursting neurons project. The decoding of the information of the three burst codes could be a topic for future studies.

The average information values calculated for the full burst code in the subiculum and MEC were in the range of 0.1 to 0.3 bits/burst. This means that on average an n-spike burst can convey 0.1 to 0.3 bits of information about the LFP, that is discriminate between $2^{0.1} = 1.07$ to $2^{0.3} = 1.23$ LFP features. However, not all bursts convey equal amount of information. In general, rare symbols in a code can contain more information than common ones, as explained in section 2.5.1. Similarly for the burst code, according to the average burst distributions (Fig. 4.2) and Eq. 2.11, the entropy of subicular bursts is $h(n=1) = 0.41 \pm 0.33$ bits, $h(n=2) = 2.59 \pm 1.05$ bits and $h(n=3) = 6.56 \pm 1.94$ bits; and the entropy of entorhinal bursts is $h(n=1) = 0.12 \pm 0.06$ bits, $h(n=2) = 4.02 \pm 0.88$ bits and $h(n=3) = 7.37 \pm 1.12$ bits. This implies that bursting neurons have the capacity to fire two-spike ($n=2$) or larger ($n=3$) bursts to encode salient feature values of the LFP.

Moreover, ensembles of hippocampal neurons usually fire together or in a sequence to encode information such as memories and space (Harris, 2005). We showed that most of the information is encoded in the firing rate of bursting neurons and, for some neurons, about 10-15% in the burst spike count. Therefore, assuming little redundancy in the burst code, a downstream neuron receiving input from a group of bursting neurons can observe the burst rate and size of its input and obtain enough information to discriminate between different LFP features. For instance, as few as three bursting neurons each encoding an average of 0.1 bits/burst about the LFP phase in their firing rate can encode four distinct phase ranges by each neuron increasing their firing rate only at a preferred phase range which is different from the other two neurons.

The information values reported in Paper 2 probably underestimate the information

capacity of the burst code. This is because the shape of the spikes within bursts changes along the burst (Kandel and Spencer, 1961; Ranck, 1973) and thus the shapes of subsequent spikes within bursts become too small or different to be clustered together with the first few spikes during spike sorting (Harris et al., 2000). Therefore, larger bursts might have been missed or split in two events. Considering bursts with three or more spikes as the same symbol for the burst code accounts for this spike sorting limitation since, even when a neuron fires a larger than three-spike burst but the last spikes are not captured, this burst is still included in the 'larger bursts' symbol even if not specifically identified.

6.4 Information transfer by LFP in the hippocampal formation

In Paper 3, we showed that interactions among delta or theta rhythms can exchange information bidirectionally between hippocampal area CA1 and subiculum. The information transferred along the two directions is not always equal. Moreover, there is a time lag between the peaks of information transfer from area CA1 to subiculum and vice versa. Area CA1 sends direct input to subiculum which, in turn, sends reciprocal input to area CA1 via indirect projections (O'Mara et al., 2001; Gigg, 2006). Based on this anatomical connectivity, the time lags might correspond to the delays between the feedforward and feedback projections.

Our finding that the phase of the rhythms transferred significantly more information (approximately double) than the amplitude is consistent with the large number of studies that emphasise the importance of LFP phase for cognitive processing such as forming memory representations (overviewed in the Introduction sections 1.3.2 and 1.4.4). Moreover, the finding that linear correlations in the LFP rhythms conveyed most of the information justifies the use of linear methods for analysing electrophysiological recordings (reviewed in Pereda et al. (2005)). However, the fact that the information transfer by LFP rhythms was slightly ($\sim$ 2-3 bits/s) but significantly higher than the information transfer by only the linear component in the rhythms implies that there is also a non-linear component involved in the LFP interactions. This non-linear component still needs to be investigated.

Our results suggest that delta and theta rhythms can route information independently from each other. This is similar to the mechanism of distinct gamma sub-band interactions for separate information flow in the hippocampal formation (Colgin et al., 2009) introduced in section 1.4.4.3. The slow frequencies that were prominent in the LFP within the hippocampal formation of anaesthetised mice might have a role in

processing separate information. More specifically, our results provide evidence for a mechanism by which delta and theta rhythms can act as two separate channels for the transmission of information between area CA1 and the subiculum.

Furthermore, we applied the transfer entropy measure to study neurological disease (Supplementary Material of Paper 3). Comparing information transfer within the CA1-subicular circuit of young 3xTg-AD mice and age-matched control mice identified both similarities and differences between the two phenotypes. Our results suggest that quantifying information transfer mediated by LFP interactions can provide an insight about the effects of neuropathology on the brain.

6.5 Conclusions

The outcomes of this project propose a mechanism by which information about local network activity (reflected in the LFP) can be transmitted in the form of spike patterns (as bursts of variable size and rate). First, we determined that bursting neuron output locks to the phase of dominant rhythms in the LFP. Subsequently, we quantified the capacity of burst rate and burst size to encode LFP features to show that a combination of both can be used in the burst code. This burst code allows distant downstream neurons to obtain information about the upstream network activity.

The second outcome provides insight into the LFP interactions that can mediate effective connectivity in the hippocampal formation. We showed that delta and theta rhythms can act as two separate channels to route information bidirectionally between two anatomically connected networks (area CA1 and subiculum). Moreover, we showed that linear components in the rhythms conveyed most of the information transmitted by the rhythms. In addition, our results suggest that phase interactions in the LFP transfer more information than amplitude. Finally, we showed that this method can also be applied in the study of neurological diseases, such as Alzheimer's disease, to identify potential impairments in information transfer as measured by LFP interactions.

6.6 Future Work

6.6.1 Further investigate the burst code

As already mentioned in section 6.2, there is still more to explore about burst coding. After determining the encoding capacity of bursting neurons to convey information

about LFP, it becomes natural to ask whether downstream neurons actually decode this information and how this affects their responses. Therefore, a next step is to record from both bursting neurons in the hippocampal formation and their downstream neurons. This will allow to determine how the output of bursting neurons affects the postsynaptic neurons and whether the latter can decode the information about LFP features.

Moreover, how this burst code affects the behaviour of animals, such as task performance, stills need to be investigated. For instance, since the burst code we described in the hippocampal formation was identified in the subicular and entorhinal regions encoding space, a follow-up study could investigate the relationship between LFP encoding by the burst code and the performance in a spatial task.

Other mechanisms might also be employed by neurons to transmit LFP information. For example, the possibility of an interval code by bursting neurons could be investigated next. In addition, the combination of other mechanisms with the burst rate and burst size codes needs to be explored in subsequent studies. For instance, how a burst code compares with the spike-timing dependent plasticity theory for transmitting LFP information still needs to be determined. Moreover, the potential of non-bursting neurons to use a combination of spike rate, spike time and sparse codes to encode LFP features could also be explored.

LFP are constantly present throughout the brain and also bursting neurons are prevalent in a number of brain systems, as discussed in the Introduction of the thesis. During this project, burst coding was investigated in the rat hippocampal formation. A next aim would be to determine whether burst coding of LFP is also possible in other brain regions, such as cortex and thalamus, where bursting neurons are common. This need not be restricted to rodents, but could also be investigated in other mammals including primates.

The most interesting question is whether this neural code is also employed in the human brain. This would require intracranial recordings from humans. This type of recordings are only possible -and ethical- when they are obtained for medical reasons, such as from epileptic patients before surgery. Thus, to answer this question, meta-analyses of simultaneous LFP and spike train recordings from human patients could determine whether bursting can encode features of LFP rhythms in the human brain.

6.6.2 Further investigate information transfer by LFP

In this thesis, information transfer was quantified as transfer entropy (TE) in units of bits/s. This quantity does not mean that there is a constant flow of information of a specific number of bits in every second, rather it standardises the measure of information transfer as explained at the end of section 2.6.2. An alternative way of reporting the information transfer values would be to use a normalisation method as in Gourevitch and Eggermont (2007); Besserve et al. (2010). The normalised transfer entropy (NTE) quantifies the fraction of information about a signal X that can be obtained by observing the past of another signal Y but not its own past. Following the notation introduced in sections 2.6.2 and 2.7.3, NTE can be obtained by:

$$NTE(Y \rightarrow X) = \frac{T_c(Y \rightarrow X)}{H(X_{t+\tau}|X_t)} \tag{6.1}$$

NTE can take values from 0 to 1; where NTE = 0 when there is no dependence between the past of Y and the present of X, and NTE approaches 1 as the dependence of the present of X on the past of Y increases. Using NTE has the advantage of presenting information transfer from signal Y to signal X independently of the dependence of X on its own past (Gourevitch and Eggermont, 2007; Besserve et al., 2010). Therefore, the next step would be to present the information transfer results of Paper 3 using the NTE measure.

Information transfer by LFP can be further investigated in future studies. For example, the results obtained from the transfer entropy analysis can be compared to other methods such as the cross-correlation of the instantaneous amplitudes which is a linear, model-independent method to estimate the direction of functional connectivity and lag between LFP in different networks (Adhikari et al., 2010). This method has already been used in other studies to measure the directionality of functional connectivity between the hippocampus and prefrontal cortex (Adhikari et al., 2010; Place et al., 2016). Moreover, a next step will be to quantify the information conveyed by the non-linear component in the LFP rhythms and also try to identify the nature of the non-linearity.

In future studies, the scope could be extended to link information transfer with task performance. This can be achieved by analysing LFP from awake behaving animals. It is interesting to determine the interactions of which rhythms in a given brain region mediate different cognitive functions. The experimental design could be chosen to test specific aspects of cognitive functioning, such as spatial navigation versus a non-spatial task, e.g. novel object recognition (Antunes and Biala, 2012).

In non-anaesthetised animals, LFP activity is more complex than under anaesthesia.

This is because the animal responds dynamically to external stimuli during wakefulness or consolidates memories during sleep. The composition of LFP is also more interesting because, for example in the hippocampus, it can contain gamma rhythms and sharp-wave ripples, which were not observed in our recordings under urethane anaesthesia. Therefore, analysing data from non-anaesthetised animals would allow the quantification of information transfer by the interplay of slower (delta or theta) with faster rhythms (ripples or gamma). These interactions could be identified by measures such as the cross-frequency coupling modulation index (Tort et al., 2010).

The effects of neurological diseases on information transfer by LFP interactions can be investigated for any type of disease, such as epilepsy, schizophrenia and Parkinson's disease, using animal models. The example of studying early Alzheimer's disease effects presented in this project can also be extended by analysing LFP recordings from the hippocampal formation at more advanced stages of the disease to determine how disease progression affects information transfer.

Information transfer can also be investigated in humans. Similar techniques as the ones used in this study can be applied to the analysis of EEG, MEG and fMRI data obtained from humans. Indeed, toolboxes have already been developed for this purpose. These include the Information Breakdown ToolBox (Magri et al., 2009) and the TRENTOOL (Lindner et al., 2011). Therefore, the final goal would be to understand how brain rhythm interactions mediate effective connectivity for cognitive processing in humans. This would be instrumental for the development of tools for the early diagnosis of neurological diseases.

References

Adhikari, A., Sigurdsson, T., Topiwala, M. A., and Gordon, J. A. (2010). Cross-correlation of instantaneous amplitudes of field potential oscillations: A straightforward method to estimate the directionality and lag between brain areas. *J. Neurosci. Methods*, 191:191–200.

Adrian, E. D. and Matthews, B. H. C. (1934). The Berger rhythm: potential changes from the occipital lobes in man. *Brain*, 57:355–385.

Adrian, E. D. and Zotterman, Y. (1926). The impulses produced by sensory nerve-endings: Part 2: The response of a single end-organ. *J. Physiol. (Lond.)*, 61:151–171.

Agarwal, G., Stevenson, I. H., Berenyi, A., Mizuseki, K., Buzsaki, G., and Sommer, F. T. (2014). Spatially distributed local fields in the hippocampus encode rat position. *Science*, 344:626–630.

Ainge, J. A., van der Meer, M. A. A., Langston, R. F., and Wood, E. R. (2007). Exploring the role of context-dependent hippocampal activity in spatial alternation behavior. *Hippocampus*, 17:988–1002.

Alitto, H. J., Weyand, T. G., and Ursey, W. M. (2005). Distinct properties of stimulus-evoked bursts in the lateral geniculate nucleus. *J. Neurosci.*, 25:514–523.

Amaral, D. G. and Witter, M. P. (1989). The three-dimensional organization of the hippocampal formation: A review of anatomical data. *Neuroscience*, 31:571–591.

Amzica, F. and Ster (1992). Delta frequency (1-4 hz) oscillations of perigeniculate thalamic neurons and their modulation by light. *Neuroscience*, 51:285–294.

Anastassiou, C. A., Perin, R., Markram, H., and Koch, C. (2011). Ephaptic coupling of cortical neurons. *Nat. Neurosci.*, 14:217–223.

Antunes, M. and Biala, G. (2012). The novel object recognition memory: neurobiology, test procedure, and its modifications. *Cogn. Process*, 13:93–110.

Arganda, S., Guantes, R., and de Polavieja, G. G. (2007). Sodium pumps adapt spike bursting to stimulus statistics. *Nat. Neurosci.*, 10:1467–1473.

Averbeck, B. B., Latham, P. E., and Pouget, A. (2006). Neural correlations, population coding and computation. *Nat. Rev. Neurosci.*, 7:358–366.

Baccala, L. A. and Sameshima, K. (2001). Partial directed coherence: a new concept in neural structure determination. *Biol. Cybern.*, 84:463–474.

Bartos, M., Vida, I., and Jonas, P. (2007). Synaptic mechanisms of synchronized gamma oscillations in inhibitory interneuron networks. *Nature Reviews Neuroscience*, 8:45–56.

Battaglia, D., Witt, A., Wolf, F., and Geisel, T. (2012). Dynamic effective connectivity of inter-areal brain circuits. *PLoS Comput. Biol.*, 8:e1002438.

Belluscio, M. A., Mizuseki, K., Schmidt, R., Kempter, R., and Buzsaki, G. (2012). Cross-frequency phase-phase coupling between theta and gamma oscillations in the hippocampus. *J. Neurosci.*, 32:423–435.

Berens, P. (2009). CircStat: a MATLAB toolbox for circular statistics. *J. Stat. Softw.*, 31:1–21.

Berger, H. (1929). Uber das Elektrenkephalogramm des Menschen. *Archiv fur Psychiatrie*, 87:527–570.

Besserve, M., Lowe, S. C., Logothetis, N. K., Scholkopf, B., and Panzeri, S. (2015). Shifts of gamma phase across primary visual cortical sites reflect dynamic stimulus-modulated information transfer. *PLoS Biol.*, 13:e1002257.

Besserve, M., Scholkopf, B., Logothetis, N. K., and Panzeri, S. (2010). Causal relationships between frequency bands of extracellular signals in visual cortex revealed by an information theoretic analysis. *J. Comput. Neurosci.*, 29:547–566.

Born, J. and Wilhelm, I. (2012). System consolidation of memory during sleep. *Psychological Research*, 76:192–203.

Borst, A. and Theunissen, F. E. (1999). Information theory and neural coding. *Nat. Neurosci.*, 2:947–957.

Bosman, C. A., Schoffelen, J. M., Brunet, N., Oostenveld, R., Bastos, A. M., Womelsdorf, T., Rubehn, B., Stieglitz, T., De Weerd, P., and Fries, P. (2012). Attentional stimulus selection through selective synchronization between monkey visual areas. *Neuron*, 75:875–888.

Braak, H. and Braak, E. (1991). Neuropathological staging of alzheimer-related changes. *Acta Neuropathol. (Berl.)*, 82:239–259.

Bremaud, P. (2002). *Mathematical Principles of Signal Processing*. Springer, New York.

Britten, K. H., Shadlen, M. N., Newsome, W. T., and Movshon, J. A. (1992). The analysis of visual motion: a comparison of neuronal and psychophysical performance. *J. Neurosci.*, 12:4745–4765.

Brun, V. H., Otnass, M. K., Molden, S., Steffenach, H. A., Witter, M. P., Moser, M. B., and Moser, E. I. (2002). Place cells and place recognition maintained by direct entorhinal-hippocampal circuitry. *Science*, 296:2243–2246.

Bryant, H. L. and Segundo, J. P. (1976). Spike initiation by transmembrane current: a white-noise analysis. *J. Physiol.*, 260:279–314.

Buzsaki, G. (2002). Theta oscillations in the hippocampus. *Neuron*, 33:325–340.

Buzsaki, G. (2004). Large-scale recording of neuronal ensembles. *Nat. Neurosci.*, 7:446–451.

Buzsaki, G. (2015). Hippocampal sharp wave-ripple: a cognitive biomarker for episodic memory and planning. *Hippocampus*, 25:1073–1188.

Buzsaki, G., Anastassiou, C. A., and Koch, C. (2012). The origin of extracellular fields and currents - EEG, ECoG, LFP and spikes. *Nat. Rev. Neurosci.*, 13:407–420.

Buzsaki, G., Bickford, R. G., Ponomareff, G., Thal, L. J., Mandel, R., and Gage, F. H. (1988). Nucleus basalis and thalamic control of neocortical activity in the freely moving rat. *J. Neurosci.*, 8:4007–4026.

Buzsaki, G. and Draguhn, A. (2004). Neuronal oscillations in cortical networks. *Science*, 304:1926–1929.

Buzsaki, G., Horvath, Z., Urioste, R., Hetke, J., and Wise, K. (1992). High-frequency network oscillation in the hippocampus. *Science*, 256:1025–1027.

Buzsaki, G. and Mizuseki, K. (2014). The log-dynamic brain: how skewed distributions affect network operations. *Nat. Rev. Neurosci.*, 15:264–278.

Buzsaki, G. and Wang, X. J. (2012). Mechanisms of gamma oscillations. *Annu. Rev. Neurosci.*, 35:203–225.

Cadotte, A. J., DeMarse, T., Mareci, T. H., Parekh, M. B., Talathi, S. S., Hwang, D. U., Ditto, W. L., Ding, M., and Carney, P. R. (2010). Granger causality relationships between local field potentials in an animal model of temporal lobe epilepsy. *J. Neurosci. Methods*, 189:121–129.

Canto, C. B., Wouterlood, F. G., and Witter, M. P. (2008). What does the anatomical organization of the entorhinal cortex tell us? *Neural Plast.*, 2008:381243.

Carr, M. F., Karlsson, M. P., and Frank, L. M. (2012). Transient slow gamma synchrony underlies hippocampal memory replay. *Neuron*, 75:700–713.

Caton, R. (1875). The electric currents of the brain. *Br. Med. J.*, 2:278.

Cauchy, A. (1826). *Exercises de mathématiques*, chapter Sur un nouveau genre de calcul analogue au calcul infinitésimal, pages 11–24. Chez de Bure frères, Paris.

Chacron, M. J., Longtin, A., and Maler, L. (2004). To burst or not to burst? *J. Comput. Neurosci.*, 17:127–136.

Chrobak, J. J. and Buzsaki, G. (1994). Selective activation of deep layer (V-VI) retrohippocampal cortical neurons during hippocampal sharp waves in the behaving rat. *Journal of Neuroscience*, 14:6160–6170.

Clement, E. A., Richard, A., Thwaites, M., Ailon, J., Peters, S., and Dickson, C. T. (2008). Cyclic and sleep-like spontaneous alternations of brain state under urethane anaesthesia. *PLoS ONE*, 3:e2004.

Colgin, L. L. (2011). Oscillations and hippocampal-prefrontal synchrony. *Current Opinion in Neurobiology*, 21:467–474.

Colgin, L. L. (2016). Rhythms of the hippocampal network. *Nat. Rev. Neurosci.*, 17:239–249.

Colgin, L. L., Denninger, T., Fyhn, M., Hafting, T., Bonnevie, T., Jensen, O., Moser, M. B., and Moser, E. I. (2009). Frequency of gamma oscillations routes flow of information in the hippocampus. *Nature*, 462:353–357.

Connors, B. W., Gutnick, M. J., and Prince, D. A. (1982). Electrophysiological properties of neocortical neurons in vitro. *J. Neurophysiol.*, 48:1302–1320.

Constantinou, M., Elijah, D. H., Squirrell, D., Gigg, J., and Montemurro, M. A. (2015). Phase-locking of bursting neuronal firing to dominant LFP frequency components. *BioSystems*, 136:73–79.

Constantinou, M., Gonzalo Cogno, S., Elijah, D. H., Kropff, E., Gigg, J., Samengo, I., and Montemurro, M. A. (2016). Bursting neurons in the hippocampal formation encode features of LFP rhythms. *Front. Comput. Neurosci.*, 10:133.

Cover, T. M. and Thomas, J. A. (2006). *Elements of Information Theory*. Wiley, New Jersey.

Cruikshank, S. J., Landisman, C. E., Mancilla, J. G., and Connors, B. W. (2005). Connexon connexions in the thalamocortical system. *Prog. Brain Res.*, 149:41–57.

Culley, D. J., Baxter, M., Yukhananov, R., and Crosby, G. (2003). The memory effects of general anesthesia persist for weeks in young and aged rats. *Anesthesia & Analgesia*, 96:1004–1009.

de Haan, W., Pijnenburg, Y. A. L., Strijers, R. L. M., van der Made, Y., van der Flier, W. M., Scheltens, P., and Stam, C. J. (2009). Functional neural network analysis in frontotemporal dementia and alzheimer's disease using eeg and graph theory. *BMC Neurosci.*, 10:101–112.

De Ruyter Van Steveninck, R. R., Lewen, G. D., Strong, S. P., Koberle, R., and Bialek, W. (1997). Reproducibility and variability in neural spike trains. *Science*, 275:1805–1808.

Debanne, D., Campanac, E., Bialowas, A., Carlier, E., and Alcaraz, G. (2011). Axon physiology. *Physiol. Rev.*, 91:555–602.

DeBusk, B. C., DeBruyn, E. J., Snider, R. K., Kabara, J. F., and Bonds, A. B. (1997). Stimulus-dependent modulation of spike burst length in cat striate cortical cells. *J. Neurophysiol.*, 78:199–213.

Dickerson, B. C. and Eichenbaum, H. (2010). The episodic memory system: neurocircuitry and disorders. *Neuropsychopharmacology*, 35:86–104.

Diekelmann, S. and Born, J. (2010). The memory function of sleep. *Nature Reviews Neuroscience*, 11:114–126.

Doeller, C. F., Barry, C., and Burgess, N. (2010). Evidence for grid cells in a human memory network. *Nature*, 463:657–661.

Einevoll, G. T., Kayser, C., Logothetis, N. K., and Panzeri, S. (2013). Modelling and analysis of local field potentials for studying the function of cortical circuits. *Nat. Rev. Neurosci.*, 14:770–785.

Einevoll, G. T., Pettersen, K. H., Devor, A., Ulbert, I., Halgren, E., and Dale, A. M. (2007). Laminar population analysis: estimating firing rates and evoked synaptic activity from multielectrode recordings in rat barrel cortex. *J. Neurophysiol.*, 97:2174–2190.

Elijah, D. H., Samengo, I., and Montemurro, M. A. (2015). Thalamic neuron models encode stimulus information by burst-size modulation. *Front. Comput. Neurosci.*, 9:113.

Engel, A. K., Fries, P., and Singer, W. (2001). Dynamic predictions: oscillations and synchrony in top-down processing. *Nat. Rev. Neurosci.*, 2:704–716.

Engel, A. K. and Singer, W. (2001). Temporal binding and the neural correlates of sensory awareness. *Trends Cogn. Sci.*, 5:16–25.

Eyherabide, H. G., Rokem, A., Herz, A. V. M., and Samengo, I. (2008). Burst firing is a neural code in an insect auditory system. *Front. Comput. Neurosci.*, 2:3.

Eyherabide, H. G., Rokem, A., Herz, A. V. M., and Samengo, I. (2009). Bursts generate a non-reducible spike-pattern code. *Front. Neurosci.*, 3:8–14.

Eyherabide, H. G. and Samengo, I. (2010a). The information transmitted by spike patterns in single neurons. *J. Physiol. Paris*, 104:147–155.

Eyherabide, H. G. and Samengo, I. (2010b). Time and category information in pattern-based codes. *Front. Comput. Neurosci.*, 4:145.

Fell, J. and Axmacher, N. (2011). The role of phase synchronization in memory processes. *Nat. Rev. Neurosci.*, 12:105–118.

Franklin, K. B. J. and Paxinos, G. (2007). *The Mouse Brain in Stereotaxic Coordinates*. Elsevier.

Freeman, W. T. (2007). Definitions of state variables and state space for brain-computer interface. *Cogn. Neurodyn.*, 1:3–14.

Fries, P. (2005). A mechanism for cognitive dynamics: neuronal communication through neuronal coherence. *Trends Cogn. Sci.*, 9:474–480.

Friston, K. J. (1994). Functional and effective connectivity in neuroimaging: a synthesis. *Human Brain Mapping*, 2:56–78.

Friston, K. J. (2011). Functional and effective connectivity: a review. *Brain Connectivity*, 1:13–36.

Fuchs, E. C., Zivkovic, A. R., Cunningham, M. O., Middleton, S., LeBeau, F. E. N., Bannerman, D. M., Rozov, A., Whittington, M. A., Traub, R. D., Rawlins, J. N. P., and Monyer, H. (2007). Recruitment of parvalbumin-positive interneurons determines hippocampal function and associated behavior. *Neuron*, 53:591–604.

Fyhn, M., Molden, S., Witter, M. P., Moser, E. I., and Moser, M. B. (2004). Spatial representation in the entorhinal cortex. *Science*, 305:1258–1264.

Georgopoulos, A. P., Kalaska, J. F., Caminiti, R., and Massey, J. T. (1982). On the relations between the direction of two-dimensional arm movements and cell discharge in primate motor cortex. *J. Neurosci.*, 2:1527–1537.

Gigg, J. (2006). Constraints on hippocampal processing imposed by the connectivity between CA1, subiculum and subicular targets. *Behav. Brain Res.*, 174:265–271.

Gigg, J., Finch, D. M., and O'Mara, S. M. (2000). Responses of rat subicular neurons to convergent stimulation of lateral entorhinal cortex and CA1 in vivo. *Brain Res.*, 884:35–50.

Giocomo, L. M., Stensola, T., Bonnevie, T., Van Cauter, T., Moser, M. B., and Moser, E. I. (2014). Topography of head direction cells in medial entorhinal cortex. *Curr. Biol.*, 24:252–262.

Gourevitch, B. and Eggermont, J. J. (2007). Evaluating information transfer between auditory cortical neurons. *J. Neurophysiol.*, 97:2533–2543.

Granger, C. W. J. (1969). Investigating causal relations by econometric models and cross-spectral methods. *Econometrica*, 37:424–438.

Gross, C. G. (2002). Genealogy of the "grandmother cell". *The Neuroscientist*, 8:512–518.

Grover, L. M., Kim, E., Cooke, J. D., and Holmes, W. R. (2009). LTP in hippocampal area CA1 is induced by burst stimulation over a broad frequency range centered around delta. *Learn. Mem.*, 16:69–81.

Guido, W. and Weyand, T. (1995). Burst responses in thalamic relay cells of the awake behaving cat. *J. Neurophysiol.*, 74:1782–1786.

Hablitz, J. J. and Johnston, D. (1981). Endogenous nature of spontaneous bursting in hippocampal pyramidal neurons. *Cell. Mol. Neurobiol.*, 1:325–334.

Hafting, T., Fyhn, M., Molden, S., Moser, M. B., and Moser, E. I. (2005). Microstructure of a spatial map in the entorhinal cortex. *Nature*, 436:801–806.

Hall, A. M. and Roberson, E. D. (2012). Mouse models of Alzheimer's disease. *Brain Research Bulletin*, 88:3–12.

Harris, K. D. (2005). Neural signatures of cell assembly organization. *Nature Reviews Neuroscience*, 6:399–407.

Harris, K. D., Henze, D. A., Csicsvari, J., Hirase, H., and Buzsaki, G. (2000). Accuracy of tetrode spike separation as determined by simultaneous intracellular and extracellular measurements. *J. Neurophysiol.*, 84:401–414.

Harris, K. D., Henze, D. A., Hirase, H., Leinekugel, X., Dragoi, G., Czurko, A., and Buzsaki, G. (2002). Spike train dynamics predicts theta-related phase precession in hippocampal pyramidal cells. *Nature*, 417:738–741.

Harris, K. D., Hirase, H., Leinekugel, X., Henze, D. A., and Buzsaki, G. (2001). Temporal interaction between single spikes and complex spike bursts in hippocampal pyramidal cells. *Neuron*, 32:141–149.

Hartley, R. V. L. (1928). Transmission of information. *Bell Syst. Tech. J.*, 7:535–563.

Hasselmo, M. E., Bodelon, C., and Wyble, B. P. (2002). A proposed function for hippocampal theta rhythm: Separate phases of encoding and retrieval enhance reversal of prior learning. *Neural Comput.*, 14:793–817.

He, Y., Chen, Z., Gong, G. L., and Evans, A. (2009). Neuronal networks in alzheimer's disease. *The Neuroscientist*, 15:333–350.

Henry, G. H., Dreher, B., and Bishop, P. O. (1974). Orientation specificity of cells in cat striate cortex. *J. Neurophysiol.*, 37:1394–1409.

Hodgkin, A. L. and Huxley, A. F. (1939). Action potentials recorded from inside a nerve fiber. *Nature*, 144:710–711.

Horner, A. J., Bisby, J. A., Zotow, E., Bush, D., and Burgess, N. (2016). Grid-like processing of imagined navigation. *Curr. Biol.*, 26:842–847.

Hubel, D. H. and Wiesel, T. N. (1959). Receptive fields of single neurones in the cat's striate cortex. *J. Physiol.*, 148:574–591.

Insausti, R. (1993). Comparative anatomy of the entorhinal cortex and hippocampus in mammals. *Hippocampus*, 3:19–26.

Ittner, L. M. and Gotz, J. (2011). Amyloid-beta and tau - a toxic pas de deux in alzheimer's disease. *Nat. Rev. Neurosci.*, 12:67–72.

Izhikevich, E. M. (2010). *Dynamical Systems in Neuroscience: The Geometry of Excitability and Bursting*. The MIT Press, London & Massachusetts.

Jacobs, J., Weidemann, C. T., Miller, J. F., Solway, A., Burke, J. F., Wei, X. X., Suthana, N., Sperling, M. R., Sharan, A. D., Fried, I., and Kahana, M. J. (2013). Direct recordings of grid-like neuronal activity in human spatial navigation. *Nat. Neurosci.*, 16:1188–1190.

Jarsky, T., Mady, R., Kennedy, B., and Spruston, N. (2008). Distribution of bursting neurons in the ca1 region and the subiculum of the rat hippocampus. *J. Comp. Neurol.*, 506:535–547.

Jefferys, J. G. (1995). Nonsynaptic modulation of neuronal activity in the brain: electric currents and extracellular ions. *Physiol. Rev.*, 75:689–723.

Jensen, O. (2006). Maintenance of multiple working memory items by temporal segmentation. *Neuroscience*, 139:237–249.

Jensen, O. and Lisman, J. E. (1998). An oscillatory short-term memory buffer model can account for data on the sternberg task. *Journal of Neuroscience*, 18:10688–10699.

Jensen, O. and Lisman, J. E. (2005). Hippocampal sequence-encoding driven by a cortical multi-item working memory buffer. *Trends in Neurosciences*, 28:67–72.

Jones, L. M., Depireux, D. A., Simons, D. J., and Keller, A. (2004a). Robust temporal coding in the trigeminal system. *Science*, 304:1986–1989.

Jones, L. M., Lee, S., Trageser, J. C., Simons, D. J., and Keller, A. (2004b). Precise temporal responses in whisker trigeminal neurons. *J. Neurophysiol.*, 92:665–668.

Kamondi, A., Acsady, L., Wang, X. J., and Buzsaki, G. (1998). Theta oscillations in somata and dendrites of hippocampal pyramidal cells in vivo: activity-dependent phase-precession of action potentials. *Hippocampus*, 8:244–261.

Kandel, E. R. and Spencer, W. A. (1961). Electrophysiology of hippocampal neurons: II. after-potentials and repetitive firing. *J. Neurophysiol.*, 24:243–259.

Kang, J., Jiang, L., Goldman, S. A., and Nedergaard, M. (1998). Astrocyte-mediated potentiation of inhibitory synaptic transmission. *Nat. Neurosci.*, 1:683–692.

Karbowski, K. (1990). Sixty years of clinical electroencephalography. *Eur. Neurol.*, 30:170–175.

Karbowski, K. (2002). Hans Berger (1873Ű1941). *J. Neurol.*, 249:1130–1131.

Katsumaru, H., Kosaka, T., Heizmann, C. W., and Hama, K. (1988). Gap junctions on gabaergic neurons containing the calcium-binding protein parvalbumin in the rat hippocampus (ca1 region). *Exp. Brain Res.*, 72:363–370.

Kayser, C., Montemurro, M. A., Logothetis, N. K., and Panzeri, S. (2009). Spike-phase coding boosts and stabilizes information carried by spatial and temporal spike patterns. *Neuron*, 61:597–608.

Kepecs, A. and Lisman, J. (2003). Information encoding and computation with spikes and bursts. *Network: Comput. Neural Syst.*, 14:103–118.

Kepecs, A. and Wang, X. J. (2000). Analysis of complex bursting in cortical pyramidal neuron models. *Neurocomputing*, 32-33:181–187.

Kepecs, A., Wang, X. J., and Lisman, J. (2002). Bursting neurons signal input slope. *J. Neurosci.*, 22:9053–9062.

Kim, S. M., Ganguli, S., and Frank, L. M. (2012). Spatial information outflow from the hippocampal circuit: distributed spatial coding and phase precession in the subiculum. *J. Neurosci.*, 32:11539–11558.

Kim, Y. and Spruston, N. (2012). Target-specific output patterns are predicted by the distribution of regular-spiking and bursting pyramidal neurons in the subiculum. *Hippocampus*, 22:693–706.

Kramis, R., Vanderwolf, C. H., and Bland, B. H. (1975). Two types of hippocampal rhythmical slow activity in both the rabbit and the rat: relations to behavior and effects of atropine, diethyl ether, urethane, and pentobarbital. *Exp. Neurol.*, 49:58–85.

Kropff, E., Carmichael, J. E., Moser, M. B., and Moser, E. I. (2015). Speed cells in the medial entorhinal cortex. *Nature*, 523:419–424.

Larson, E. B., Kukull, W. A., and Katzman, R. L. (1992). Cognitive impairment: Dementia and alzheimer's disease. *Annu. Rev. Public Health*, 13:431–449.

Latuske, P., Toader, O., and Allen, K. (2015). Interspike intervals reveal functionally distinct cell populations in the medial entorhinal cortex. *J. Neurosci.*, 35:10963–10976.

Lee, A. K. and Wilson, M. A. (2002). Memory of sequential experience in the hippocampus during slow wave sleep. *Neuron*, 36:1183–1194.

Lega, B. C., Jacobs, J., and Kahana, M. (2012). Human hippocampal theta oscillations and the formation of episodic memories. *Hippocampus*, 22:748–761.

Lesica, N. A. and Stanley, G. B. (2004). Encoding of natural scene movies by tonic and burst spikes in the lateral geniculate nucleus. *J. Neurosci.*, 24:10731–10740.

Leung, L. W. S. and Yim, C. Y. C. (1991). Intrinsic membrane potential oscillations in hippocampal neurons in vitro. *Brain Res.*, 553:261–274.

Lever, C., Burton, S., Jeewajee, A., O'Keefe, J., and Burgess, N. (2009). Boundary vector cells in the subiculum of the hippocampal formation. *J. Neurosci.*, 29:9771–9777.

Linden, H., Tetzlaff, T., Potjans, T. C., Pettersen, K. H., Grun, S., Diesmann, M., and Einevoll, G. T. (2011). Modeling the spatial reach of the lfp. *Neuron*, 72:859–872.

Lindner, M., Vicente, R., Priesemann, V., and Wibral, M. (2011). TRENTOOL: A Matlab open source toolbox to analyse information flow in time series data with transfer entropy. *BMC Neurosci.*, 12:119.

Lisman, J. (2005). The theta/gamma discrete phase code occuring during the hippocampal phase precession may be a more general brain coding scheme. *Hippocampus*, 15:913–922.

Lisman, J. and Buzsaki, G. (2008). A neural coding scheme formed by the combined function of gamma and theta oscillations. *Schizophrenia Bulletin*, 34:974–980.

Lisman, J. E. (1997). Bursts as a unit of neural information: making unreliable synapses reliable. *Trends Neurosci.*, 20:38–43.

Lisman, J. E. and Idiart, M. A. P. (1995). Storage of 7+/-2 short-term memories in oscillatory subcycles. *Science*, 267:1512–1515.

Llinas, R. R. (1988). The intrinsic electrophysiological properties of mammalian neurons: insights into central nervous system function. *Science*, 242:1654–1664.

Logothetis, N. K. (2003). The underpinnings of the bold functional magnetic resonance imaging signal. *J. Neurosci.*, 23:3963–3971.

Louie, K. and Wilson, M. A. (2001). Temporally structured replay of awake hippocampal ensemble activity during rapid eye movement sleep. *Neuron*, 29:145–156.

Lubenov, E. V. and Siapas, A. G. (2009). Hippocampal theta oscillations are travelling waves. *Nature*, 459:534–539.

MacKay, D. J. C. (2003). *Information Theory, Inference, and Learning Algorithms*. Cambridge University Press, Cambridge.

MacKay, D. M. and McCullock, W. S. (1952). The limiting information capacity of a neuronal link. *Bull. Math. Biophys.*, 14:127–135.

Magri, C., Whittingstall, K., Singh, V., Logothetis, N. K., and Panzeri, S. (2009). A toolbox for the fast information analysis of multiple-site LFP, EEG and spike train recordings. *BMC Neurosci.*, 10:81.

Maguire, E. A., Gadian, D. G., Johnsrude, I. S., Good, C. D., Ashburner, J., Frackowiak, R. S. J., and Frith, C. D. (2000). Navigation-related structural change in the hippocampi of taxi drivers. *Proc. Natl. Acad. Sci. U. S. A.*, 97:4398–4403.

Maguire, E. A., Woollett, K., and Spiers, H. J. (2006). London taxi drivers and bus drivers: A structural mri and neuropsychological analysis. *Hippocampus*, 16:1091–1101.

Mainen, Z. F. and Sejnowski, T. J. (1995). Reliability of spike timing in neocortical neurons. *Science*, 268:1503–1506.

Marple, S. L. (1999). Computing the discrete-time 'analytic' signal via FFT. *IEEE Trans. Signal Proces.*, 47:2600–2603.

Marsat, G. and Pollack, G. S. (2006). A behavioral role for feature detection by sensory bursts. *J. Neurosci.*, 26:10542–10547.

Marsat, G. and Pollack, G. S. (2010). The structure and size of sensory bursts encode stimulus information but only size affects behavior. *J. Comp. Physiol. A*, 196:315–320.

Martinez-Conde, S., Macknik, S. L., and Hubel, D. H. (2002). The function of bursts of spikes during visual fixation in the awake primate lateral geniculate nucleus and primary visual cortex. *Proc. Natl. Acad. Sci. U. S. A.*, 99:13920–13925.

Masquelier, T., Hugues, E., Deco, G., and Thorpe, S. J. (2009). Oscillations, phase-of-firing coding, and spike timing-dependent plasticity: an efficient learning scheme. *J. Neurosci.*, 29:13484–13493.

Mazzoni, A., Panzeri, S., Logothetis, N. K., and Brunel, N. (2008). Encoding of naturalistic stimuli by local field potential spectra in networks of excitatory and inhibitory neurons. *PLoS Comput. Biol.*, 4:e1000239.

McCormick, D. A., Connors, B. W., Lighthall, J. W., and Prince, D. A. (1985). Comparative electrophysiology of pyramidal and sparsely spiny stellate neurons of the neocortex. *J. Neurophysiol.*, 54:782–806.

McCormick, D. A. and Contreras, D. (2001). On the cellular and network bases of epileptic seizures. *Annu. Rev. Physiol.*, 63:815–846.

McNaughton, B. L., Battaglia, F. P., Jensen, O., Moser, E. I., and Moser, M. B. (2006). Path integration and the neural basis of the 'cognitive map'. *Nat. Rev. Neurosci.*, 7:663–678.

Mitzdorf, U. (1985). Current source-density method and application in cat cerebral cortex: investigation of evoked potentials and EEG phenomena. *Physiol. Rev.*, 65:37–100.

Mizuseki, K., Sirota, A., Pastalkova, E., and Buzsaki, G. (2009). Theta oscillations provide temporal windows for local circuit computation in the entorhinal-hippocampal loop. *Neuron*, 64:267–280.

Moldestad, O., Karlsen, P., Molden, S., and Storm, J. F. (2009). Tracheotomy improves experiment success rate in mice during urethane anesthesia and stereotaxic surgery. *J. Neurosci. Methods*, 176:57–62.

Molle, M. and Born, J. (2011). Slow oscillations orchestrating fast oscillations and memory consolidation. *Prog. Brain Res.*, 193:93–110.

Montemurro, M. A., Panzeri, S., Maravall, M., Alenda, A., Bale, M. R., Brambilla, M., and Petersen, R. S. (2007a). Role of precise spike timing in coding of dynamic vibrissa stimuli in somatosensory thalamus. *J. Neurophysiol.*, 98:1871–1882.

Montemurro, M. A., Rasch, M. J., Murayama, Y., Logothetis, N. K., and Panzeri, S. (2008). Phase-of-firing coding of natural visual stimuli in primary visual cortex. *Curr. Biol.*, 18:375–380.

Montemurro, M. A., Senatore, R., and Panzeri, S. (2007b). A downward biased estimator of spike timing information. *Neurocomputing*, 70:1777–1781.

Montemurro, M. A., Senatore, R., and Panzeri, S. (2007c). Tight data-robust bounds to mutual information combining shuffling and model selection techniques. *Neural Comput.*, 19:2913–2957.

Nemenman, I., Bialek, W., and De Ruyter Van Steveninck, R. R. (2004). Entropy and information in neural spike trains: Progress on the sampling problem. *Phys. Rev. E*, 69:056111.

Nobelprize.org (2016). The nobel prize in physiology or medicine 2014.

Nyquist, H. (1924). Certain factors affecting telegraph speed. *Bell Syst. Tech. J.*, 3:324–346.

Nyquist, H. (1928). Certain topics in telegraph transmission theory. *A.I.E.E. Trans.*, 47:617–644.

Oddo, S., Caccamo, A., Shepherd, J. D., Murphy, M. P., Golde, T. E., Kayed, R., Metherate, R., Mattson, Y. A., and LaFerla, F. M. (2003). Triple-transgenic model of Alzheimer's dsease with plaques and tangles: intracellular Abeta and synaptic dysfunction. *Neuron*, 39:409–421.

O'Keefe, J. and Dostrovsky, J. (1971). The hippocampus as a spatial map. preliminary evidence from unit activity in the freely-moving rat. *Brain Res.*, 34:171–175.

O'Keefe, J. and Nadel, L. (1978). *The Hippocampus as a Cognitive Map*. Oxford University Press.

O'Keefe, J. and Recce, M. L. (1993). Phase relationship between hippocampal place units and the EEG theta rhythm. *Hippocampus*, 3:317–330.

O'Mara, S. M., Commins, S., Anderson, M., and Gigg, J. (2001). The subiculum: a review of form, physiology and function. *Prog. Neurobiol.*, 64:129–155.

Oswald, A. M. M., Chacron, M. J., Doiron, B., Bastian, J., and Maler, L. (2004). Parallel processing of sensory input by bursts and isolated spikes. *J. Neurosci.*, 24:4351–4362.

Oswald, A. M. M., Doiron, B., and Maler, L. (2007). Interval coding. I. Burst interspike intervals as indicators of stimulus intensity. *J. Neurophysiol.*, 97:2731–2743.

Pagliardini, S., Funk, G. D., and Dickson, C. T. (2013a). Breathing and brain state: Urethane anesthesia as a model for natural sleep. *Respir. Physiol. Neurobiol.*, 188:324–332.

Pagliardini, S., Gosgnach, S., and Dickson, C. T. (2013b). Spontaneous sleep-like brain state alternations and breathing characteristics in urethane anesthetized mice. *PLoS ONE*, 8:e70411.

Paninski, L. (2003). Estimation of entropy and mutual information. *Neural Comput.*, 5:1191–1253.

Panzeri, S., Brunel, N., Logothetis, N. K., and Kayser, C. (2010). Sensory neural codes using multiplexed temporal scales. *Trends Neurosci.*, 33:111–120.

Panzeri, S., Petersen, R. S., Schultz, S. R., Lebedev, M., and Diamond, M. E. (2001). The role of spike timing in the coding of stimulus location in rat somatosensory cortex. *Neuron*, 29:769–777.

Panzeri, S., Petroni, F., Petersen, R. S., and Diamond, M. E. (2003). Decoding neuronal population activity in rat somatosensory cortex: role of columnar organization. *Cereb. Cortex*, 13:45–52.

Panzeri, S., Schultz, S. R., Treves, A., and Rolls, E. T. (1999). Correlations and the encoding of information in the nervous system. *Proc. R. Soc. Lond. B*, 266:1001–1012.

Panzeri, S., Senatore, R., Montemurro, M. A., and Petersen, R. S. (2007). Correcting for the sampling bias problem in spike train information measures. *J. Neurophysiol.*, 98:1064–1072.

Panzeri, S. and Treves, A. (1996). Analytical estimates of limited sampling biases in different information measures. *Network: Comput. Neural Syst.*, 7:87–107.

Papoulis, A. (1977). *Signal Analysis*. McGraw-Hill Book Company, New York.

Patel, J., Fujisawa, S., Berenyi, A., Royer, S., and Buzsaki, G. (2012). Traveling theta waves along the entire septotemporal axis of the hippocampus. *Neuron*, 75:410–417.

Paxinos, G. and Watson, C. (2007). *Rat Brain Atlas*. Academic Press, London.

Penttonen, M. and Buzsaki, G. (2003). Natural logarithmic relationship between brain oscillators. *Thalamus & Related Systems*, 2:145–152.

Pereda, E., Quiroga, R. Q., and Bhattacharya, J. (2005). Nonlinear multivariate analysis of neurophysiological signals. *Prog. Neurobiol.*, 77:1–37.

Petersen, R. S., Panzeri, S., and Diamond, M. E. (2002). Population coding in somatosensory cortex. *Curr. Opin. Neurobiol.*, 12:441–447.

Pettersen, K. H., Hagen, E., and Einevoll, G. T. (2008). Estimation of population firing rates and current source densities from laminar electrode recordings. *J. Comput. Neurosci.*, 24:291–313.

Pinsky, P. F. and Rinzel, J. (1994). Intrinsic and network rhythmogenesis in a reduced Traub model for CA3 neurons. *J. Comput. Neurosci.*, 1:39–60.

Place, R., Farovik, A., Brockmann, M., and Eichenbaum, H. (2016). Bidirectional prefrontalhippocampal interactions support context-guided memory. *Nat. Neurosci.*, 19:992–994.

Poskanzer, K. E. and Yuste, R. (2011). Astrocytic regulation of cortical up states. *Proc. Natl. Acad. Sci. U. S. A.*, 108:18453–18458.

Prandoni, P. and Vetterli, M. (2008). *Signal Processing for Communications*. EPFL Press, Lausanne.

Prichard, D. and Theiler, J. (1994). Generating surrogate data for time series with several simultaneously measured variables. *Phys. Rev. Lett.*, 73:951–954.

Prince, D. A. (1978). Neurophysiology of epilepsy. *Ann. Rev. Neurosci.*, 1:395–415.

Proakis, J. G. and Manolakis, D. G. (1996). *Digital Signal Processing*. Prentice-Hall, Inc., New Jersey.

Querfurth, H. W. and LaFerla, F. M. (2010). Alzheimer's disease. *N. Engl. J. Med.*, 362:329–344.

Quian Quiroga, R. (2012). Concept cells: the building blocks of declarative memory functions. *Nat. Rev. Neurosci.*, 13:587–597.

Quian Quiroga, R., Kraskov, A., Koch, C., and Fried, I. (2009). Explicit encoding of multimodal percepts by single neurons in the human brain. *Curr. Biol.*, 19:1308–1313.

Quian Quiroga, R., Kreiman, G., Koch, C., and Fried, I. (2008). Sparse but not 'Grandmother-cell' coding in the medial temporal lobe. *Trends Cogn. Sci.*, 12:87–91.

Quian Quiroga, R. and Panzeri, S. (2009). Extracting information from neuronal populations: information theory and decoding approaches. *Nat. Rev. Neurosci.*, 10:173–185.

Quian Quiroga, R., Reddy, L., Koch, C., and Fried, I. (2007). Decoding visual inputs from multiple neurons in the human temporal lobe. *J. Neurophysiol.*, 98:1997–2007.

Ranck, J. B. J. (1973). Studies on single neurons in dorsal hippocampal formation and septum in unrestrained rats. I. Behavioral correlates and firing repertoires. *Exp. Neurol.*, 41:461–531.

Rasch, B. and Born, J. (2013). About sleep's role in memory. *Physiol. Rev.*, 93:681–766.

Rieke, F., Warland, D., De Ruyter Van Steveninck, R. R., and Bialek, W. (1997). *Spikes: Exploring the Neural Code*. MIT Press, Cambridge, MA.

Royer, S., Zemelman, B. V., Losonczy, A., Kim, J., Chance, F., Magee, J. C., and Buzsaki, G. (2012). Control of timing, rate and bursts of hippocampal place cells by dendritic and somatic inhibition. *Nat. Neurosci.*, 15:769–775.

Sabourin, P. and Pollack, G. S. (2009). Behaviorally relevant burst coding in primary sensory neurons. *J. Neurophysiol.*, 102:1086–1091.

Samengo, I., Mato, G., Elijah, D. H., Schreiber, S., and Montemurro, M. A. (2013). Linking dynamical and functional properties of intrinsically bursting neurons. *J. Comput. Neurosci.*, 35:213–230.

Samengo, I. and Montemurro, M. A. (2010). Conversion of phase information into a spike-count code by bursting neurons. *PLoS ONE*, 5:e9669.

Sameshima, K. and Baccala, L. A. (1999). Using partial directed coherence to describe neuronal ensemble interactions. *Journal of Neuroscience Methods*, 94:93–103.

Scheffer-Teixeira, R., Belchior, H., Leao, R. N., Ribeiro, S., and Tort, A. B. L. (2013). On high-frequency field oscillations (>100 hz) and the spectral leakage of spiking activity. *J. Neurosci.*, 33:1535–1539.

Schiller, J., Major, G., Koester, H. J., and Schiller, Y. (2000). Nmda spikes in basal dendrites of cortical pyramidal neurons. *Nature*, 404:285–289.

Schneidman, E., Bialek, W., and Berry, M. J. (2003). Synergy, redundancy, and independence in population codes. *J. Neurosci.*, 23:11539–11553.

Schomburg, E. W., Anastassiou, C. A., Buzsaki, G., and Koch, C. (2012). The spiking component of oscillatory extracellular potentials in the rat hippocampus. *J. Neurosci.*, 32:11798–11811.

Schomburg, E. W., Fernandez-Ruiz, A., Mizuseki, K., Berenyi, A., Anastassiou, C. A., Koch, C., and Buzsaki, G. (2014). Theta phase segregation of input-specific gamma patterns in entorhinal-hippocampal networks. *Neuron*, 84:470–485.

Schreiber, T. (2000). Measuring information transfer. *Phys. Rev. Lett.*, 85:461–464.

Scoville, W. B. and Milner, B. (1957). Loss of recent memory after bilateral hippocampal lesions. *Journal of Neurology Neurosurgery and Psychiatry*, 20:11–21.

Shannon, C. E. (1948). A mathematical theory of communication. *Bell System Technical Journal*, 27:379–423,623–656.

Sharma, A. V., Wolansky, T., and Dickson, C. T. (2010). A comparison of sleeplike slow oscillations in the hippocampus under ketamine and urethane anesthesia. *J. Neurophysiol.*, 104:932–939.

Sharp, P. E. and Green, C. (1994). Spatial correlates of firing patterns of single cells in the subiculum of the freely moving rat. *J. Neurosci.*, 14:2339–2356.

Shein-Idelson, M., Ondracek, J. M., Liaw, H. P., Reiter, S., and Laurent, G. (2016). Slow waves, sharp waves, ripples, and REM in sleeping dragons. *Science*, 352:590–595.

Sherman, S. M. (2001). A wake-up call from the thalamus. *Nat. Neurosci.*, 4:344–346.

Siapas, A. G. and Wilson, M. A. (1998). Coordinated interactions between hippocampal ripples and cortical spindles during slow-wave sleep. *Neuron*, 21:1123–1128.

Siegel, M., Donner, T. H., and Engel, A. K. (2012). Spectral fingerprints of large-scale neuronal interactions. *Nat. Rev. Neurosci.*, 13:121–134.

Silva, L. R., Amitai, Y., and Connors, B. W. (1991). Intrinsic oscillations of neocortex generated by layer 5 pyramidal neurons. *Science*, 251:432–435.

Sirota, A. and Buzsaki, G. (2005). Interaction between neocortical and hippocampal networks via slow oscillations. *Thalamus Relat. Syst.*, 3:245–259.

Skaggs, W. E., McNaughton, B. L., Gothard, K. M., and Markus, E. J. (1993). An information-theoretic approach to deciphering the hippocampal code. In Hanson, S. J., Cowan, J. D., and Giles, C. L., editors, *Advances in Neural Information Processing Systems*, volume 5, pages 1030–1037, San Marco, CA. Morgan Kaufmann.

Skaggs, W. E., McNaughton, B. L., Permenter, M., Archibeque, M., Vogt, J., Amaral, D. G., and Barnes, C. A. (2007). EEG sharp waves and sparse ensemble unit activity in the macaque hippocampus. *J. Neurophysiol.*, 98:898–910.

Skaggs, W. E., McNaughton, B. L., Wilson, M. A., and Barnes, C. A. (1996). Theta phase precession in hippocampal neuronal populations and the compression of temporal sequences. *Hippocampus*, 6:149–172.

Solstad, T., Boccara, C. N., Kropff, E., Moser, M. B., and Moser, E. I. (2008). Representation of geometric borders in the entorhinal cortex. *Science*, 322:1865–1868.

Squire, L. R. (2009). The legacy of patient hm for neuroscience. *Neuron*, 61:6–9.

Squire, L. R. and Wixted, J. T. (2011). The cognitive neuroscience of human memory since hm. *Annu. Rev. Neurosci.*, 34:259–288.

Staff, N. P., Jung, H. Y., Thiagarajan, T., Yao, M., and Spruston, N. (2000). Resting and active properties of pyramidal neurons in subiculum and ca1 of rat hippocampus. *J. Neurophysiol.*, 84:2398–408.

Stam, C. J., de Haan, W., Daffertshofer, A., Jones, B. F., Manshanden, I., van Walsum, A. M. V., Montez, T., Verbunt, J. P. A., de Munck, J. C., van Dijk, B. W., Berendse, H. W., and Scheltens, P. (2009). Graph theoretical analysis of magnetoencephalographic functional connectivity in alzheimers disease. *Brain*, 132:213–224.

Steriade, M. (2006). Grouping of brain rhythms in corticothalamic systems. *Neuroscience*, 137:1087–1106.

Steriade, M., McCormick, D. A., and Sejnowski, T. J. (1993a). Thalamocortical oscillations in the sleeping and aroused brain. *Science*, 262:679–685.

Steriade, M., Nunez, A., and Amzica, F. (1993b). A novel slow (<1 hz) oscillation of neocortical neurons in vivo: depolarizing and hyperpolarizing components. *J. Neurosci.*, 13:3252–3265.

Strange, B. A., Witter, M. P., Lein, E. S., and Moser, E. I. (2014). Functional organization of the hippocampal longitudinal axis. *Nat. Rev. Neurosci.*, 15:655–669.

Strong, S. P., Koberle, R., De Ruyter Van Steveninck, R. R., and Bialek, W. (1998). Entropy and information in neural spike trains. *Phys. Rev. Lett.*, 80:197–200.

Sugase, Y., Yamane, S., Ueno, S., and Kawano, K. (1999). Global and fine information coded by single neurons in the temporal visual cortex. *Nature*, 400:869–873.

Suthana, N. A., Ekstrom, A. D., Moshirvaziri, S., Knowlton, B., and Bookheimer, S. Y. (2009). Human hippocampal ca1 involvement during allocentric encoding of spatial information. *J. Neurosci.*, 29:10512–10519.

Swadlow, H. A. and Gusev, A. G. (2001). The impact of 'bursting' thalamic impulses at a neocortical synapse. *Nat. Neurosci.*, 4:402–408.

Taube, J. S. (1993). Electrophysiological properties of neurons in the rat subiculum in vitro. *Exp. Brain Res.*, 96:304–318.

Taube, J. S., Muller, R. U., and Ranck, J. B. (1990a). Head-direction cells recorded from the postsubiculum in freely moving rats. I. Description and quantitative analysis. *J. Neurosci.*, 10:420–435.

Taube, J. S., Muller, R. U., and Ranck, J. B. (1990b). Head-direction cells recorded from the postsubiculum in freely moving rats. II. Effects of environmental manipulations. *J. Neurosci.*, 10:436–447.

Theiler, J., Eubank, S., Longtin, A., Galdrikian, B., and Farmer, J. D. (1992). Testing for nonlinearity in time series: the method of surrogate data. *Physica D*, 58:77–94.

Tort, A. B. L., Komorowski, R., Eichenbaum, H., and Kopell, N. (2010). Measuring phase-amplitude coupling between neuronal oscillations of different frequencies. *J. Neurophysiol.*, 104:1195–1210.

Tovee, M. J., Rolls, E. T., Treves, A., and Bellis, R. P. (1993). Information encoding and the responses of single neurons in the primate temporal visual cortex. *J. Neurophysiol.*, 70:640–654.

Townsend, G., Peloquin, P., Kloosterman, F., Hetke, J. F., and Leung, L. S. (2002). Recording and marking with silicon multichannel electrodes. *Brain Res. Brain Res. Protoc.*, 9:122–129.

Traub, R. D., Wong, R. K. S., Miles, R., and Michelson, H. (1991). A model of a CA3 hippocampal pyramidal neuron incorporating voltage-clamp data on intrinsic conductances. *J. Neurophysiol.*, 66:635–650.

Treves, A. and Panzeri, S. (1995). The upward bias in measures of information derived from limited data samples. *Neural Comput.*, 7:399–407.

Uhlhaas, P. J. and Singer, W. (2006). Neural synchrony in brain disorders: relevance for cognitive dysfunctions and pathophysiology. *Neuron*, 52:155–168.

Uhlhaas, P. J. and Singer, W. (2010). Abnormal neural oscillations and synchrony in schizophrenia. *Nature Reviews Neuroscience*, 11:100–113.

Wang, X. J. (2010). Neurophysiological and computational principles of cortical rhythms in cognition. *Physiol. Rev.*, 90:1195–1268.

Ward, L. M. (2003). Synchronous neural oscillations and cognitive processes. *Trends Cogn. Sci.*, 7:553–559.

Watson, B. O. and Buzsaki, G. (2015). Sleep, memory & brain rhythms. *Daedalus*, 144:67–82.

Welch, P. D. (1967). The use of Fast Fourier Transform for the estimation of power spectra: A method based on time averaging over short, modified periodograms. *IEEE Trans. Audio and Electroacoust.*, AU-15:70–73.

West, M. J., Coleman, P. D., Flood, D. G., and Troncoso, J. C. (1994). Differences in the pattern of hippocampal neuronal loss in normal aging and alzheimer's disease. *The Lancet*, 344:769–772.

Wiener, N. (1956). *Modern mathematics for engineers*, chapter The theory of prediction. McGraw-Hill, New York.

Witter, M. P., Naber, P. A., van Haeften, T., Machielsen, W. C. M., Rombouts, S. A. R. B., Barkhof, F., Scheltens, P., and Lopes da Silva, F. H. (2000). Cortico-hippocampal communication by way of parallel parahippocampal-subicular pathways. *Hippocampus*, 10:398–410.

Wolansky, T., Clement, E. A., Peters, S. R., Palczak, M. A., and Dickson, C. T. (2006). Hippocampal slow oscillation: A novel EEG state and its coordination with ongoing neocortical activity. *J. Neurosci.*, 26:6213–6229.

Womelsdorf, T., Schoffelen, J. M., Oostenveld, R., Singer, W., Desimone, R., Engel, A. K., and Fries, P. (2007). Modulation of neuronal interactions through neuronal synchronization. *Science*, 316:1609–1612.

Wong, R. K. S., Prince, D. A., and Basbaum, A. I. (1979). Intradendritic recordings from hippocampal neurons. *Proc*, 76:986–990.

Wood, E. R., Dudchenko, P. A., Robitsek, R. J., and Eichenbaum, H. (2000). Hippocampal neurons encode information about different types of memory episodes occurring in the same location. *Neuron*, 27:623–633.

Ylinen, A., Bragin, A., Nadasdy, Z., Jando, G., Szabo, I., Sik, A., and Buzsaki, G. (1995). Sharp wave-associated high-frequency oscillation (200 hz) in the intact hippocampus: network and intracellular mechanisms. *J. Neurosci.*, 15:30–46.

Zhang, S. J., Ye, J., Couey, J. J., Witter, M. P., Moser, E. I., and Moser, M. B. (2014). Functional connectivity of the entorhinal-hippocampal space circuit. *Phil. Trans. R. Soc. B*, 369:20120516.